AD NUMBER

**AD231291**

LIMITATION CHANGES

TO:

**Approved for public release; distribution is unlimited.**

FROM:

**Distribution authorized to U.S. Gov't. agencies and their contractors;
Administrative/Operational Use; SEP 1959. Other requests shall be referred to Wright Air Development Center (USAF), Wright-Patterson AFB, OH 45433.**

AUTHORITY

**AFFDL ltr, 21 Oct 1974**

# DISCLAIMER NOTICE

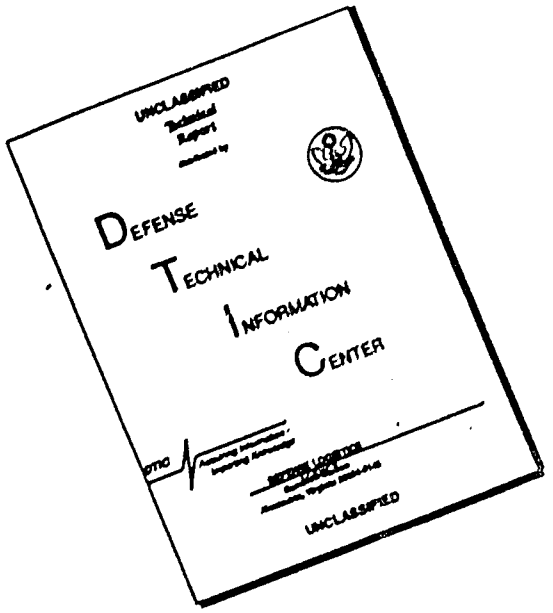


THIS DOCUMENT IS BEST QUALITY AVAILABLE. THE COPY FURNISHED TO DTIC CONTAINED A SIGNIFICANT NUMBER OF PAGES WHICH DO NOT REPRODUCE LEGIBLY.

49

WADC TECHNICAL REPORT 59-457

# APPLICATION OF THE WATER SURFACE WAVE ANALOGY IN VISUALIZING THE WAVE PATTERN OF A NUMBER OF PRIMARY AND SECONDARY BODY COMBINATIONS IN SUPERSONIC FLOW

FC

HELMUT G. HEINRICH
and
SHUKRY K. IBRAHIM

DEPARTMENT OF AERONAUTICAL ENGINEERING
UNIVERSITY OF MINNESOTA



SEPTEMBER 1959



This report is not to be announced or distributed automatically to foreign governments (AFR 205-43A, paragraph 6d.)

WRIGHT AIR DEVELOPMENT CENTER

AF-WP-B-DEC 59 175

WADC TECHNICAL REPORT 59-457

# APPLICATION OF THE WATER SURFACE WAVE ANALOGY IN VISUALIZING THE WAVE PATTERN OF A NUMBER OF PRIMARY AND SECONDARY BODY COMBINATIONS IN SUPERSONIC FLOW

HELMUT G. HEINRICH
and
SHUKRY K. IBRAHIM

DEPARTMENT OF AERONAUTICAL ENGINEERING
UNIVERSITY OF MINNESOTA

SEPTEMBER 1959

AERONAUTICAL ACCESSORIES LABORATORY
Contract No. AF 33(616)-6372
Project 6065-60252

WRIGHT AIR DEVELOPMENT CENTER
AIR RESEARCH AND DEVELOPMENT COMMAND
UNITED STATES AIR FORCE
WRIGHT-PATTERSON AIR FORCE BASE, OHIO

FOREWORD

This report was prepared by the Department of Aeronautical Engineering of the University of Minnesota in compliance with Air Force Contract No. AF 33(616)-3955.

The work being accomplished under this contract is sponsored jointly by the Quartermaster Research and Engineering Command, Department of the Army; Bureau of Aeronautics and Bureau of Ordnance, Department of the Navy; and Air Research and Development Command, Department of the Air Force, and is directed by a Tri-Service Steering Committee concerned with Aerodynamic Retardation. Contract administration is conducted by Wright Air Development Center (ARDC) and Mr. Rudi J. Berndt of the Parachute Branch, Aeronautical Accessories Laboratory, Wright Air Development Center, is Project Engineer.

The facility development and initial experimentation were done by Mr. James Grant. The scientific guidance and analysis were performed by Mr. Shukry Ibrahim, Research Associate, and Dr. H. G. Heinrich, Professor of Aeronautical Engineering. The main part of the experimental work and related analysis was carried out by Mr. Edward Riebesehl and a number of other graduate and undergraduate students. Mr. Riebesehl also contributed significantly in the preparation of this report.

## ABSTRACT

The Water Surface Wave Analogy has been applied to obtain a visual representation of the wave pattern for a number of primary-secondary body combinations representing systems in which the secondary body is located totally or partially in the wake of the primary body. The systems represent potential shapes of flying objects in connection with aerodynamic deceleration devices at a simulated Mach Number of 2. The distance between primary and secondary bodies varied between 2 and 8 diameters of the primary body.

The mathematical basis of the analogy and its main limitations are discussed. The test equipment and the experimental procedure are described.

Photographs of the wave pattern for a series of tests involving all possible combinations of five primary bodies and six secondary bodies with diameter ratio: $\frac{D \text{ secondary}}{D \text{ primary}} = 2$ are given.

Within the limitations outlined, the analogy is found to provide a convenient and inexpensive means for a qualitative study of the wave pattern which can serve as a preliminary information in the layout of aerodynamic deceleration systems and as a guide in the establishment of a program for supersonic wind tunnel tests.


## PUBLICATION REVIEW

This report has been reviewed and is approved.

For the Commander:

Warren P. Shepardson

WARREN P. SHEPARDSON
Chief, Parachute Branch
Aeronautical Accessories Laboratory

TABLE OF CONTENTS

## LIST OF ILLUSTRATIONS

## LIST OF SYMBOLS

| | |
|---|---|
| $a$ | - Speed of sound in a gas. |
| $C_p$ | - Specific heat at constant pressure. |
| $C_v$ | - Specific heat at constant volume. |
| $d$ | - Water depth. |
| $h$ | - Enthalpy of a gas. |
| $g$ | - Acceleration of gravity. |
| $m$ | - Mass. |
| $T$ | - Absolute temperature. |
| $p$ | - Pressure of a gas. |
| $u,v$ | - Components of velocity in x-direction and y-direction, respectively. |
| $x,y$ | - Rectangular coordinate axes. |
| $V$ | - Velocity of flow. |
| $c$ | - Velocity of propagation of surface waves in fluid. |
| $\gamma$ | - Adiabatic gas constant, ratio of $C_p$ to $C_v$ of gas. |
| $\theta$ | - Wedge angle. |
| $\lambda$ | - Wave length of surface wave in liquid. |
| $\rho$ | - Mass density. |
| $\sigma$ | - Surface tension of liquid. |
| $\phi$ | - Velocity potential in two dimensional flow. |

Subscript o refers to stagnation condition.

Subscript w refers to water flow.

Subscript A refers to air flow.

Subscripts x, y indicate partial differentiation w.r.t. x, y.

## SECTION 1

## INTRODUCTION

One of the objectives of the research program concerning aerodynamic retardation is the establishment of the principal flow pattern and the related velocity and pressure distribution as they occur when two bodies are immersed in a fluid, and one body is located in the wake of the preceding one. The body in the originally undisturbed flow is called the primary and the one in the wake is called the secondary body. The primary and secondary bodies investigated in the following study are basic forms representing actual or contemplated configurations of flying objects and trailing aerodynamic deceleration devices.

The entire program is rather large and would be very expensive if all interesting combinations were to be investigated in subsonic and supersonic wind tunnels. Therefore, studies, by means of the water analogy method, were conceived as a possibility to explore the principal flow phenomena which will occur when objects are immersed in fluid as described above.

In view of the circumstances, the main objective of these studies is the establishment of preliminary information for the engineering layout of retardation systems and for extensive wind tunnel studies on promising body combinations.

The Water Analogy has, in recent years, become a valuable tool to the investigator who desires, without making expensive wind tunnel tests, to make a qualitative study of the fluid flow around a body in transonic and supersonic flow. In water a hydraulic jump occurs which is similar

---

Manuscript released by the author 25 Sept 59 for publication

to a shock wave in a gas and the analogy provides a method of visualizing the wave pattern.

The theory of the hydraulic analogy, which provides the mathematical basis for relating the hydraulic jump in the water tank to a shock wave in a two-dimensional supersonic flow and indicates the possibilities and limitations of this analogy, is given in Section 2 of this report.

There are two types of water tables used in hydraulic analogy investigations. One type has a fixed model with water flowing past it. The velocity and depth of the water are maintained through a reservoir and sluice gate arrangement and by controlling the slope of the table. The other type has placid water at a specified depth and the model is towed through it at an easily measured velocity. The latter system was used in the water analogy studies at the University of Minnesota.

## SECTION 2

## THEORY OF THE HYDRAULIC ANALOGY

The analogy between the flow of a liquid with a free surface in a gravity field and the two-dimensional flow of a compressible gas has been known for some time. The mathematical Basis of this analogy was first presented in 1932 by Riabouchinsky. In 1938, Preiswerk made a comprehensive, theoretical and experimental study and demonstrated the application of the methods of gas dynamics to water flow with a free surface with and without hydraulic jumps (Reference 1).

The following summarized presentation of the mathematical theory of the analogy is largely based on that reference.

### 2.1 Water Flow Equations

The following assumptions are made in the derivation of the water flow equations:

1) The flow is frictionless, i.e., there is no conversion of energy into heat.

2) The flow is irrotational; this assumption implies the existence of a Velocity Potential.

3) The vertical accelerations are negligible compared with the acceleration of gravity. It follows from this assumption that the pressure in the fluid at any point depends only on the height of the free surface above that point.

#### 2.1.1 Energy Equations

The energy equation simply states that the sum of the potential

and kinetic energy of a water particle is constant during its motion.

If one considers a flow filament originating at the point $P_o$ ($x_o$, $y_o$, $z_o$) (Fig 1) at which the velocity is assumed to be zero (Stagnation Condition), then Bernoulli's Equation applied to any point P (x,y, z) on the same filament that originates at $P_o$ gives:

$$p + 1/2\,\rho V_w^2 + \rho g z = p_o + \rho g z_o \tag{2.1a}$$

where $V_w$ represents the resultant water velocity at P

Equation (2.1a) may be written as

$$V_w^2 = 2g(z_o - z) + \frac{2}{\rho}(p_o - p) \tag{2.1b}$$

From assumption 3), there follows:

$$p_o = \rho g(d_o - z_o) \tag{2.2a}$$

and $$p = \rho g(d - z) \tag{2.2b}$$

By substitution into (2.1b) there follows:

$$V_w^2 = 2g(d_o - d) \tag{2.3a}$$

This is a simple form of the energy equation and it indicates that the velocity at any internal point is independent of z and hence constant over the entire depth.

The maximum velocity is given by:

$$V_{w_{max}} = \sqrt{2gd_o} \tag{2.4}$$

and the velocity ratio

$$\left(\frac{V}{V_{max}}\right)_w = \sqrt{\frac{d_o - d}{d_o}} \tag{2.5}$$

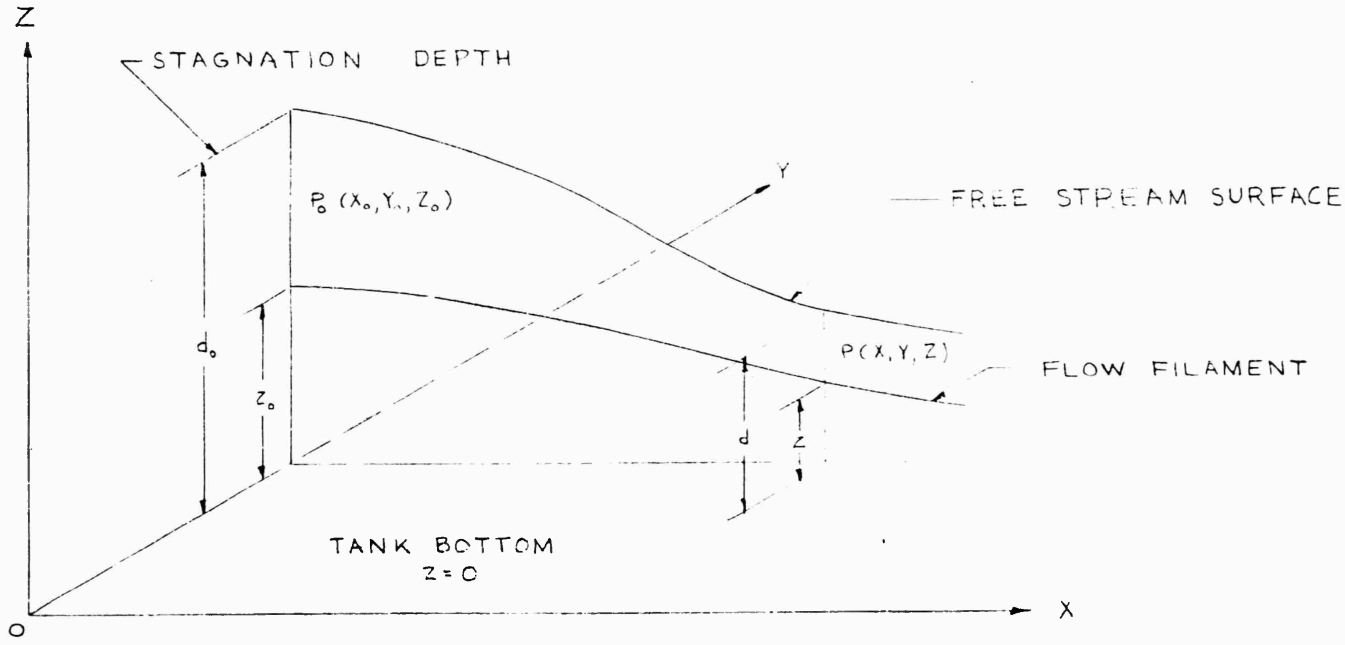


FIG. 1 NOTATION FOR THE WATER FLOW EQUATIONS

2.1.2 Continuity Equation

The equation of continuity is given by:

$$\frac{\partial(du)}{\partial x} + \frac{\partial(dv)}{\partial y} = 0 \qquad (2.6a)$$

which may be expanded into:

$$d\,\frac{\partial u}{\partial x} + u\,\frac{\partial d}{\partial x} + d\,\frac{\partial v}{\partial y} + v\,\frac{\partial d}{\partial y} = 0 \qquad (2.6b)$$

2.1.3 Potential Function

The energy equation (2.3a) may be written in the form

$$d = d_o - \frac{V_w^2}{2g} \qquad (2.3b)$$

Since $V_w^2 = u^2 + v^2$

Then

$$\frac{\partial d}{\partial x} = -\frac{1}{g}\left(u\,\frac{\partial u}{\partial x} + v\,\frac{\partial v}{\partial x}\right) \qquad (2.7a)$$

and $$\frac{\partial d}{\partial y} = -\frac{1}{g}\left(u\,\frac{\partial u}{\partial y} + v\,\frac{\partial v}{\partial y}\right) \qquad (2.7b)$$

By substitution from (2.7a) and (2.7b) into (2.6b) there is obtained:

$$\frac{\partial u}{\partial x}\left(1 - \frac{u^2}{gd}\right) - \frac{uv}{gd}\left(\frac{\partial u}{\partial y} + \frac{\partial v}{\partial x}\right) + \frac{\partial v}{\partial y}\left(1 - \frac{v^2}{gd}\right) = 0 \qquad (2.8)$$

The assumption of irrotationality (Assumption 2) is expressed mathematically by:

$$\frac{\partial v}{\partial x} - \frac{\partial u}{\partial y} = 0$$

It implies the existence of a velocity potential function $\phi(x, y)$ such that

$$u = \frac{\partial \phi}{\partial x}; \qquad v = \frac{\partial \phi}{\partial y} \tag{2.10}$$

By substitution from (2.10) into (2.8), the differential equation for the velocity potential of the free surface water flow is obtained, namely,

$$\phi_{xx}\left(1 - \frac{\phi^2_x}{gd}\right) - 2\phi_{xy}\frac{\phi_x\phi_y}{gd} + \phi_{yy}\left(1 - \frac{\phi^2_y}{gd}\right) = 0 \tag{2.11}$$

## 2.2 Two-dimensional Compressible Gas Flow Equations

These equations and the assumptions underlying their derivation are well known and are given in many textbooks on Compressible Fluid Flow as, for example, Reference 9. Only the equations directly relevant to the present analogy are listed below.

The Equation of State for an ideal gas is given by

$$p = gR\rho T \tag{2.12}$$

The assumption of adiabatic flow, i.e., that no heat is added or removed from the flow yields the relations:

$$\frac{p}{p_o} = \left(\frac{\rho}{\rho_o}\right)^{\gamma} \tag{2.13a}$$

$$\frac{\rho}{\rho_o} = \left(\frac{T}{T_o}\right)^{\frac{1}{\gamma-1}} \tag{2.13b}$$

$$\frac{p}{p_o} = \left(\frac{T}{T_o}\right)^{\frac{1}{\gamma-1}} \tag{2.13c}$$

### 2.2.1 Energy Equation

Using the concept of enthalpy given by:

$$h = gC_pT \tag{2.14}$$

The energy equation may be written in the forms

$$gh + \tfrac{1}{2} V_A^2 = gh_o \tag{2.15}$$

$$\text{or} \quad gC_pT + \tfrac{1}{2} V_A^2 = gC_pT_o \tag{2.16}$$

where subscript $_o$ refers to stagnation conditions and $V_A$,T represent the resultant air velocity and temperature at any specified point P in the flow.

Hence, the air flow velocity at P is given by

$$V_A^2 = 2g(h_o - h) = 2gC_p(T_o - T) \tag{2.17}$$

The maximum velocity is given by

$$V_{A\ max} = \sqrt{2gh_o} = \sqrt{2gC_pT_o} \tag{2.18}$$

and the velocity ratio:

$$\left(\frac{V}{V_{max}}\right)_A = \sqrt{\frac{T_o - T}{T_o}} = \sqrt{\frac{h_o - h}{h_o}} \tag{2.19}$$

2.2.2 Continuity Equation

This is given by

$$\frac{\partial}{\partial x}(\rho u) + \frac{\partial}{\partial y}(\rho v) = 0 \tag{2.20}$$

2.2.3 Potential Function

The equation for the velocity potential of a two-dimensional compressible flow is given by:

$$\phi_{xx}\left(1 - \frac{\phi_x^2}{a^2}\right) - 2\phi_{xy}\frac{\phi_x\phi_y}{a^2} + \phi_{yy}\left(1 - \frac{\phi_y^2}{a^2}\right) = 0 \tag{2.21}$$

## 2.3 Correspondence Between the Water Flow Equations and the Two-Dimensional Compressible Gas Flow Equations

Comparison between equations (2.5) and (2.19) shows that the nondimensional velocity ratios for water and gas flow will be the same if

$$\frac{d_o - d}{d_o} = \frac{T_o - T}{T_o} = \frac{h_o - h}{h_o}$$

i.e. $$\frac{d}{d_o} = \frac{T}{T_o} = \frac{h}{h_o} \qquad (2.22)$$

For analogy, the water depth ratio would correspond to the gas temperature ratio or the enthalpy ratio.

Equations (2.6a) and (2.20) expressing the continuity condition for the two flows have the same form and since the velocities are analogous, a further condition for the analogy is that the water depth be identified with the air density, namely,

$$\frac{d}{d_o} = \frac{\rho}{\rho_o} \qquad (2.23)$$

By using (2.22), it follows that

$$\frac{d}{d_o} = \frac{\rho}{\rho_o} = \frac{T}{T_o} \qquad (2.24)$$

However, the adiabatic condition specified that

$$\frac{\rho}{\rho_o} = \left(\frac{T}{T_o}\right)^{\frac{1}{\gamma-1}} \qquad (2.13b)$$

Equations (2.13b) and (2.24) can be consistent only if

$$\frac{1}{\gamma-1} = 1 \qquad \text{i.e.} \quad \gamma = 2$$

Thus, an intrinsic limitation of the analogy is that it is correct only for a gas having $\gamma = 2$.

Such a gas does not exist but fortunately, there are many flow problems which are not greatly affected by a change of $\gamma$ and for these problems, the analogy can be very fruitful.

Equations (2.11) and (2.21) for the velocity potentials of the two flows indicate that the quantity $\sqrt{gd}$ in the water flow is identifiable with a, the velocity of sound in the gas flow.

Physically, the quantity $\sqrt{gd}$ represents the velocity of propagation of surface waves having wave lengths that are large in comparison to the water depth.

The ratio $\frac{V_w}{\sqrt{gd}}$ in the liquid flow corresponds to the Mach Number $\frac{V_A}{a}$ in the gas flow.

Two flow regimes can be distinguished:

a) The case $\frac{V_w}{\sqrt{gd}} < 1$ corresponding to $\frac{V_A}{a} < 1$ i.e. subsonic flow.

The water flow in this case is termed "streaming."

b) The case $\frac{V_w}{\sqrt{gd}} > 1$ corresponding to $\frac{V_A}{a} > 1$ i.e. supersonic flow.

The water flow is known as "shooting."

Hydraulic jumps occur in shooting flow and equation (2.23) shows that the jump in depth corresponds to the step function in the density.

Small intensity hydraulic jumps are propagated with the velocity $c = \sqrt{gd}$ thereby creating a wave pattern which corresponds to the Mach waves in a gas flow.

From the Equation of State (Equation 2.12), it follows that:

$$\frac{P}{P_o} = \frac{\rho T}{\rho_o T_o}$$

The Analogy has already established that

$$\frac{T}{T_o} = \frac{d}{d_o} \tag{2.22}$$

and $$\frac{\rho}{\rho_o} = \frac{d}{d_o} \tag{2.23}$$

Hence

$$\frac{p}{p_o} = \left(\frac{d}{d_o}\right)^2 \tag{2.26}$$

Thus the pressure ratios in the compressible gas flow field are analogous to the square of the depth ratio in the incompressible water flow field.

## 2.4 Some Limitations of the Analogy

One inherent limitation of the analogy is that it applies to a hypothetical gas having $\gamma = 2$. It is necessary therefore to keep in mind the possible changes of flow characteristics resulting from the difference between the actual and hypothetical values.

Another important limitation of the analogy is that since the water depth (direction of z axis) represents the density, only two other dimensions remain for the geometric representation of the flow field and hence only two-dimensional shapes can be geometrically represented.

In a critical examination of the analogy, Laitone has discussed in Reference 4 some additional restrictive assumptions and limitations of the analogy. One of these restrictions stems from the fact that the actual velocity of wave propagation is not given exactly by $c = \sqrt{gd}$ as assumed but more accurately by:

$$c = \sqrt{\frac{g\lambda}{2\pi} + \frac{2\pi\sigma}{\rho\lambda} \tanh \frac{2\pi d}{\lambda}}$$

The expansion of $\tanh \frac{2\pi d}{\lambda}$ as a power series in $\frac{2\pi d}{\lambda}$ is given by:

$$\tanh \frac{2\pi d}{\lambda} = \frac{2\pi d}{\lambda} - \frac{1}{3}\left(\frac{2\pi d}{\lambda}\right)^3 + \frac{2}{15}\left(\frac{2\pi d}{\lambda}\right)^5 - \frac{17}{315}\left(\frac{2\pi d}{\lambda}\right)^7 + \cdots \quad (2.28)$$

This is valid for

$$-\frac{\pi}{2} < \frac{2\pi d}{\lambda} < \frac{\pi}{2}$$

By substitution from (2.28) into (2.27) one obtains

$$c = \sqrt{gd}\left[1 + \frac{4\pi^2\sigma}{g\rho\lambda^2} + \text{terms of order } \frac{d^2}{\lambda^2} \text{ or higher}\right]^{\frac{1}{2}} \quad (2.29)$$

The actual wave propagation velocity depends not only on the liquid depth d but also its surface tension $\sigma$ and the wavelength $\lambda$.

For the case $d \to o$ the second term in (2.29) containing the surface tension will become predominant for small $\lambda$. These wavelengths correspond to the capillary waves and should be disregarded since they form no part of the analogy. The third term of Equation (2.29) shows that the vertical acceleration is not negligible unless $d \ll \lambda$ i.e. the water depth is very much smaller than the wavelength.

The disturbance wavelength in shallow water is proportional to the model size and hence relatively large models should be used to reduce the capillary ripples.

In view of the above restrictions and the fact that the available water channel of the University of Minnesota is only 4 ft. wide, the model dimensions given in Figures 7b and 7c when used in conjunction with a water depth of .25 in. appeared to provide the best compromise.

A further restriction of the analogy discussed in Reference 4 arises in the investigation of shock waves.

Equation (2.22) indicates that the local water depth directly corresponds to the local value of the enthalpy or temperature in the

two-dimensional compressible gas flow. In an adiabatic gas flow, there is no change in the stagnation temperature across a shock wave. In the hydraulic jump, however, there exists a certain loss in the stagnation water depth due to the formation of eddies that eventually increase the water temperature. This additional loss of available energy has no counterpart in the analogous case of ordinary shock waves in gas flow. The analogy, therefore, should be strictly limited to that range of Mach Numbers and flow deflections where the loss of stagnation depth is negligible.

A comparison of data on normal shocks indicates that the analogy is within 1% if $M < 1.5$. Beyond $M = 1.5$, some of the hydraulic jump relations differ appreciably from the perfect gas relations and an analysis should be undertaken to determine the relative order of magnitude of the discrepancies.

## 2.5 Summary of the Analogy

| Two-Dimensional Compressible Gas Flow | Liquid Flow with Free Surface in Gravity Field |
|---|---|
| **Flow Medium** | **Flow Medium** |
| Hypothetical Compressible Gas with $\gamma = \frac{C_p}{C_v} = 2$ | Incompressible liquid |
| **Field Geometry** | **Field Geometry** |
| Two-dimensional field. Model and side boundaries geometrically similar | Shallow water with horizontal bottom and free top surface. Model and sides geometrically similar |
| **Corresponding Quantities** | **Corresponding Quantities** |
| Velocity ratio: $\left(\frac{V}{V_{max}}\right)_A$ | Velocity ratio: $\left(\frac{V}{V_{max}}\right)_w$ |
| Temperature ratio: $\frac{T}{T_o}$ | Water depth ratio: $\frac{d}{d_o}$ |
| Density ratio: $\frac{\rho}{\rho_o}$ | Water depth ratio: $\frac{d}{d_o}$ |
| Pressure ratio: $\frac{p}{p_o}$ | Square of water depth ratio: $\left(\frac{d}{d_o}\right)^2$ |
| Velocity of sound $a = \sqrt{\frac{\gamma p}{\rho}}$ | Wave velocity $c = \sqrt{gd}$ |
| Mach Number: $\frac{V_A}{a}$ | Mach Number: $\frac{V_w}{\sqrt{gd}}$ |
| Subsonic Flow | Streaming Flow |
| Supersonic Flow | Shooting Flow |
| Shock Wave | Hydraulic Jump |

SECTION 3

## Experimental Equipment

### 3.1 Water Channel

The water channel used in the investigation is one which already existed in the University of Minnesota Aerodynamic Laboratory. The channel was utilized for this study by making a few alterations in the model tow system.

The water channel is made up of the following four main components:

1) A water basin

2) A model track

3) A model carriage

4) A power and speed control unit

The water basin in this installation is an L-shaped table having a glass floor and plywood side walls (Fig. 2). The table is supported by a steel framework with adjustable legs which allow the basin floor to be properly leveled. In this investigation, only the long leg of the L is being used. It measures 4 feet wide by 12 feet long. A more detailed description of the water basin may be found in Ref. 2.

The model track or guide rails are mounted on the sides of the basin (Fig. 2). The elevation of the rails as well as the horizontal distance between them is adjustable.

The model carriage shown in Fig. 2 is made of 1" tubular steel welded together to form a rigid support for the model or models. The model support bars are long enough to accomodate two models at a wide range of length diameter ratios. The carriage is guided along a straight path by means of a small wheel mounted at each corner in the horizontal plane. These wheels are in contact with the outside edges of the guide rails, thus preventing any cross-channel movement of the model.

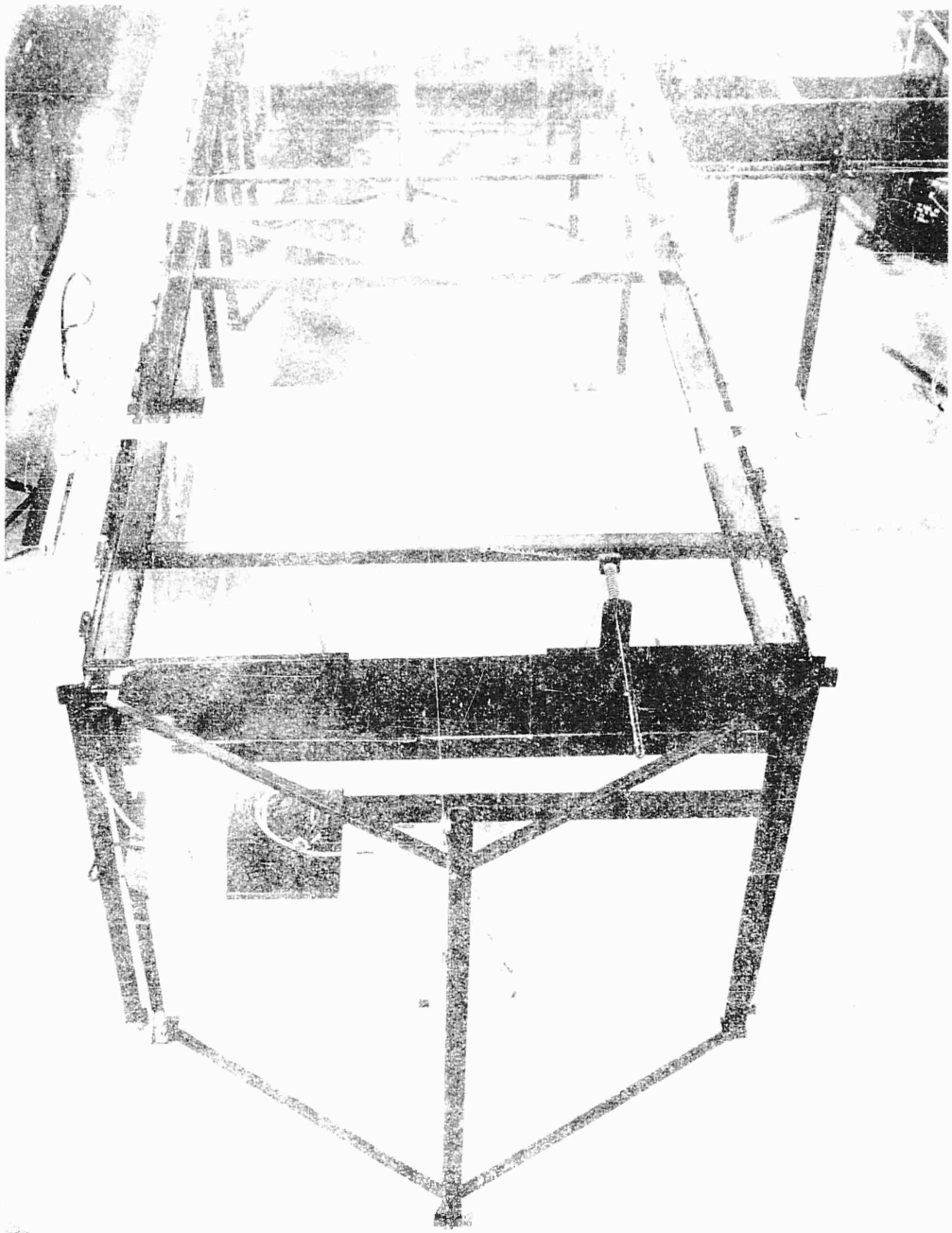

FIG. 2 [illegible] WITH CALIPER ASSEMBLY AT [illegible] PATH.

Model mounting brackets shown in Fig. 3 were designed so as to allow quick interchangeability and exact positioning of the models, and the brackets are hinged so that the models will always maintain sliding contact with the channel floor.

A General Electric "Thymotrol Drive" system is used for towing the carriage at different speeds and with a water depth of 0.25 inches.a simulated Mach Number range of 1 to 7 may be obtained. It is not suggested, however, that the analogy remains valid at high Mach Number as already indicated in Section 2.

For proper interpretation of the experiments, the speed of the carriage must be measured with considerable accuracy. For this purpose, a timing device consisting of an electric motor with constant RPM is combined with a standard automobile distributor with coil and a spark plug to produce marks upon a strip of electrically sensitive paper (Fig. 4). The spark plug is fastened to the carriage and the electrically sensitive paper to the track. Exactly three sparks are emitted per second and by measuring the distance between adjacent marks on the paper the speed can be determined with sufficient accuracy.

Since the speed of propagation of surface waves in a liquid is dependent on depth, it is necessary to measure accurately the water depth in the basin. For this purpose a small table large enough to hold a depth micrometer was built. The table is placed on the floor of the water basin and the micrometer is adjusted until the sharp point touches the water. Because of the meniscus which forms around the point the instant of contact can clearly be determined and the water depth can be measured with an accuracy in the order of $\pm$ 0.002 inch. Fig. 5 shows schematically this depth measuring device.

For pictures taken from a fixed point a photo platform is used,

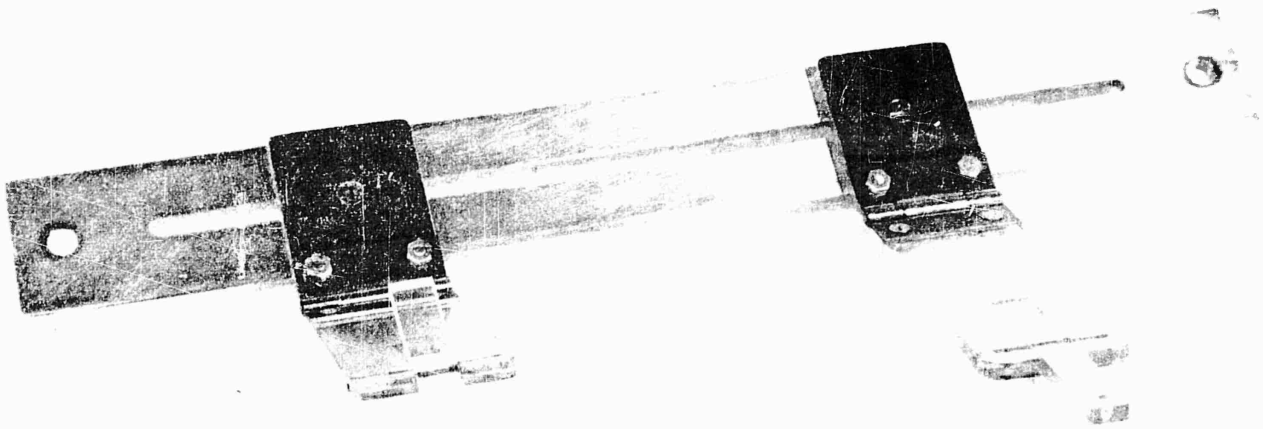

FIG. 3 ADJUSTABLE MODEL MOUNTING BRACKET FOR WATER ANALOGY STUDIES.

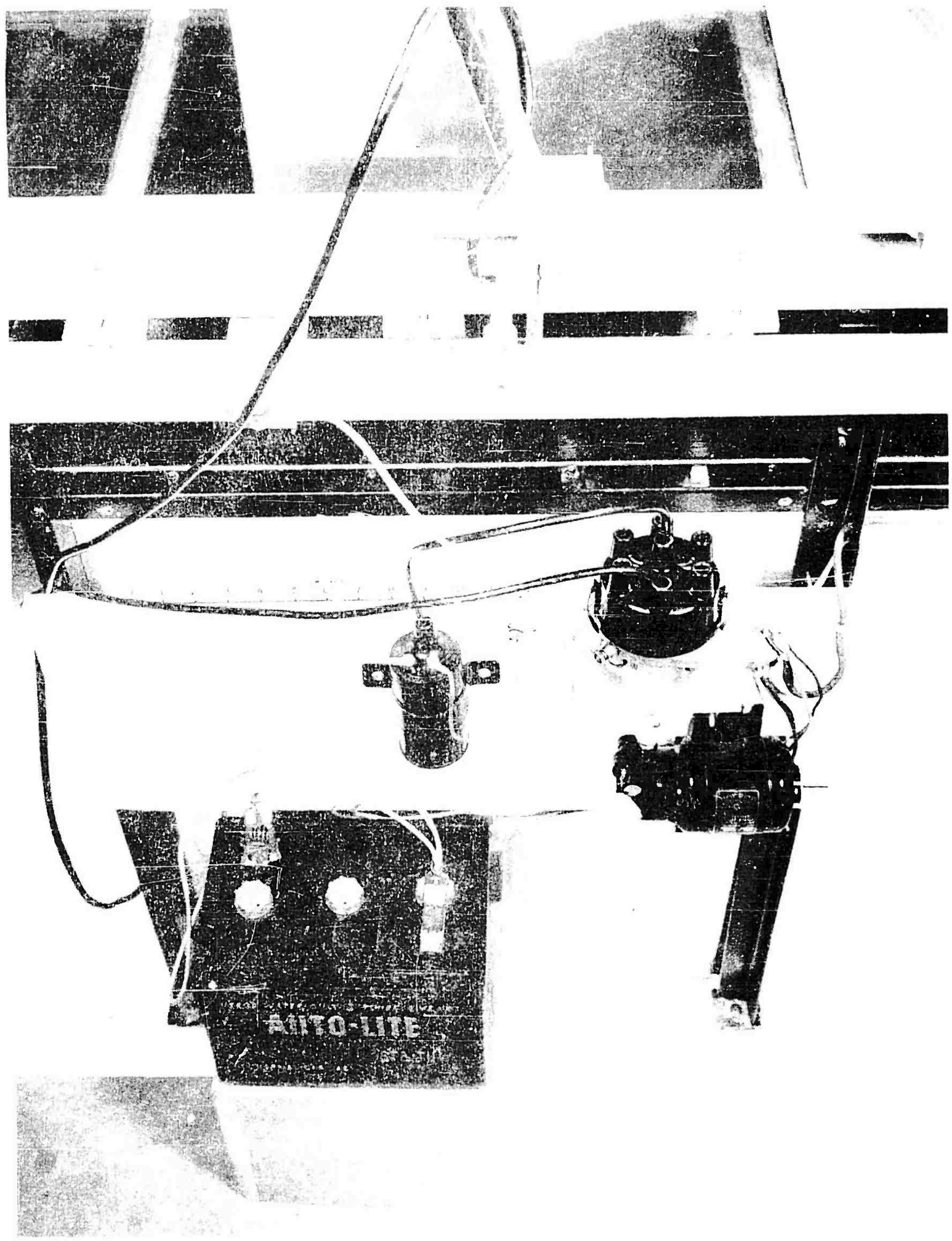


FIG. 4 ARRANGEMENT FOR MEASURING THE CARRIAGE VELOCITY.

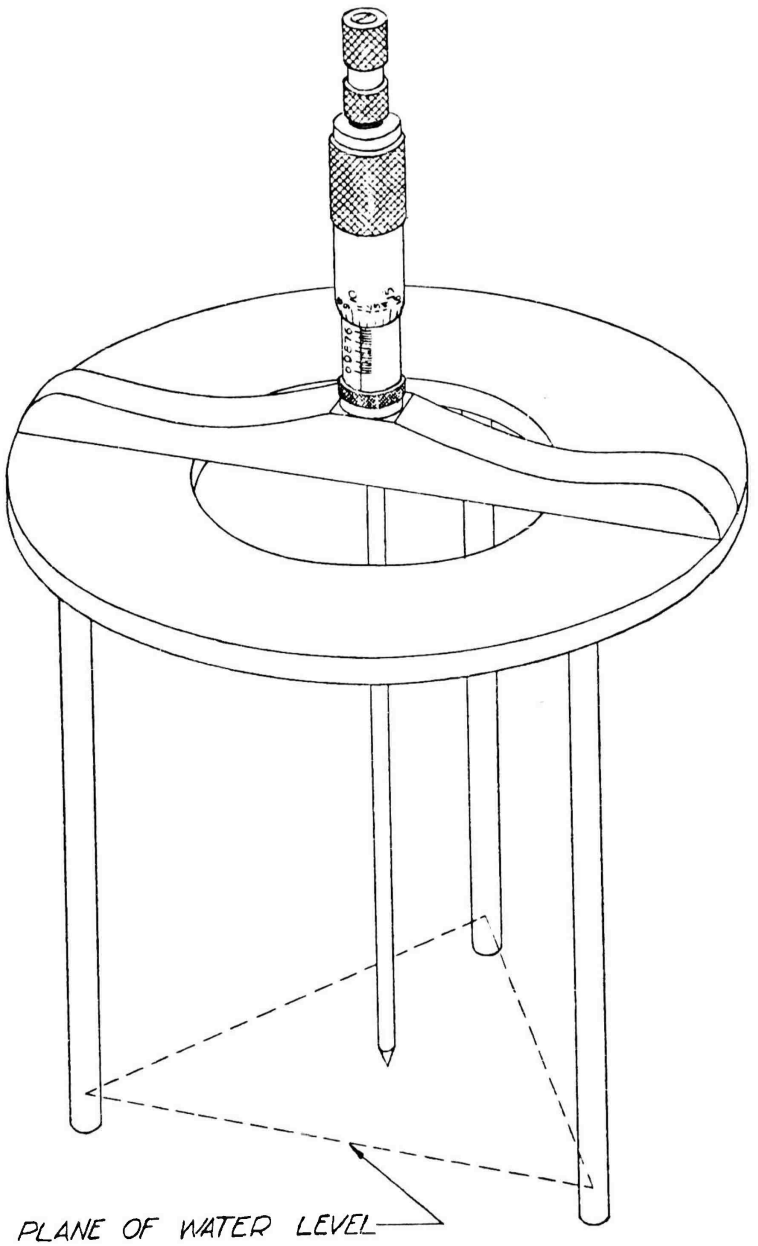


FIG. 5 - WATER DEPTH MEASURING DEVICE

which is shown in Fig. 6a. For studies of subsonic flow phenomena, it is sometimes desirable to photograph the water motion with a camera moving with the model. For this purpose a support is provided which allows mounting the camera on the carriage. This arrangement is shown in Fig. 6b.

3.2 Models

In view of the objective of this study the following bodies were considered.

Primary Bodies

1) Cylinder, tangent ogival nose, blunt tail, L/D = 4.5

2) Cylinder, blunt ends, L/D = 3

3) Ellipsoid, a/b = 2

4) Cylinder, tangent ogival nose, converging cone tail, L/D = 5.34

5) Sphere

Secondary Bodies

5) Sphere

6) Hollow Hemisphere

7) Truncated Cone, 45° half angle, t/D = .15

8) Flat Plate, t/D = .10

9) Cone, 30° half angle, L/D = .866

10) Cone, 45° half angle, L/D = .50

All primary and secondary bodies are symmetrical about the longitudinal axis (flow direction). However, for the water surface analogy experiments, only two dimensional shapes can be represented. It is known that the wave pattern for some axi-symmetric bodies and their corresponding two-dimensional representation are qualitatively similar as, for example, the wave patterns for cones and wedges.

The models tested in the water channel were suitable two-dimensional representations of the primary and secondary shapes listed above. These

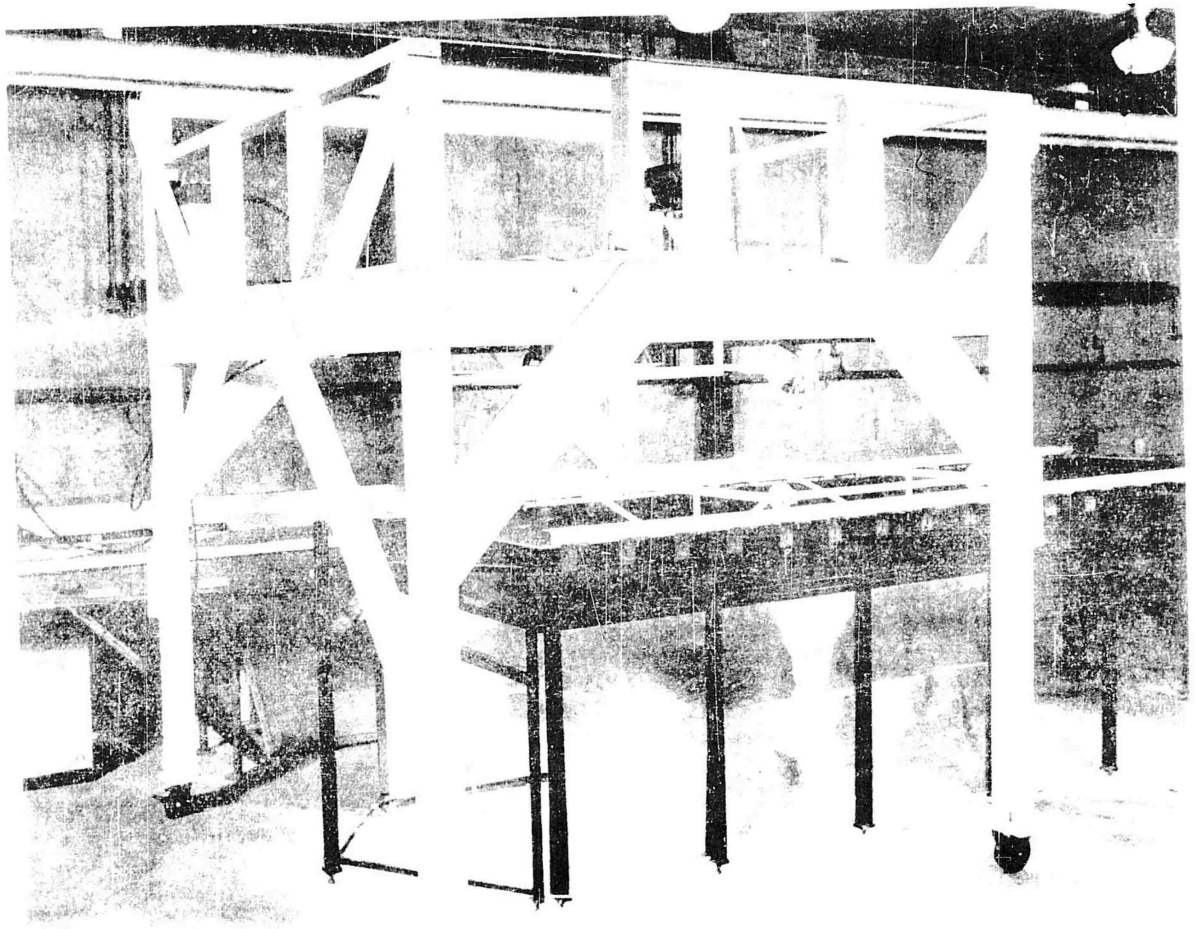

FIG. 6-a MOBILE PHOTOGRAPHIC PLATFORM IN OPERATIONAL POSITION.

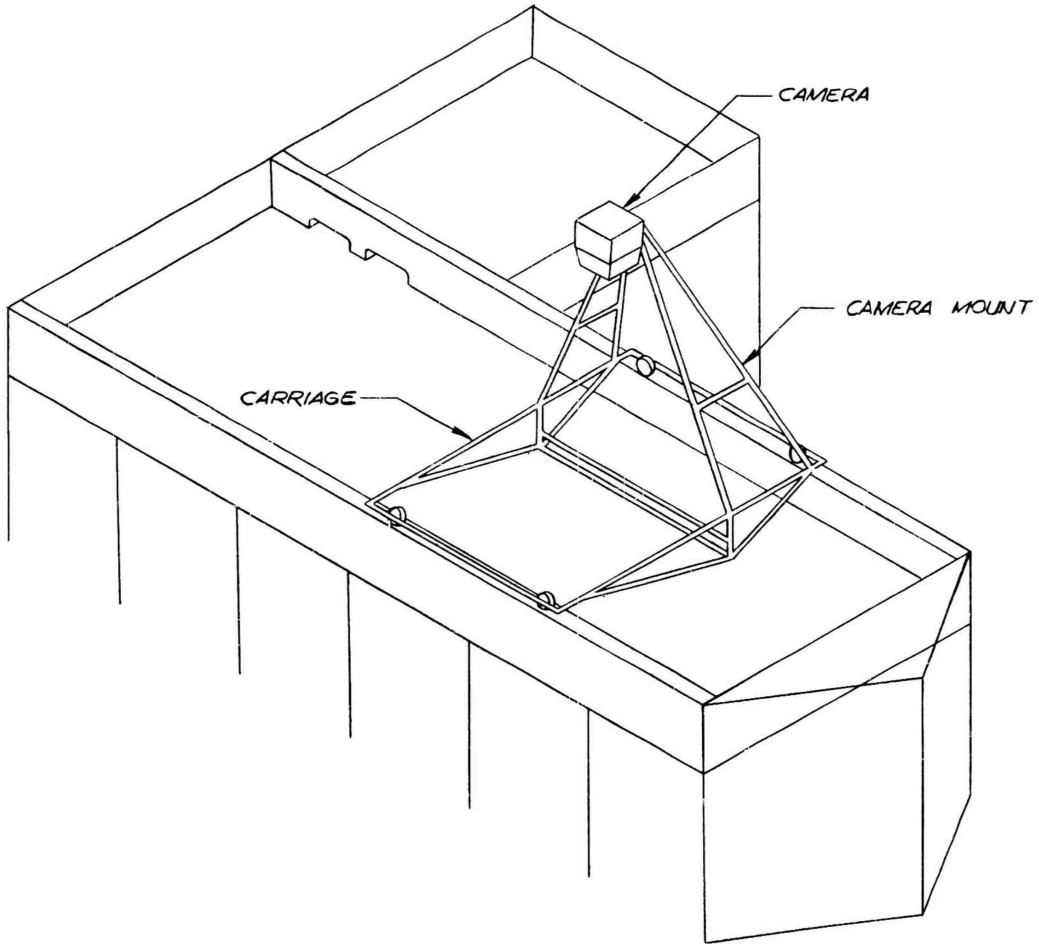


FIG. 6-b PICTORIAL OF FACILITY WITH MOVING CAMERA

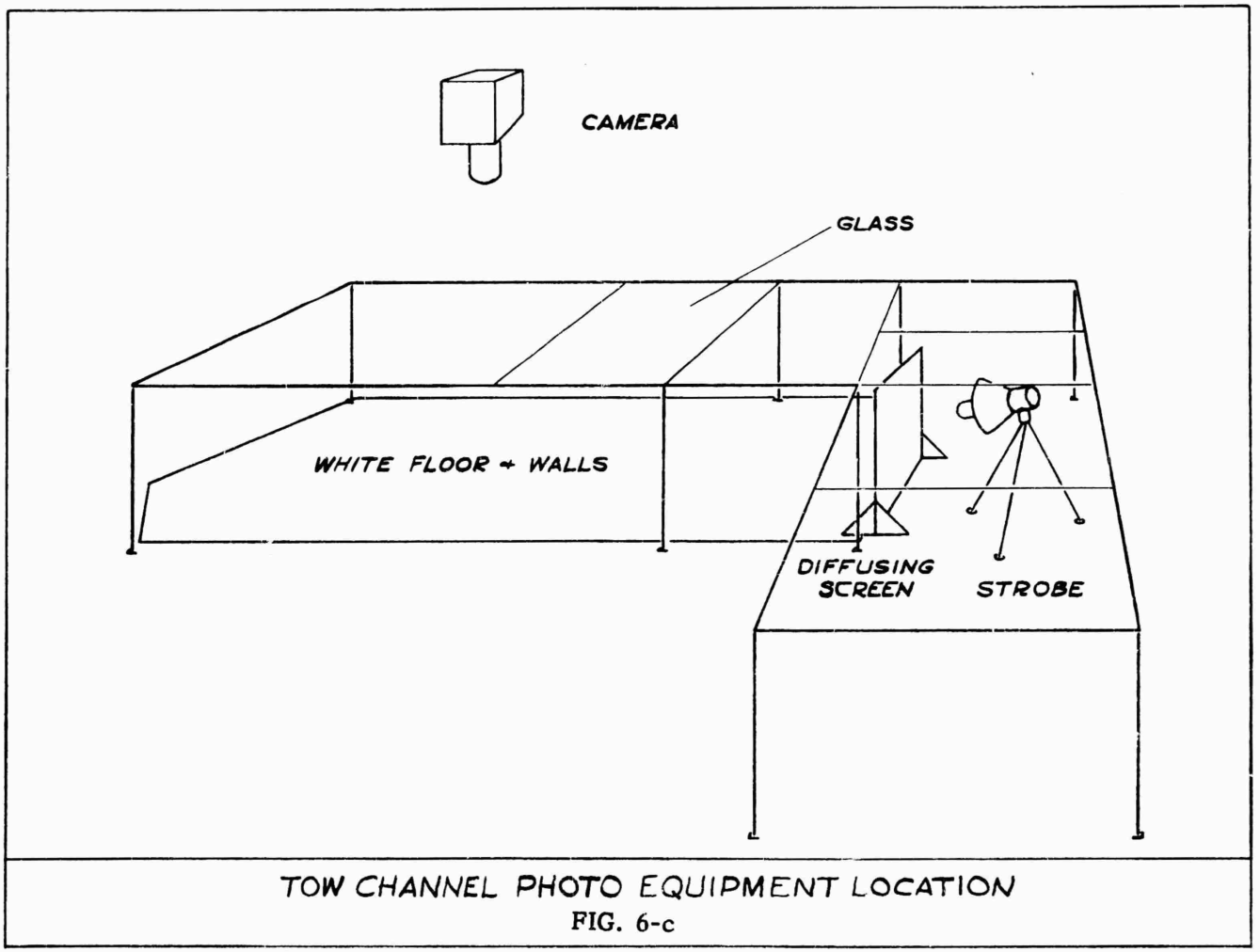


TOW CHANNEL PHOTO EQUIPMENT LOCATION

FIG. 6-c

two-dimensional models were made of plexiglass. They are shown in Fig. 7a, and their dimensions are given in Fig. 7b. In the series of tests reported here, the diameter of the secondary body is twice as large as that of the primary body.

Two additional models were used in the investigation (Fig. 7c). They were:

a) Double Wedge, $10^{o}$ half angle

b) Cluster of three hollow hemispheres

The double wedge was used for an experimental determination of the Mach Number in the wake of the primary bodies. The shock wave angle generated by the double wedge could be measured and compared with previously recorded data.

The hollow hemisphere cluster was added to the test program as requested by the Procuring Agency. This model was towed behind each primary body. It was realized, however, that this model was not an adequate representation of a parachute cluster since a parachute cluster does not have axial symmetry and is essentially a three-dimensional configuration which cannot be adequately represented by a two-dimensional body. The tests of the cluster are not included in this report.

3.3 Photographic Equipment

The Photographic Equipment consisted of a 4" x 5" portrait camera, and a light source. The lens used is a 6 inch, f/6.8 "Golden Dagor" with a Synchro Compur shutter capable of speeds to 1/500 sec. The shutter is equipped with a solenoid, actuated by a switch which is located on the water tow basin and tripped as the carriage passes through the test area. Film used is Kodak Contrast Process Panchromatic which shows up very well the highlights and shadows of the water surface. Exposure is f/19 and 1/500 of a sec.

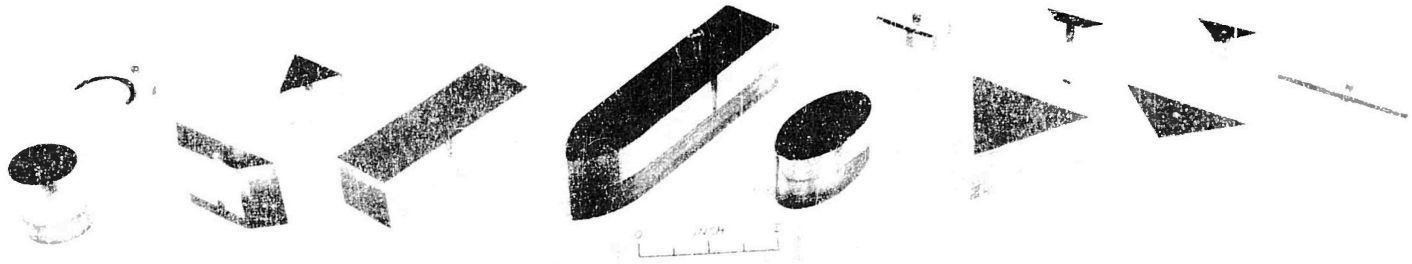

FIG. 7-a WATER TOW MODELS

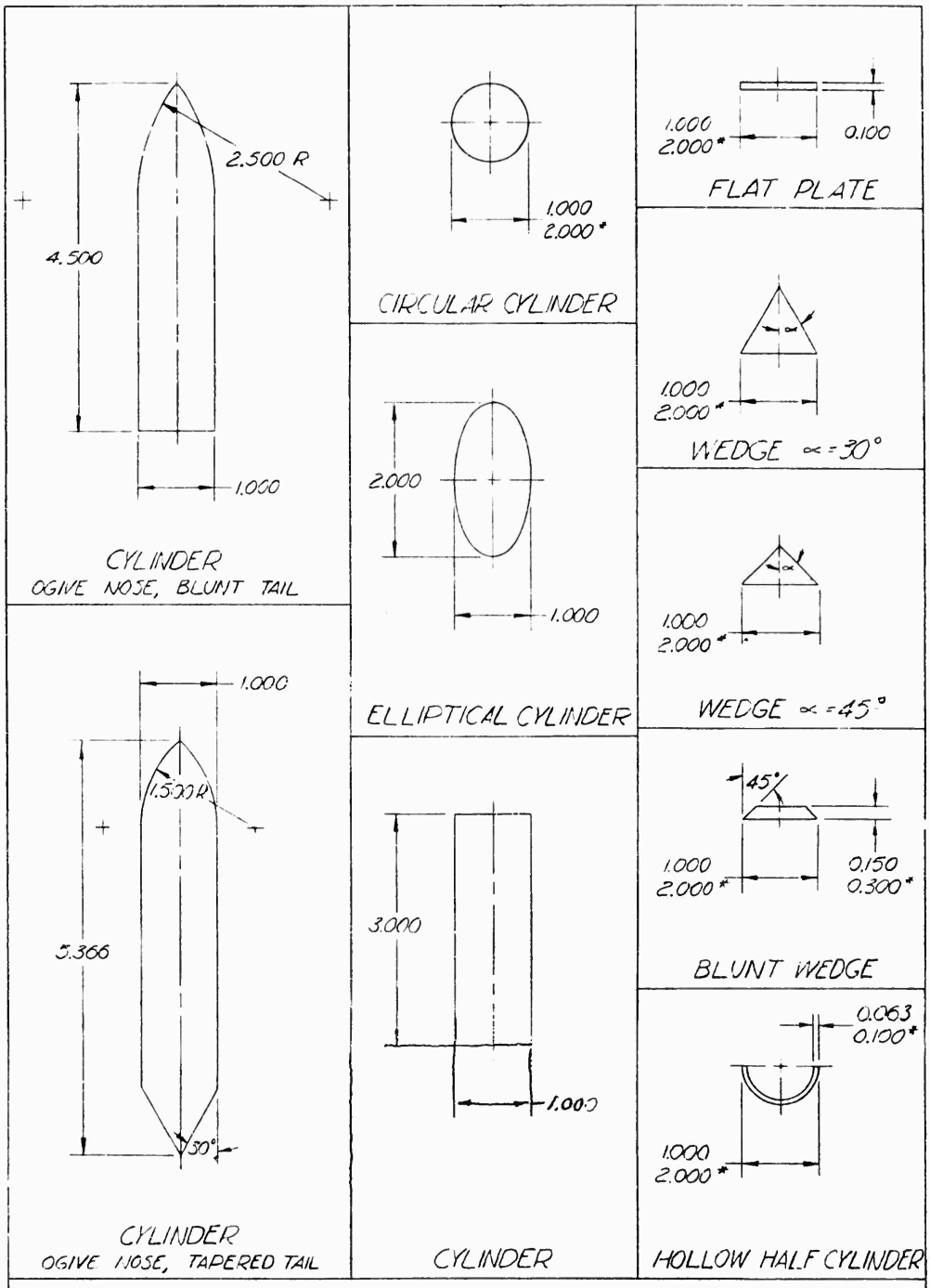


FIG. 7-6 - WATER TOW MODELS

*DIMENSION OF SECOND SET OF SECONDARY MODELS

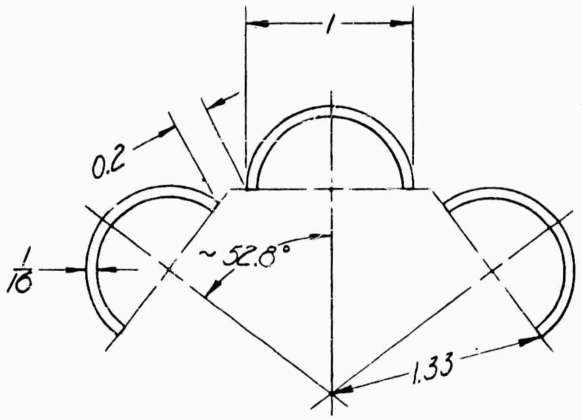


HOLLOW HALF CYLINDER CLUSTER

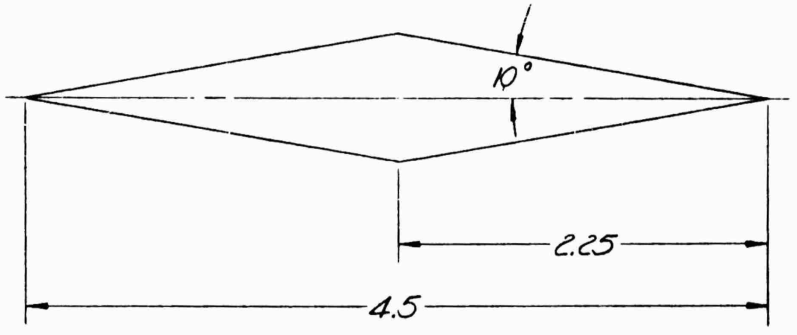


DOUBLE WEDGE (10° HALF ANGLE)

FIG. 7c-ADDITIONAL WATER TOW MODELS

A 1000 watt-sec strobe light is used as the light source for photographing the wave forms. The strobe light is placed below the water basin and downstream of the test section. Figure 6c (Page 24) shows achematically the photo set-up.

SECTION 4

## Experimental Procedure

In order to conduct tests in the water channel it is first necessary to determine the related speed of the model in the water in order to simulate the assumed speed in the analogous gas.

From theory we assume that

$$c = \sqrt{gd} \tag{4.1}$$

for a water depth of 1/4" we have:

$$c = 0.82 \text{ fps}$$

To simulate M = 2

$$V_w = Mc$$

and with c from above

$$V_w = 1.64 \text{ fps}$$

Thus, a speed of 1.64 fps in 1/4" water will simulate M = 2 in the analogous gas.

After determining the proper speed for the model, the corresponding distance between adjacent marks on the electrically sensitive tape is computed as follows:

$$X = \frac{Mc}{K} \tag{4.2}$$

where M = Mach Number to be simulated

c = speed of propagation of surface waves

K = number of sparks emitted per sec

X = distance between marks in inches

For M = 2, c = 0.82 fps and K = 3 we obtain

$$X = 6.56 \text{ in.}$$

For good distinction of models and wave patterns the upper surface of the models was painted red.

All of the models and combinations were tested at a speed which is analogous to M = 2 in a hypothetical gas where $\gamma = 2$. In cases where combinations of primary and secondary models were tested, the secondary model was arranged at length/diameter (L/D) ratios of 2, 4, 6, 8, and 10.

In order to determine at what L/D ratio the Mach Number in the wake had returned to free stream conditions, a 10° half-angle double wedge was used. This was towed at the various L/D values behind the primary models and the attached shock wave of the wedge was measured for the Mach Number determination. (For the water analogy, values of Mach Number as a function of oblique shock wave angle may be found in Reference 6). The results of these tests are given in Section 5 of this report.

SECTION 5

## 5.0 Results and Discussion

As explained before, the present investigation was conducted mainly for the purpose of obtaining qualitative information to be used as a guide for the wind tunnel studies.

A photographic record was made of the wave formation for all possible combinations of 5 primary and 6 secondary bodies with diameter ratio $\frac{D \text{ secondary}}{D \text{ primary}} = 2$ and a range of L/D ratios of 2 and 10.

The photographing of water surface waves over a large area proved to be a rather difficult task. In an effort to obtain pictures with good contrast, various methods of lighting the water surface were tried. Lighting by reflection gave fairly good results but, when the light was placed above the channel, there were many undesirable shadows from the model carriage, model and model brackets. The system finally adopted was lighting by refraction. A strobe light was placed on the floor beneath the channel and the light was then reflected off the white painted floor through the glass bottom of the channel. This system gave very satisfactory results when a high contrast film (Kodak Contrast Process Panchromatic) was used.

## 5.1 Tests on Single Models - Comparison Between Theory and Experiment

First, the wave pattern of all the body shapes when towed alone in a uniform stream was obtained and this pattern was compared with the theoretical wave shapes for these bodies in free stream as calculated by the theory of Reference 3. This theory provides an approximate method for predicting the form and location of detached shock waves ahead of plane and axially symmetric bodies. Several investigators have found that results obtained with this method were in fair agreement with experimental results of wind tunnel tests.

Our calculations using the method of Reference 3 invariably place the shock wave much closer to the body than indicated by the water tow experiments.

Figures 8 through 18 are photographs of experiments at a simulated Mach 2. It is apparent that, in almost all cases, the form of the experimental wave is nearly the same as that predicted by the theory but the stand-off distance of the experimentally obtained shock wave is much greater. The same discrepancy was noted in Reference 7. It has been shown by other investigators that a contributing factor to the lack of agreement in predicting the location of bow shock waves is the fact that the flow conditions may not have become steady. The distance travelled by the model in the water tank is about 8 feet which, in our case, corresponds to about 10,000 feet in air. The error in location of the shock wave seems to differ by a constant factor for all models tested, and was found to be about 1.70. Reference 7 showed similar results. The discrepancy may be due to the factor previously mentioned, i.e., the possibility of unsteady flow conditions. Other factors, which may have a significant influence on the flow pattern, are water depth, model size and surface tension of the liquid, and further studies would be necessary to determine the effects of each one of these factors on the wave form and location. For the purpose of this study, the discrepancy in the stand-off distances may not be too significant.

In addition to the general configuration of the detached shock waves, Figs. 8 through 18 also illustrate the wave formation behind the different primary and secondary bodies when towed alone. The tail wave is significant since it affects the flow characteristics on the secondary body. The figures show all the main features of supersonic flow and compare well with Figure 19 which is a schematic drawing illustrating the

FIG. 3 COMPARISON OF THEORETICAL AND EXPERIMENTAL SHOCK SHAPES AT MACH NO 1.410 ON THE OGIVE CYLINDER

FIG. 9. COMPARISON OF THEORETICAL AND EXPERIMENTAL SHOCK SHAPES ON THE CYLINDER

FIG. 16. COMPARISON OF MEASURED STEADY AIRFOIL SHAPE AT MACH NO. 1.25 WITH DESIGN SHAPE

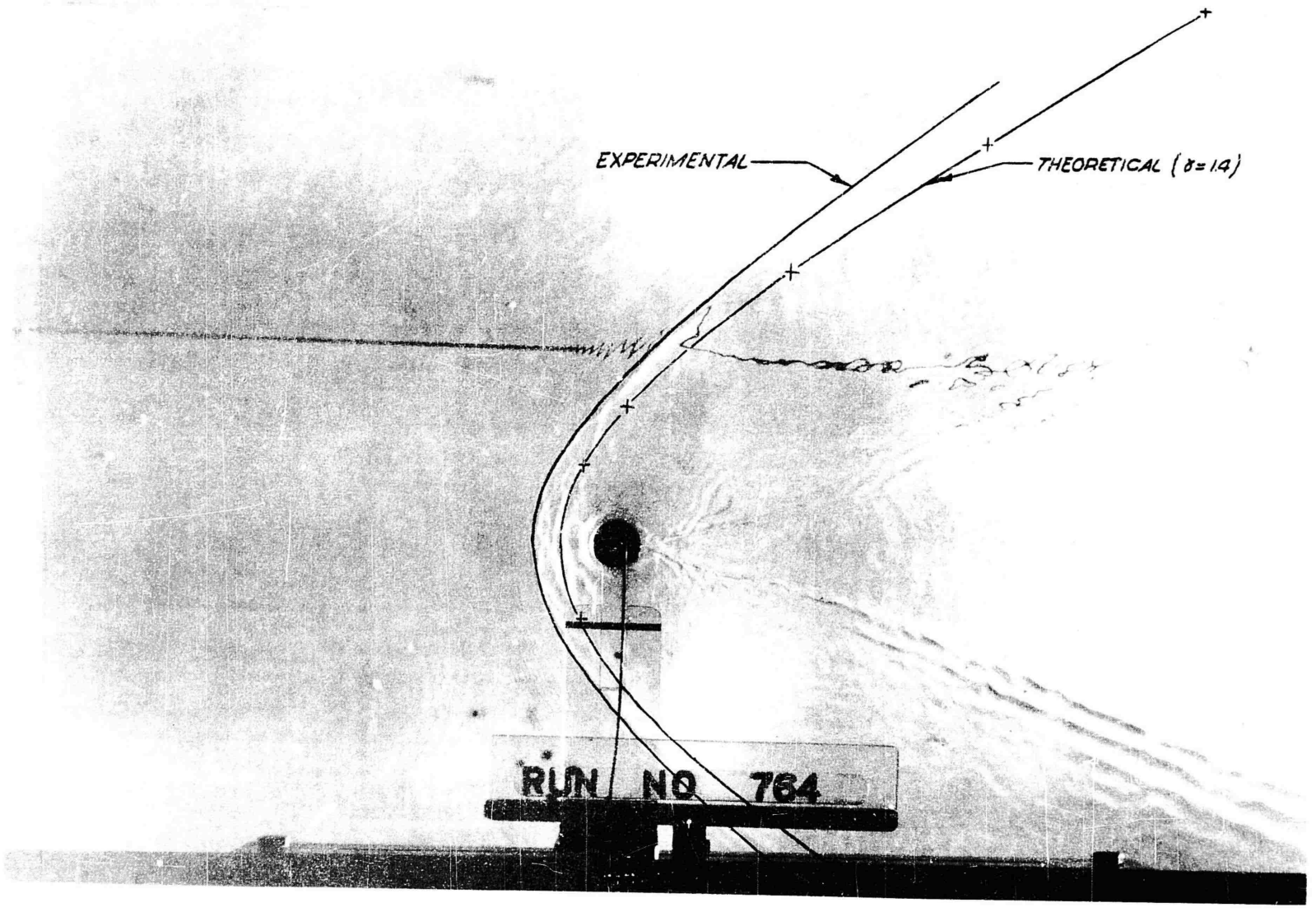


FIG. 11. COMPARISON OF THEORETICALLY DERIVED SHOCK WAVE AND THE OBSERVED SHOCK OF THE CIRCULAR CYLINDER (PRIMARY)

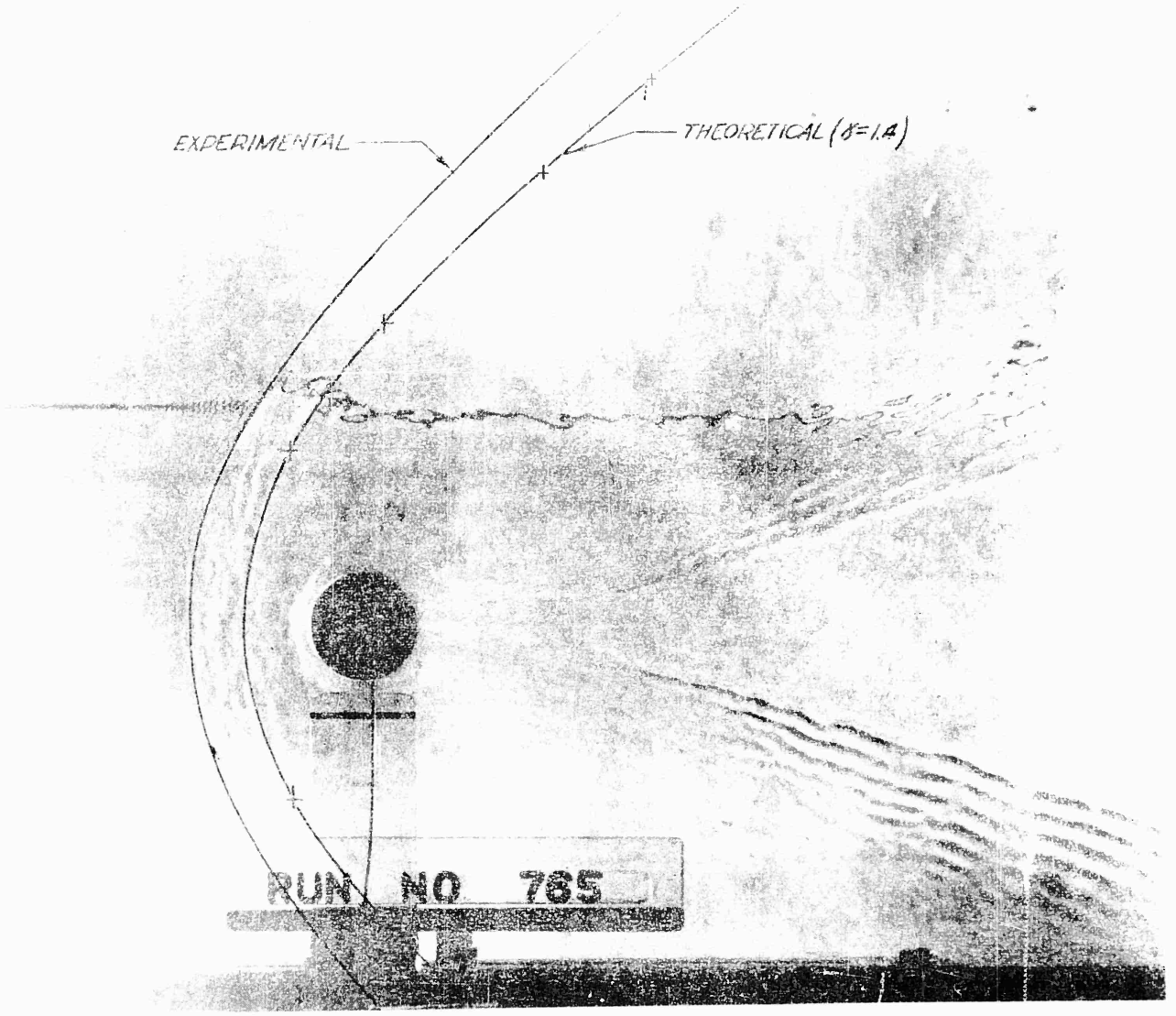


FIG. 12. COMPARISON OF THEORETICALLY DERIVED SHOCK WAVE AND THE OBSERVED SHOCK OF THE CIRCULAR CYLINDER (SECONDARY)

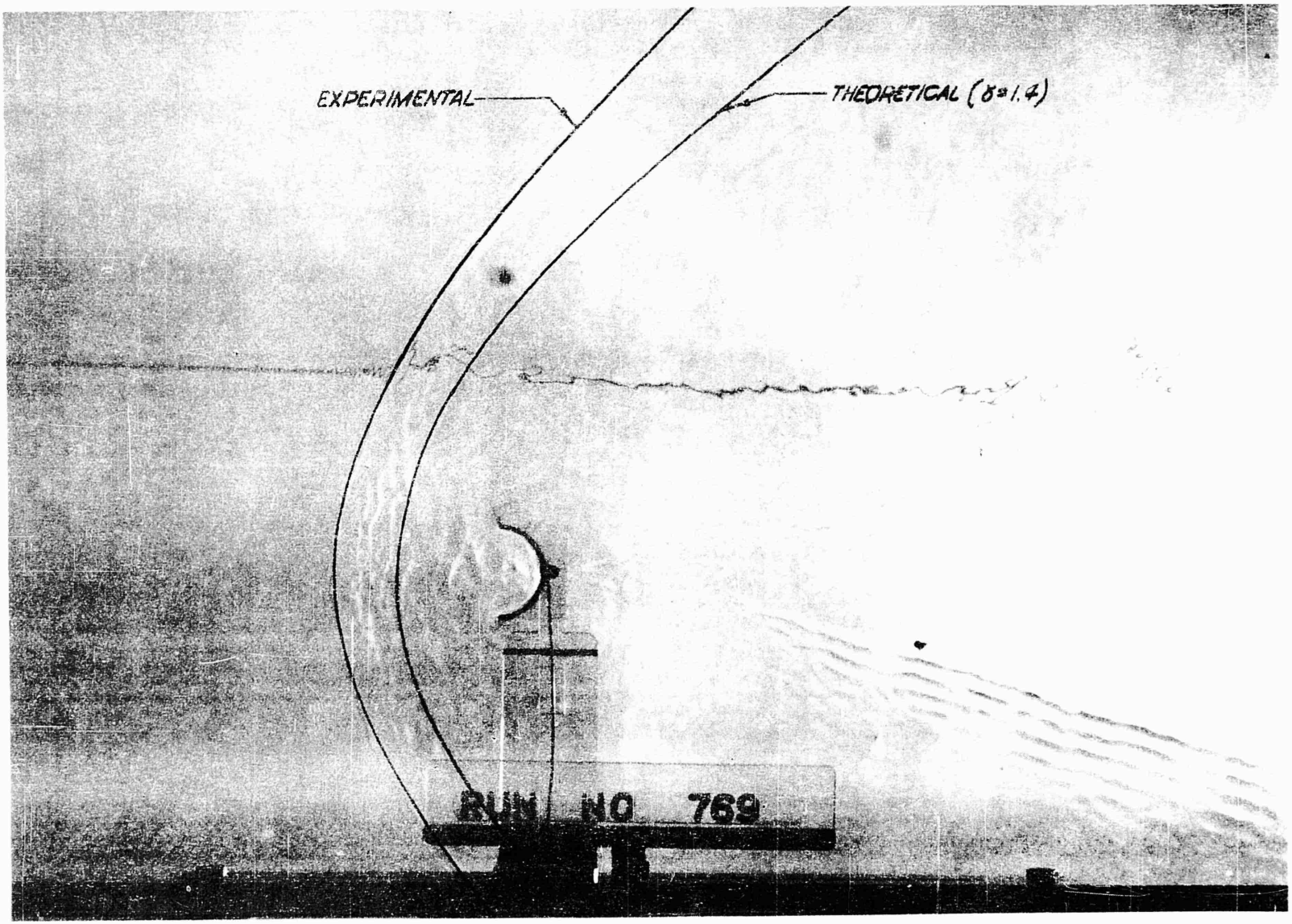


FIG. 13. COMPARISON OF THEORETICALLY DERIVED SHOCK WAVE AND THE OBSERVED SHOCK OF THE HOLLOW HALF CYLINDER

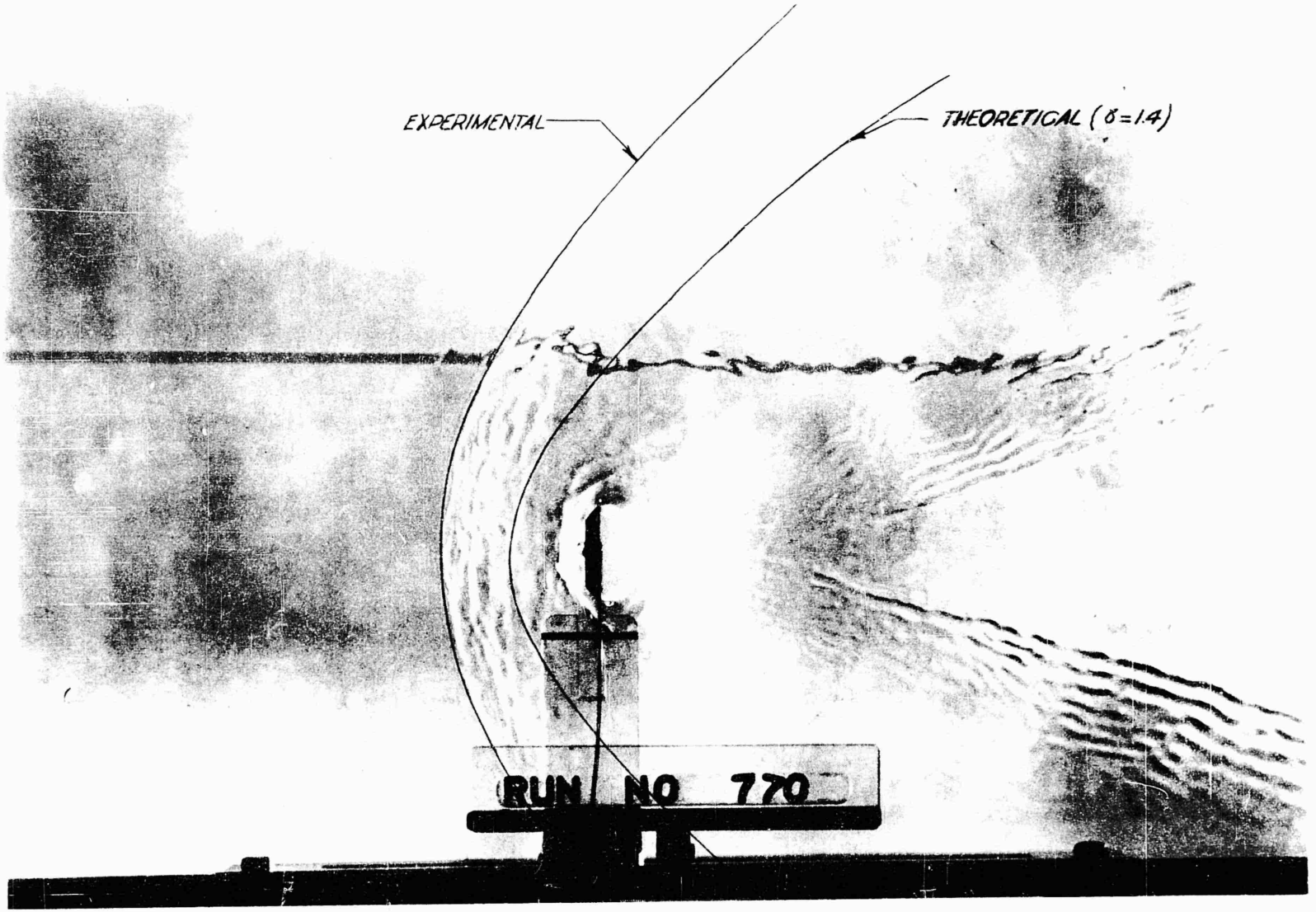


FIG. 14. COMPARISON OF THEORETICALLY DERIVED SHOCK WAVE AND THE OBSERVED SHOCK OF THE BLUNT WEDGE (MODEL FOR TRUNCATED CONE)

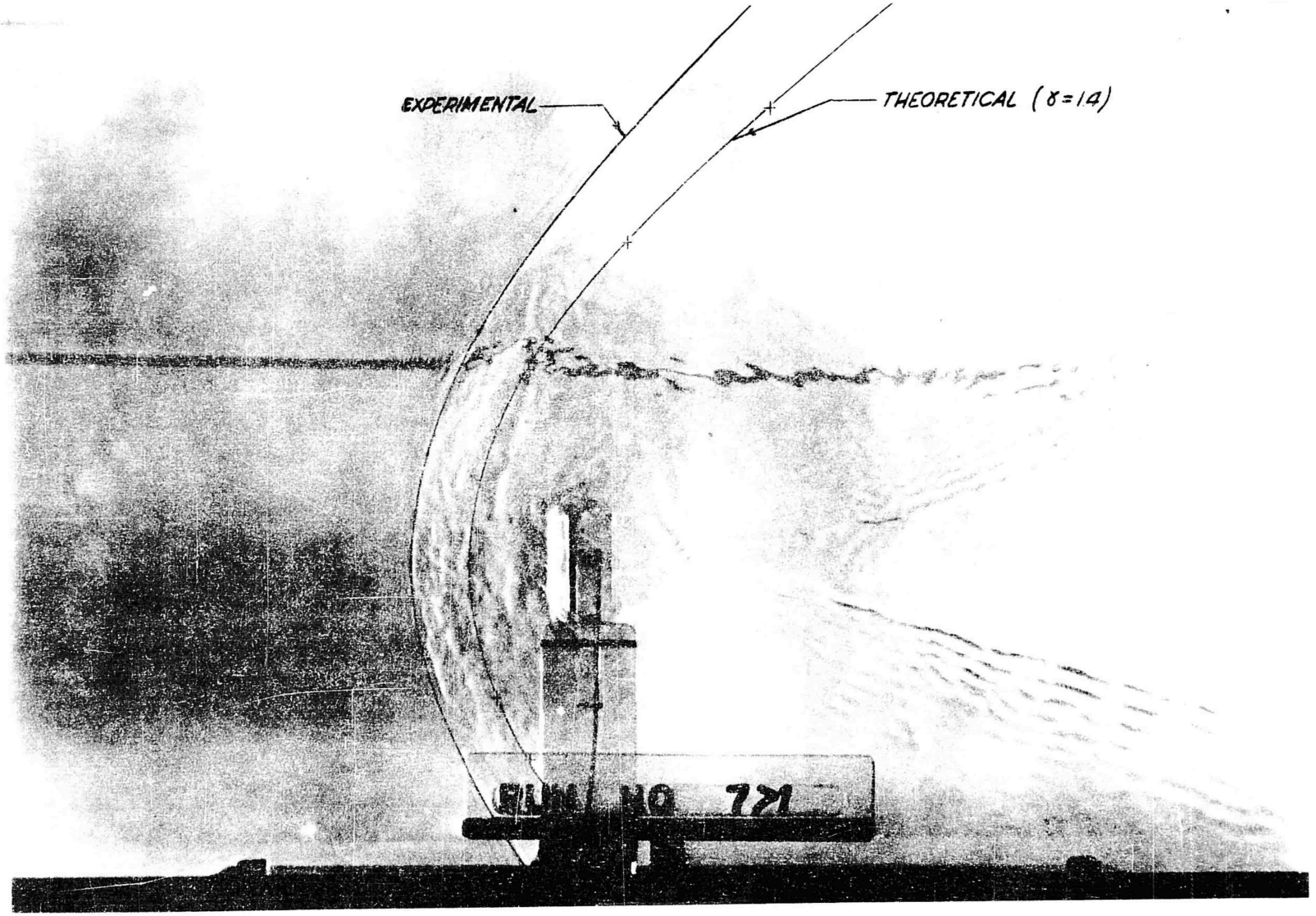


FIG. 15. COMPARISON OF THEORETICALLY DERIVED SHOCK WAVE AND THE OBSERVED SHOCK OF THE FLAT PLATE

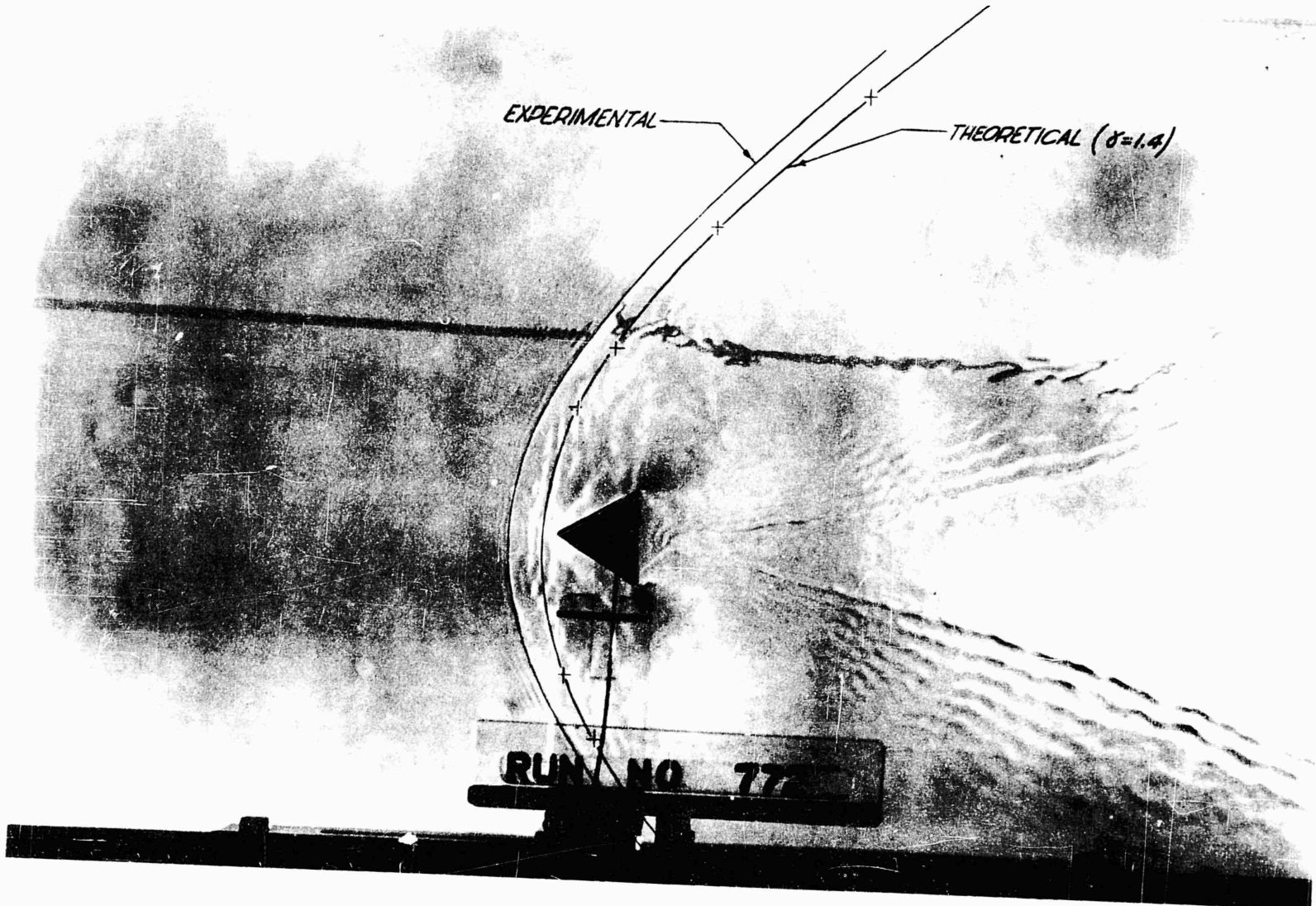


FIG. 16. COMPARISON OF THEORETICALLY DERIVED SHOCK WAVE AND THE OBSERVED SHOCK OF THE 30° HALF ANGLE WEDGE (MODEL FOR CONE)

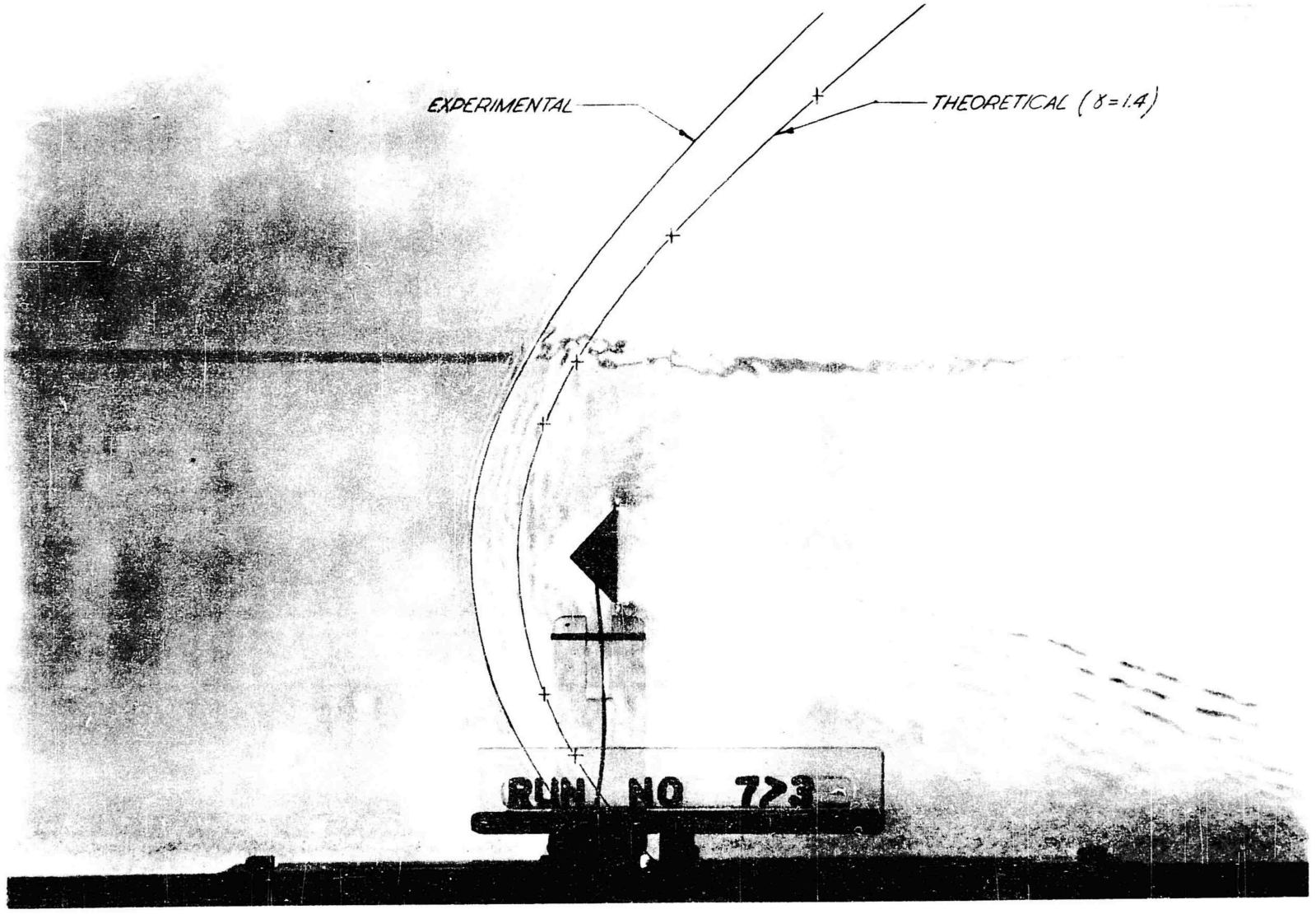


FIG. 17. COMPARISON OF THEORETICALLY DERIVED SHOCK WAVE AND THE OBSERVED SHOCK OF THE 45° HALF ANGLE WEDGE (MODEL FOR CONE)

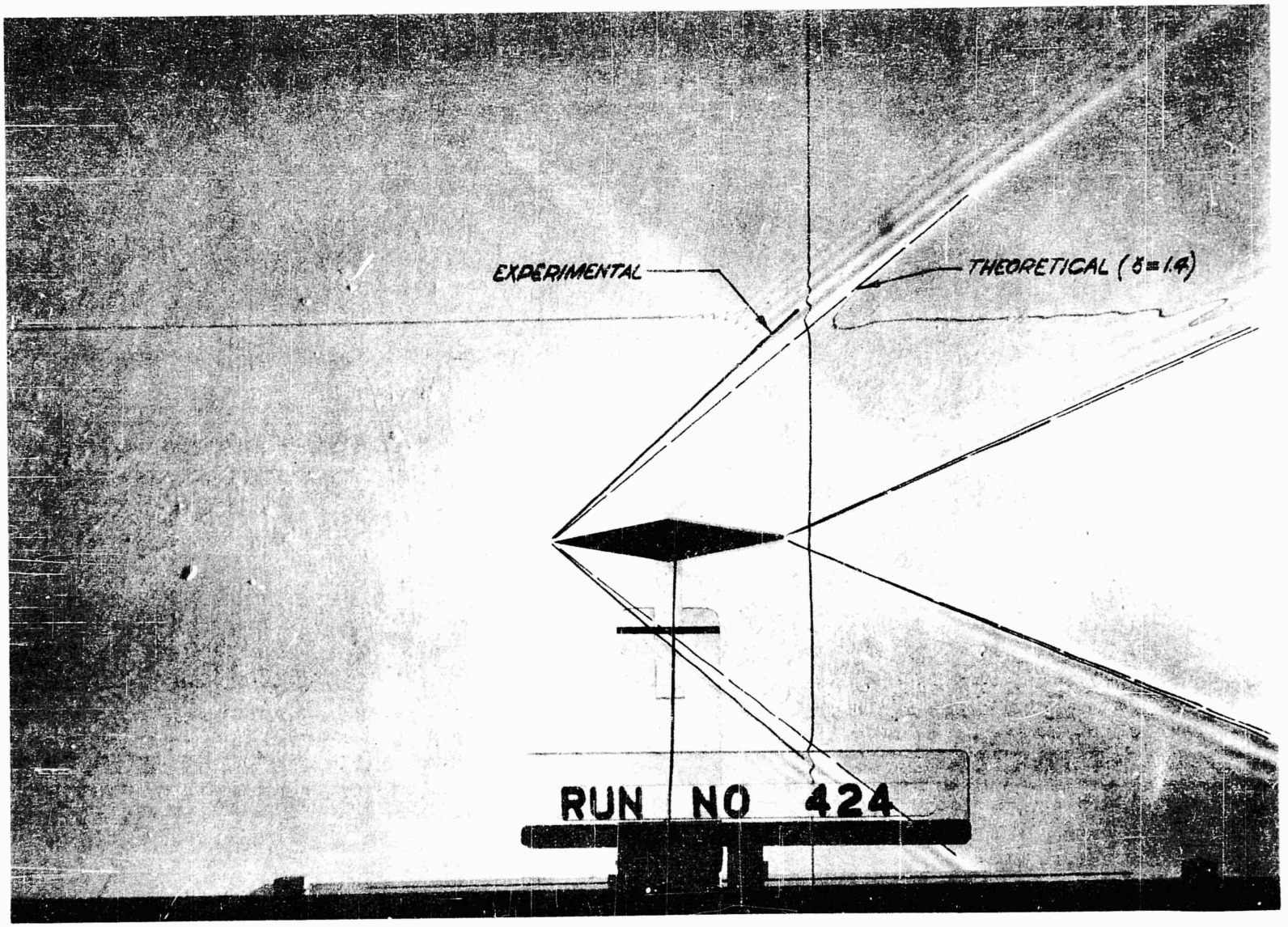


FIG. 18. COMPARISON OF THEORETICALLY DERIVED SHOCK WAVE AND THE OBSERVED SHOCK OF THE 10° HALF ANGLE DOUBLE WEDGE

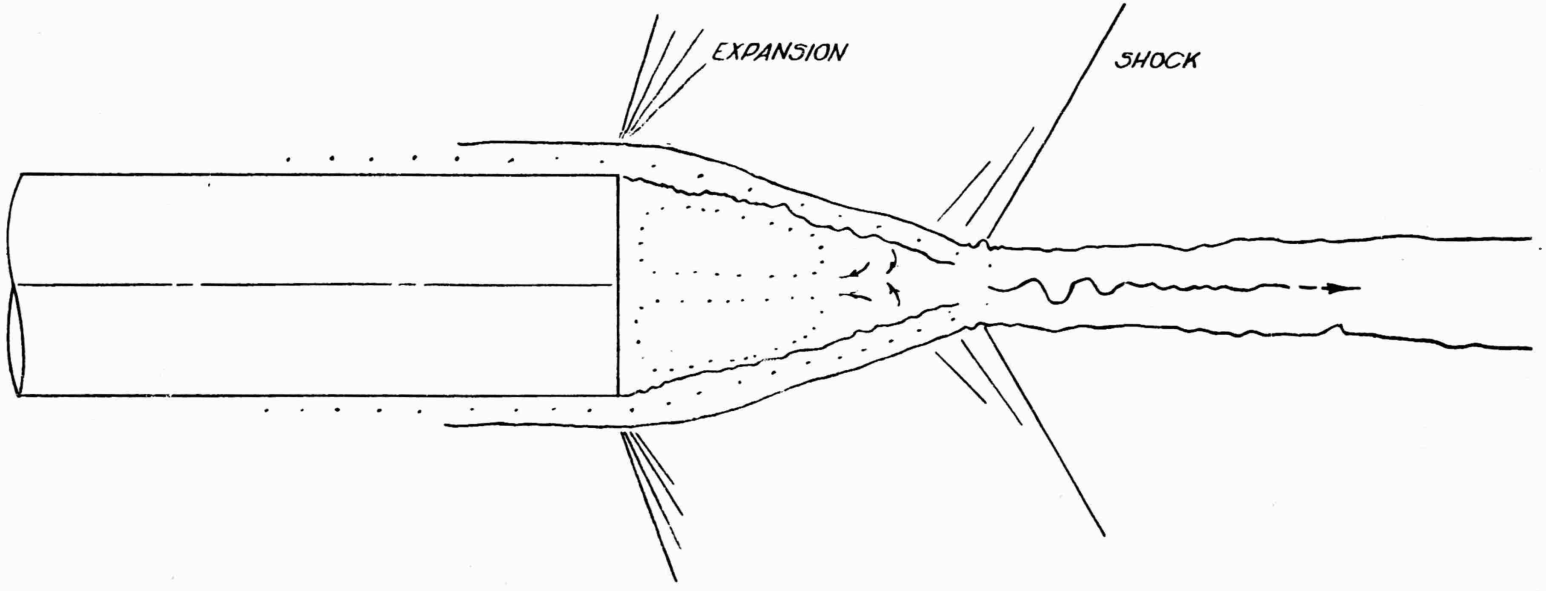


FIG. 19. BASIC FLOW PATTERN PAST THE BASE OF A THREE-DIMENSIONAL PROJECTILE OR MISSILE BODY IN SUPER-SONIC FLOW.

general nature of the flow behind a cylindrical body in supersonic flow as determined from well-established theoretical considerations and experimental tests.

It was shown in Section II that the water surface analogy assumes a hypothetical gas for which $\gamma = 2.0$. In order to show the effect of $\gamma$ on the wave form and location, calculations were made for air and for the gas with $\gamma = 2$ and the results are illustrated in Figure 11. It is apparent that the effect of $\gamma$ on the wave form and location is very slight in our case. This result was confirmed by calculations on other models.

## 5.2 Tests on Model Combinations

Having obtained the basic wave pattern for each one of the model shapes when towed alone at a simulated Mach 2 and having ascertained the relatively slight effect due to a change of $\gamma$, systematic tests were conducted on various model combinations over a range of Length/Diameter ratio L/D from 2 to 10. Comparison of the pictures taken at L/D = 8 and 10 indicated that the wave patterns were essentially the same. Therefore, the pictures for L/D = 10 are not included in this report.

### 5.2.1 Wave Formation With Ogival Nose Cylinder as Primary Body

Figures 20 through 25 show the wave patterns for the model representing combinations of an ogival nose cylinder with blunt tail as a primary body and the six secondary bodies at L/D ratios of 2, 4, 6, and 8.

It is apparent from this series of pictures that, for L/D = 2, the wave pattern, particularly the tail wave of the primary body and detached shock wave of the secondary body, is considerably different from that of the same bodies in free stream (Figs. 20A, 21A, 22A, 23A, 24A, and 25A).

At L/D = 4, the tail wave of the primary body and detached shock wave of the secondary body begin to be established for the trailing sphere (Fig. 20B) and trailing cones (Figs. 24B and 25B). However, for the more

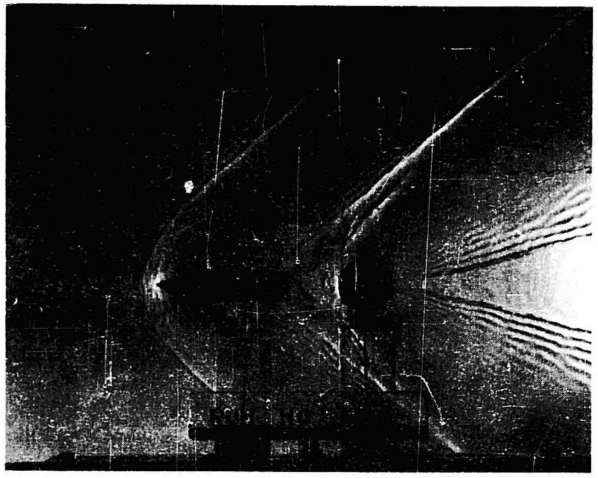

(A) L/D = 2

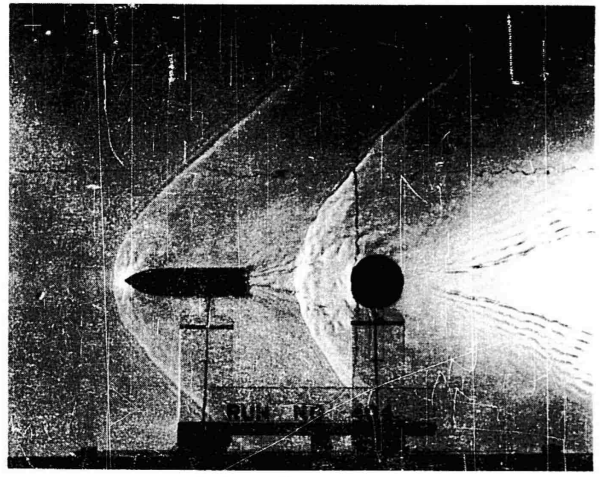

(B) L/D = 4

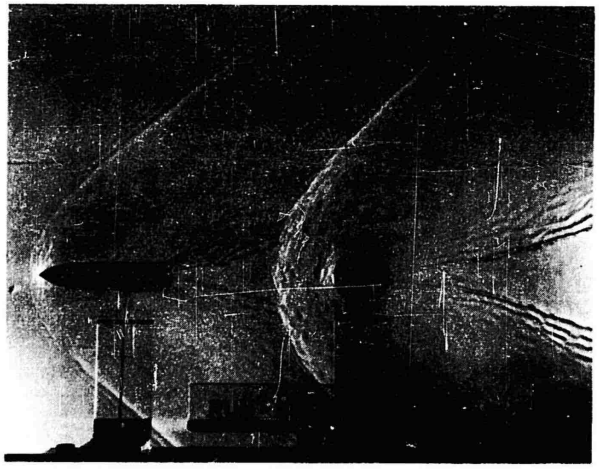

(C) L/D = 6

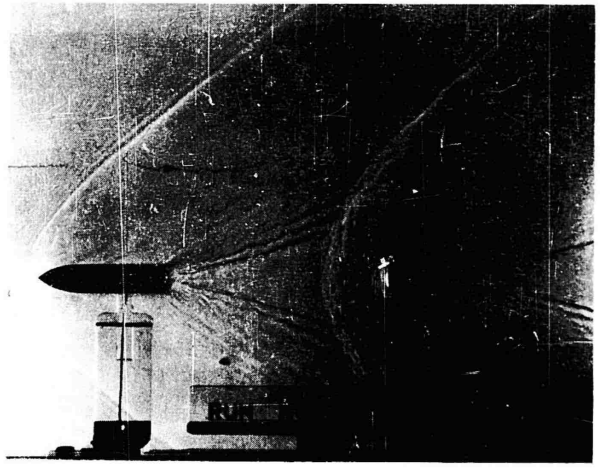

(D) L/D = 8

FIG. 20. REPRESENTATION OF OGIVAL NOSE CYLINDER WITH TRAILING SPHERE

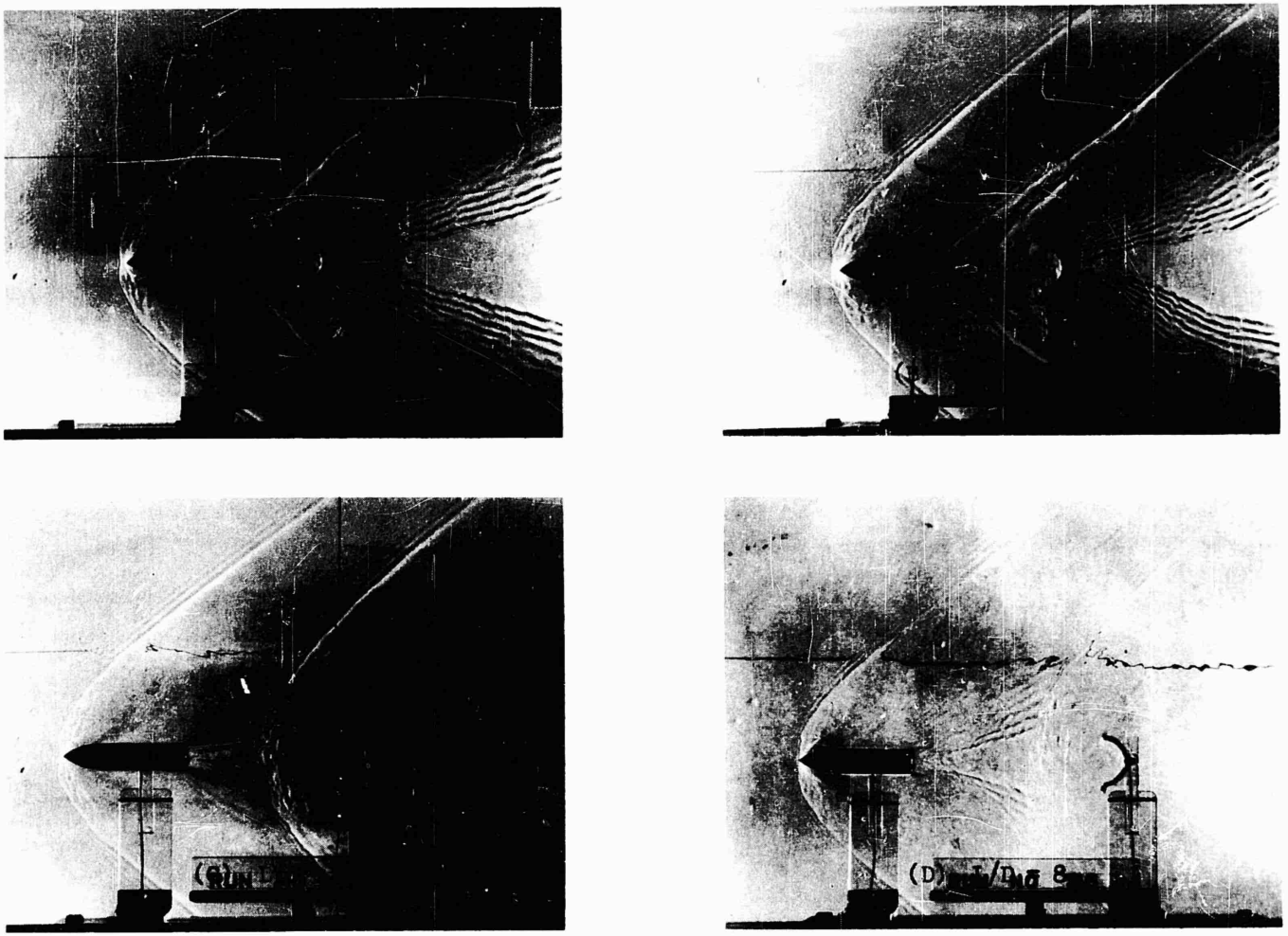

FIG. 21. REPRESENTATION OF OGIVAL NOSE CYLINDER WITH TRAILING HOLLOW HEMISPHERE

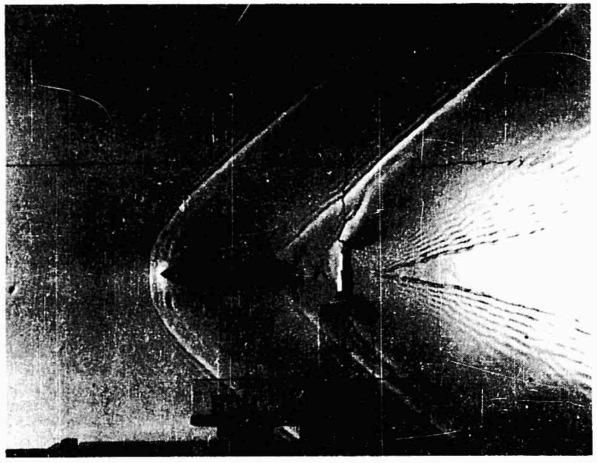

(A) L/D = 2

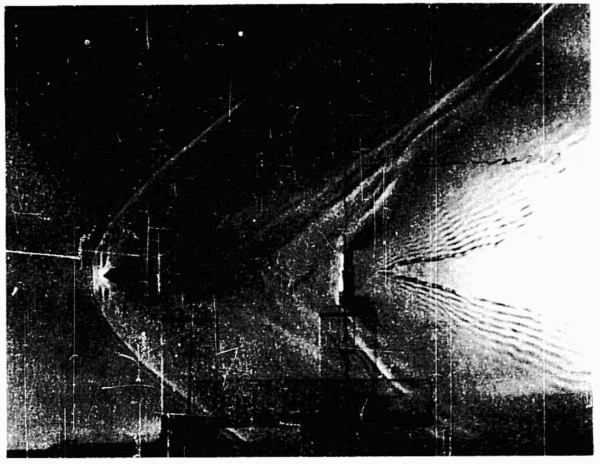

(B) L/D = 4

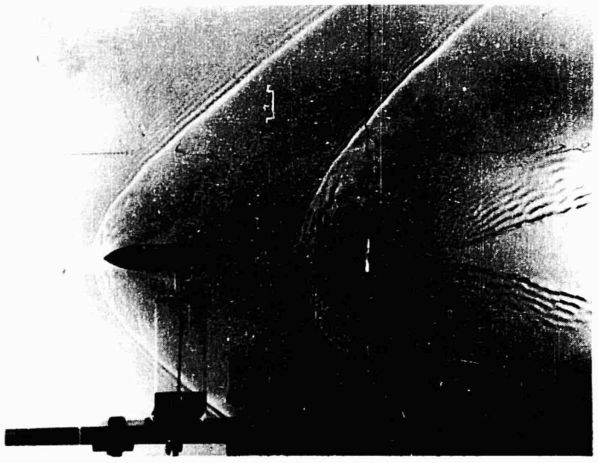

(C) L/D = 6

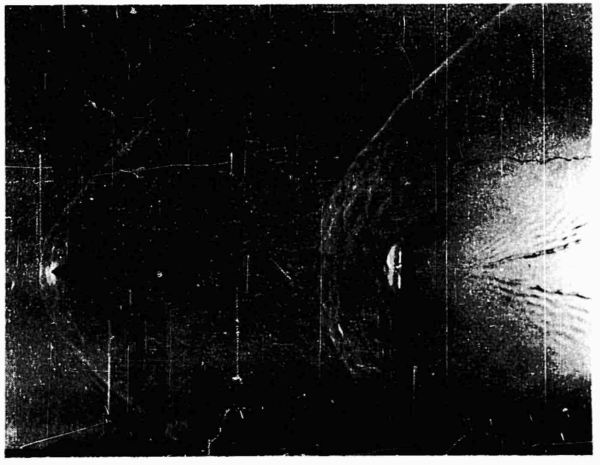

(D) L/D = 8

FIG. 22 REPRESENTATION OF OGIVAL NOSE CYLINDER WITH TRAILING TRUNCATED CONE

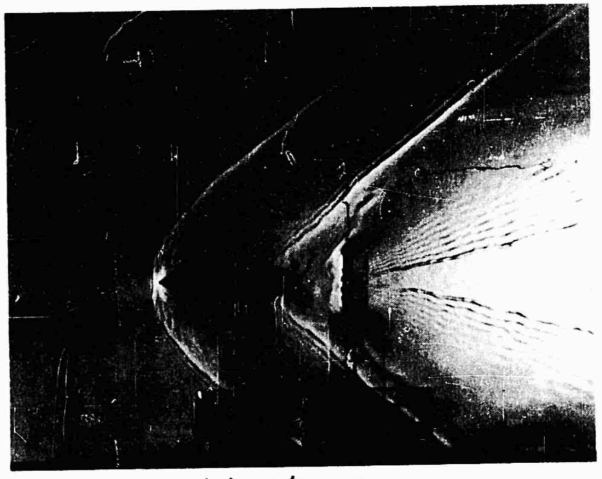

(A) L/D = 2

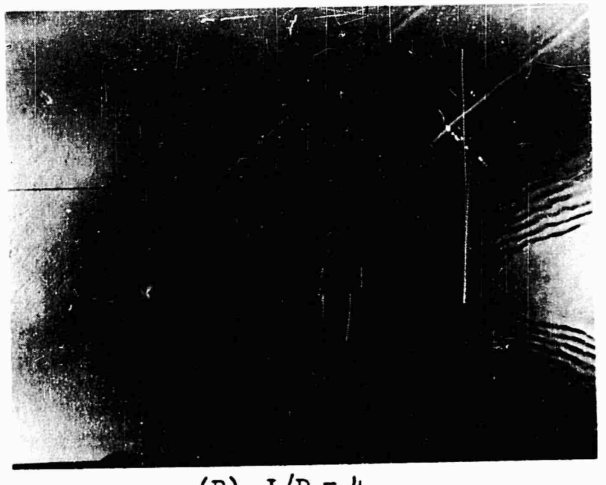

(B) L/D = 4

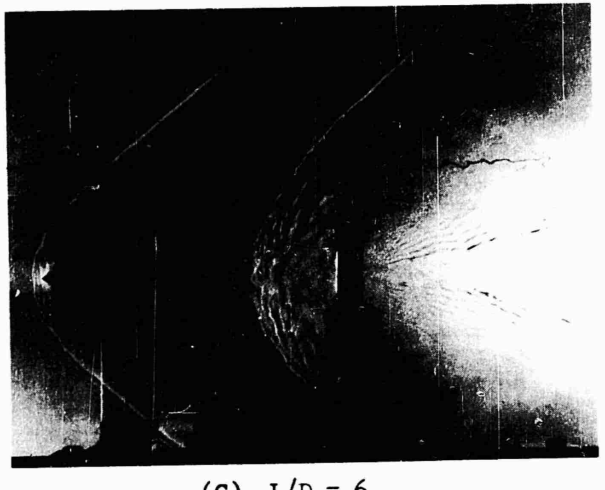

(C) L/D = 6

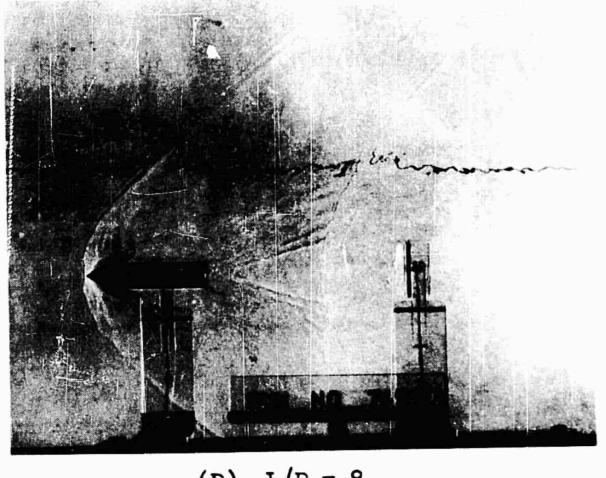

(D) L/D = 8

FIG. 23. REPRESENTATION OF OGIVAL NOSE CYLINDER WITH TRAILING FLAT PLATE

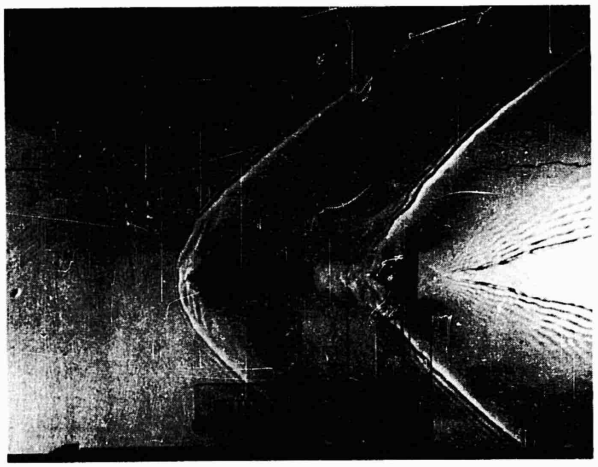

(A) L/D = 2

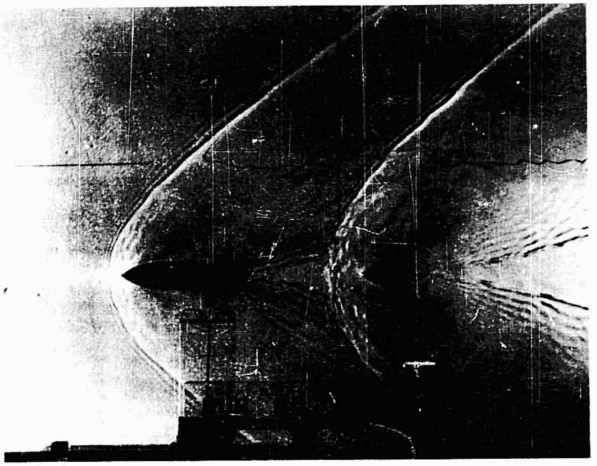

(B) L/D = 4

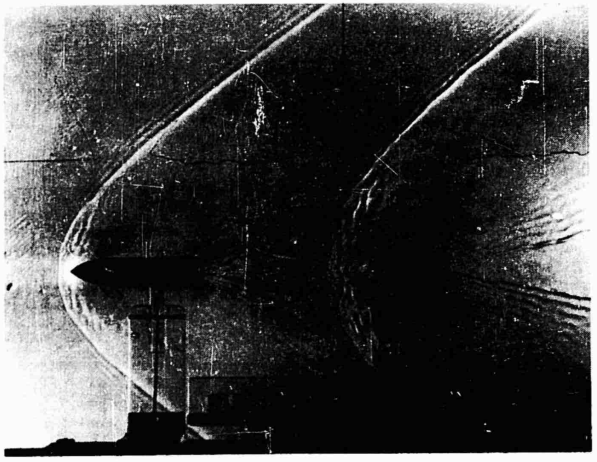

(C) L/D = 6

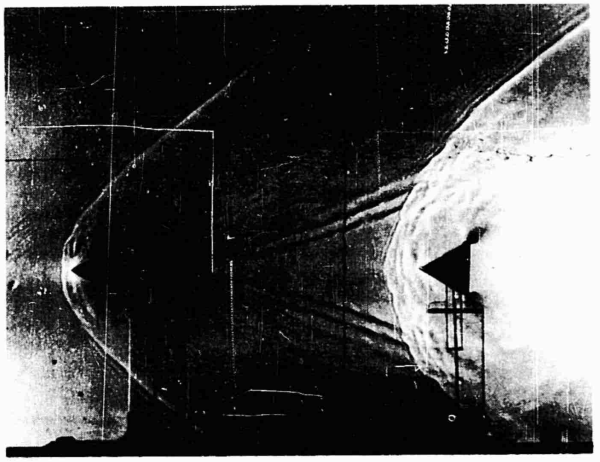

(D) L/D = 8

FIG. 24. REPRESENTATION OF OGIVAL NOSE CYLINDER WITH TRAILING CONE (30° HALF ANGLE)

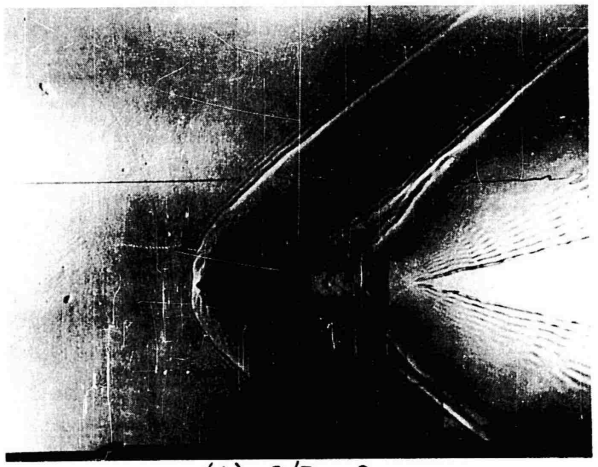

(A) L/D = 2

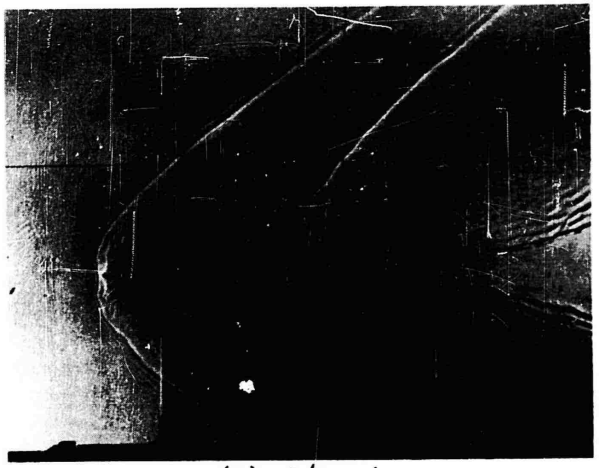

(B) L/D = 4

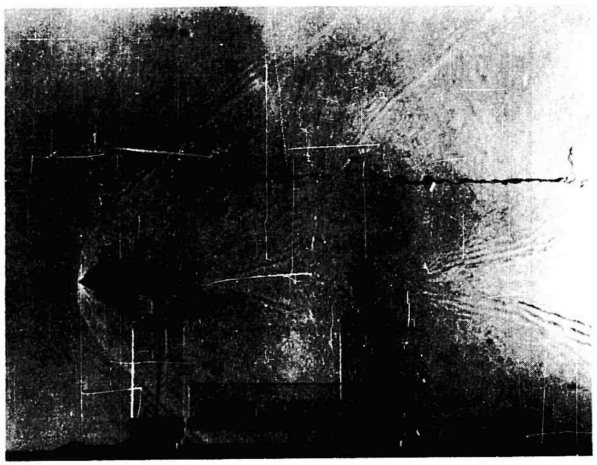

(C) L/D = 6

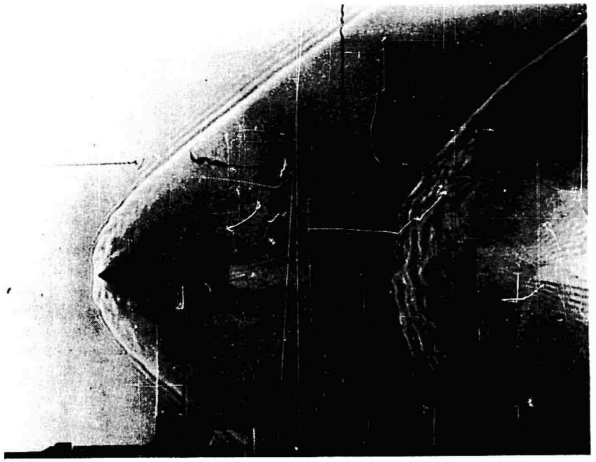

(D) L/D = 8

FIG. 25. REPRESENTATION OF OGIVAL NOSE CYLINDER WITH TRAILING CONE (45° HALF ANGLE)

blunt secondary bodies, i.e., the hollow hemisphere (Fig. 21), truncated cone (Fig. 22) and flat plate (Fig. 23) the full wave pattern becomes established only at L/D = 6.

5.2.2 Wave Formation With Blunt Ended Cylinder as Primary Body

Figures 26 through 31 show the wave patterns for the representation of a cylinder with blunt nose and tail as a primary body and the six secondary bodies.

The wave patterns of the secondary bodies resemble those of the previous set except that the tail wave of the primary and detached shock wave of the secondary bodies are not established for all secondary shapes until L/D = 6. This may be due to the fact that the flow disturbances behind the blunt ended cylinder are greater than those behind the ogival nose cylinder as can be inferred from Figures 8 and 9.

5.2.3 Wave Formation With Ellipsoid as Primary Body

Figures 32 through 37 show the wave patterns for the model representing an ellipsoid as the primary body and the six secondary bodies.

It can be seen from this set of figures that, for the same L/D ratios, the detached shock wave of the secondary body closely resembles the corresponding case with the ogival nose cylinder.

5.2.4 Wave Formation With Ogival Nose Cylinder With Cone Tail as Primary Body

Figures 38 through 43 show that the presence of the cone tail on the primary body helps to reduce the wake disturbance, thereby resulting in the establishment of the typical shock wave pattern for the secondary body at a smaller L/D ratio than was the case with the blunt ended ogival nose cylinder.

5.2.5 Wave Formation With Sphere as Primary Body

Comparison of the experimental representation of the sphere (Figs. 44 to 49) with those of the ellipsoid (Figs. 32 through 37) shows a general

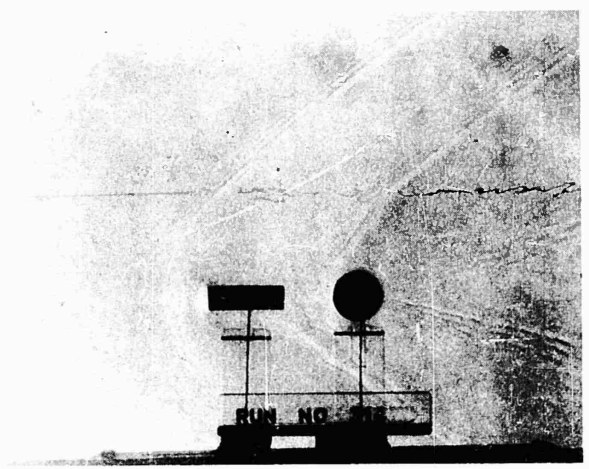

(A) L/D = 2

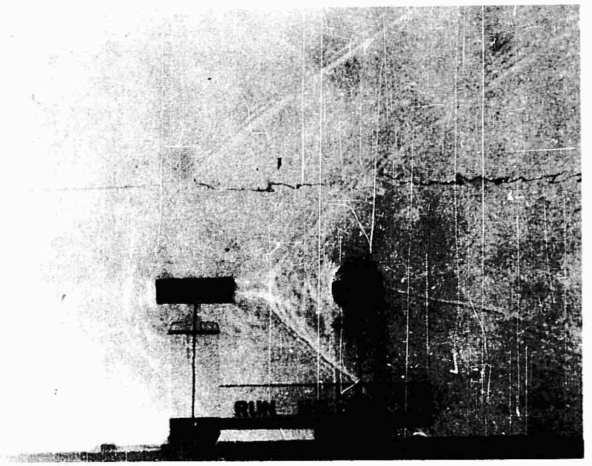

(B) L/D = 4

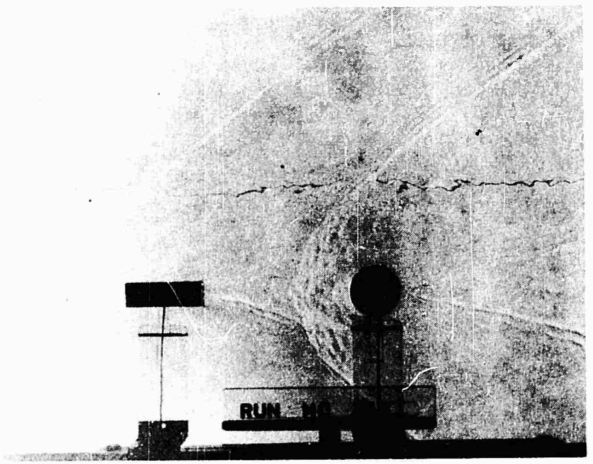

(C) L/D = 6

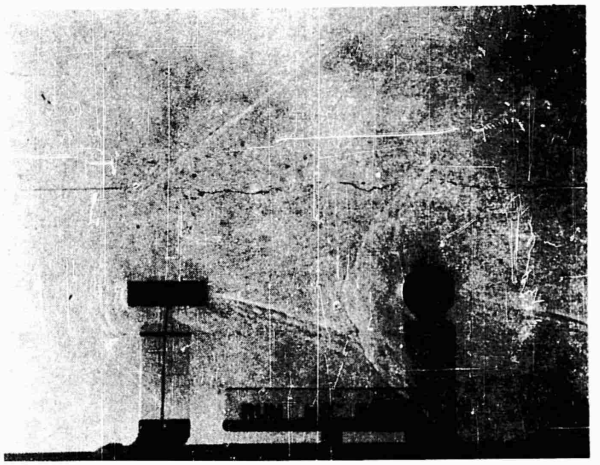

(D) L/D = 8

FIG. 26. REPRESENTATION OF CYLINDER WITH TRAILING SPHERE

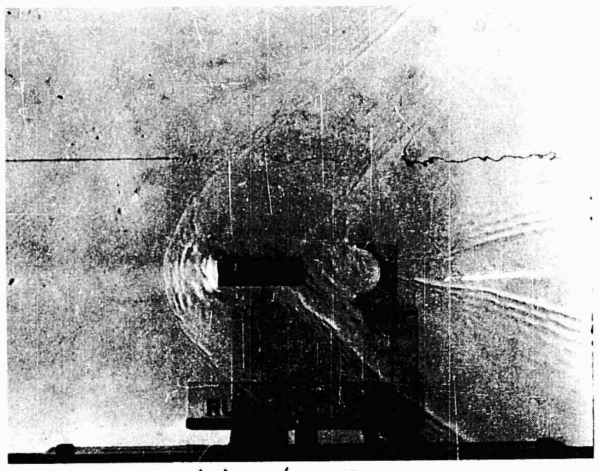

(A) L/D = 2

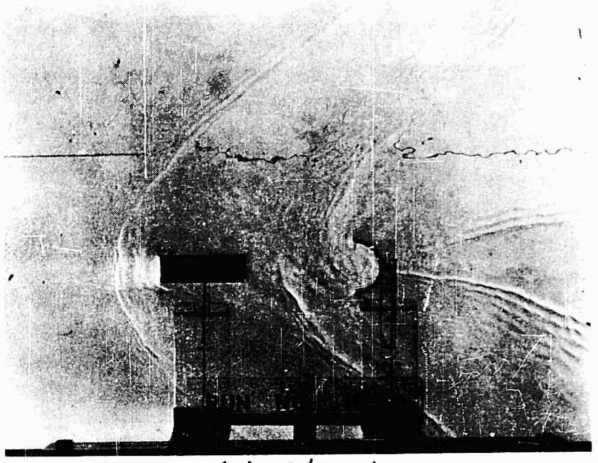

(B) L/D = 4

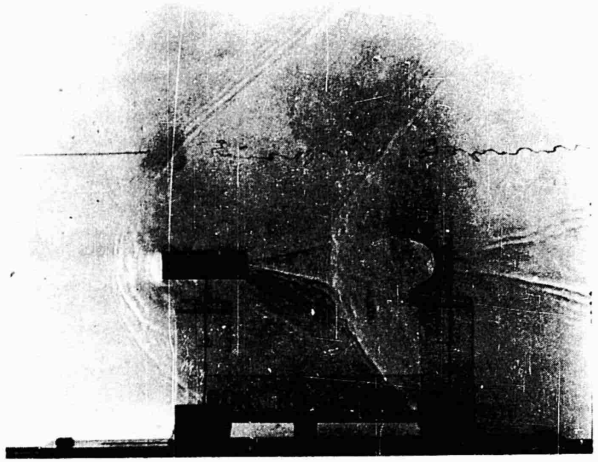

(C) L/D = 6

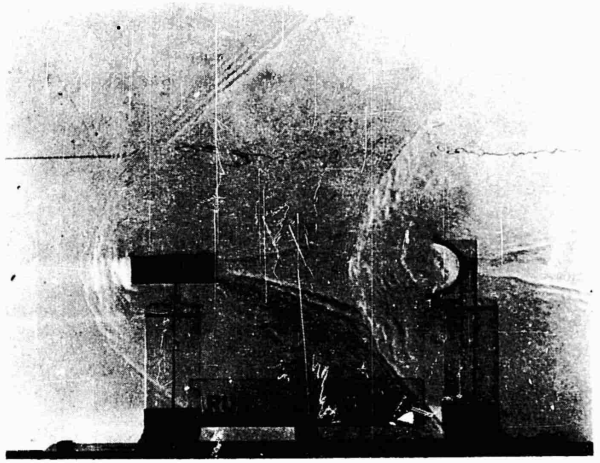

(D) L/D = 8

FIG. 27. REPRESENTATION OF CYLINDER WITH TRAILING HOLLOW HEMISPHERE

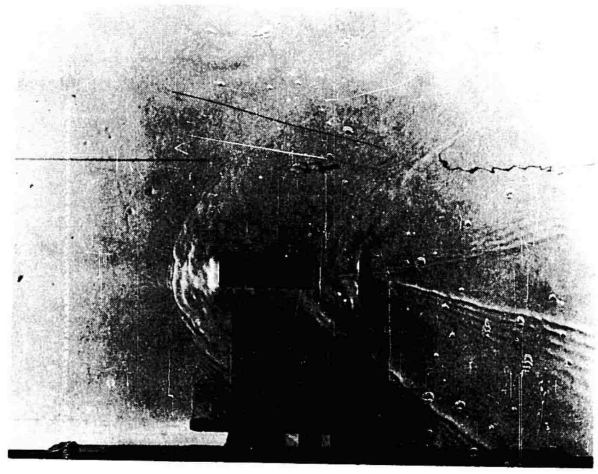

(A) L/D = 2

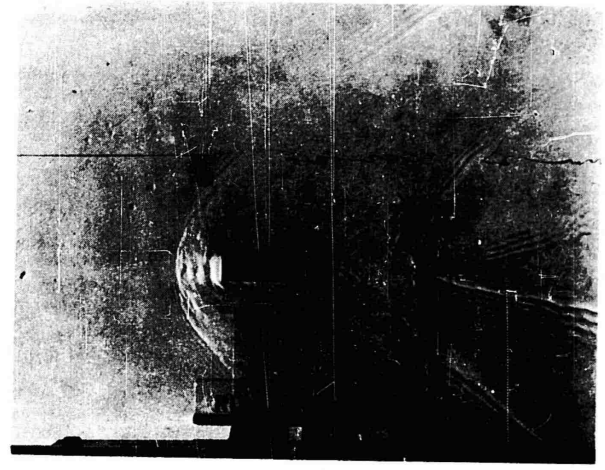

(B) L/D = 4

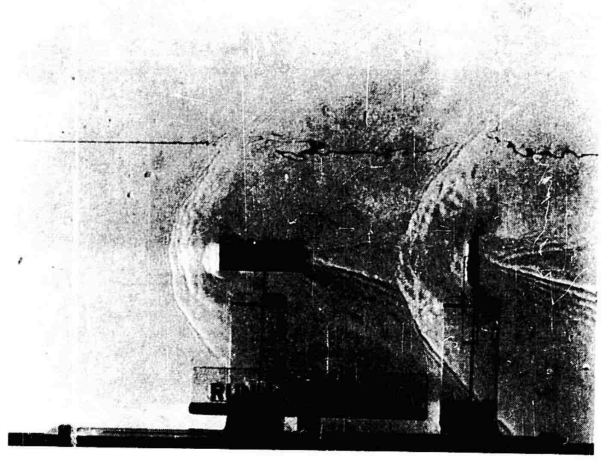

(C) L/D = 6

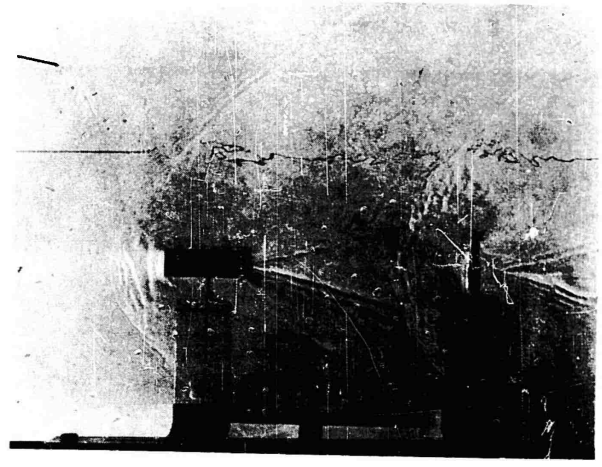

(D) L/D = 8

FIG. 28. REPRESENTATION OF CYLINDER WITH TRAILING TRUNCATED CONE

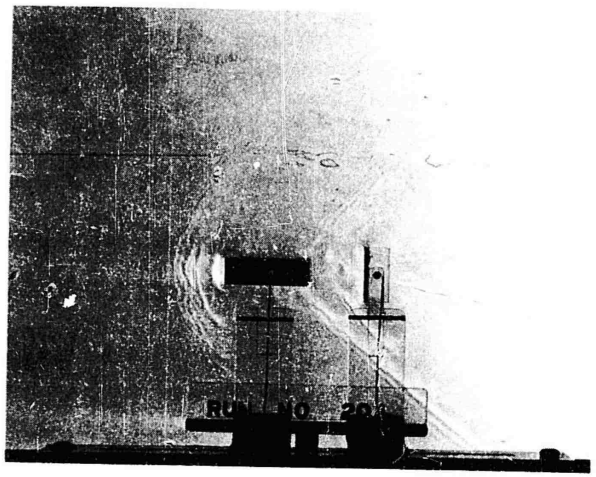

(A) L/D = 2

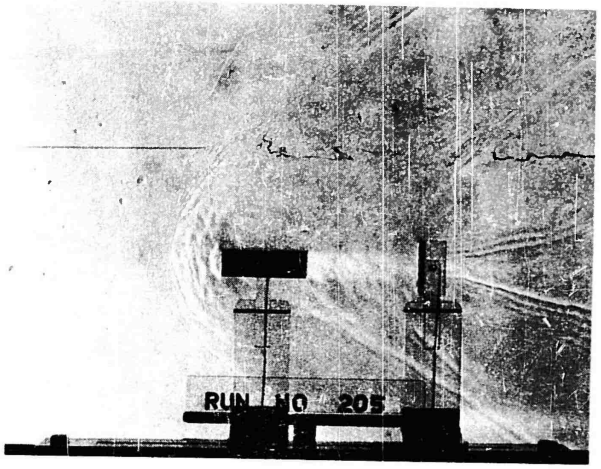


(B) L/D = 4

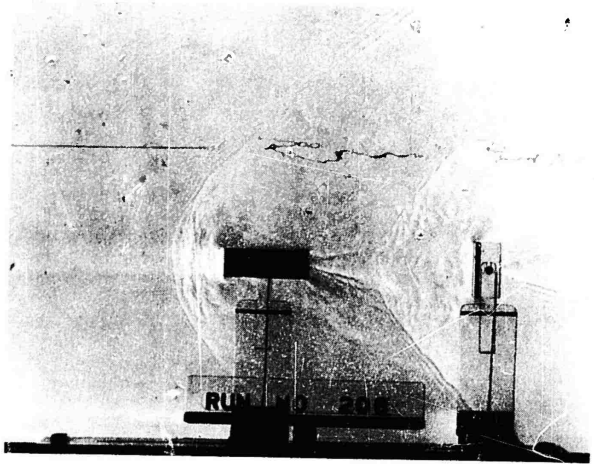

(C) L/D = 6

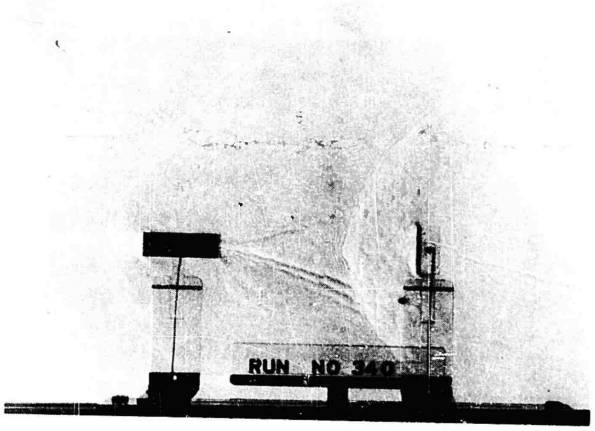


(D) L/D = 8

FIG. 29. REPRESENTATION OF CYLINDER WITH TRAILING FLAT PLATE

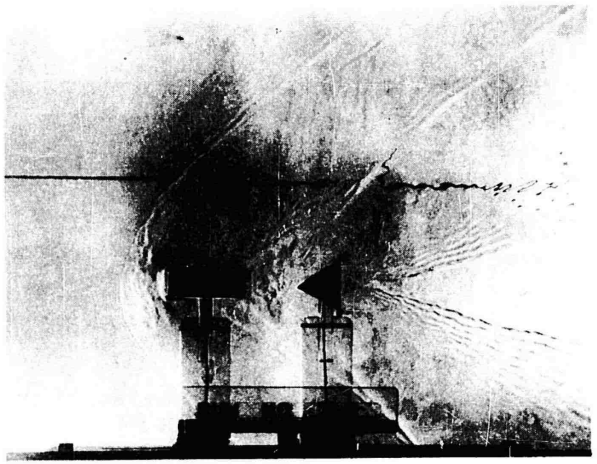

(A) L/D = 2

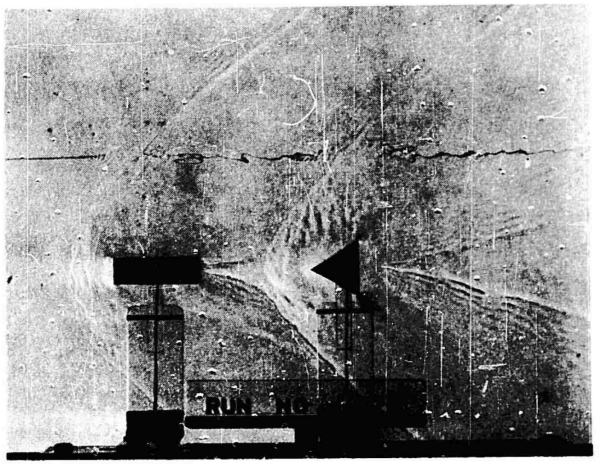

(B) L/D = 4

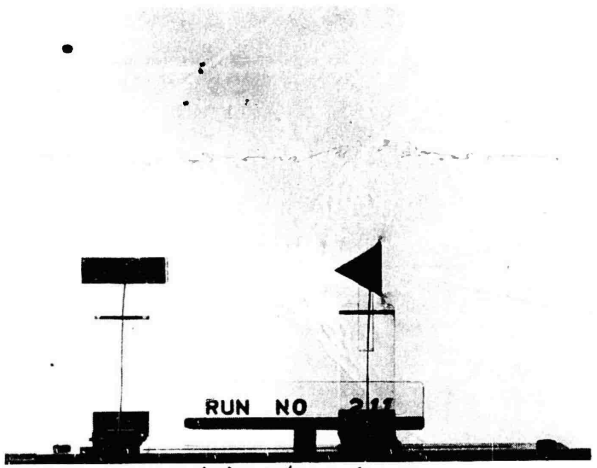


(C) L/D = 6

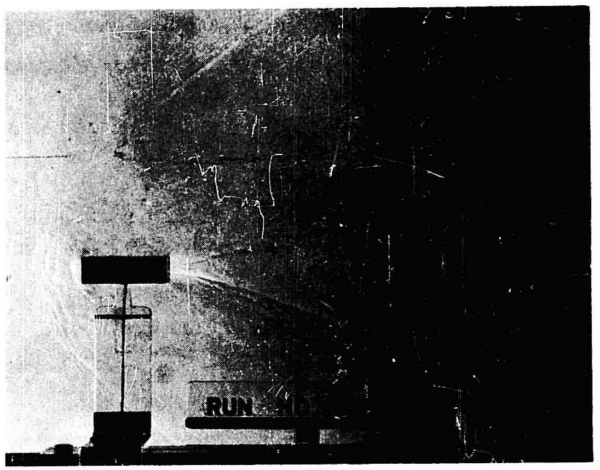

(D) L/D = 8

FIG. 30. REPRESENTATION OF CYLINDER WITH TRAILING CONE (30° HALF ANGLE)

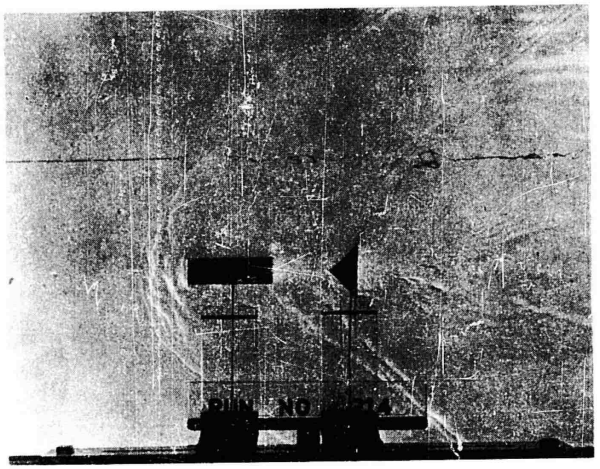

(A) L/D = 2

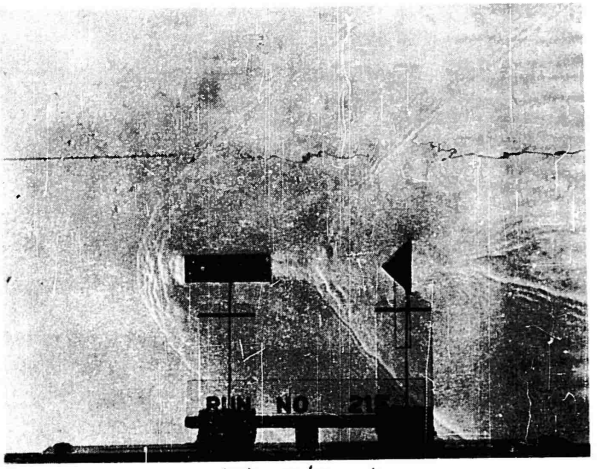

(B) L/D = 4

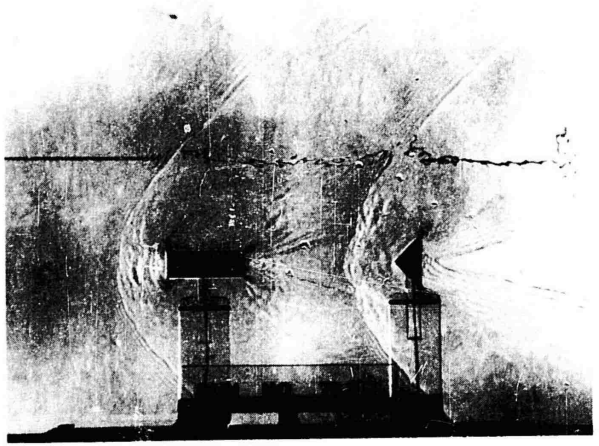

(C) L/D = 6

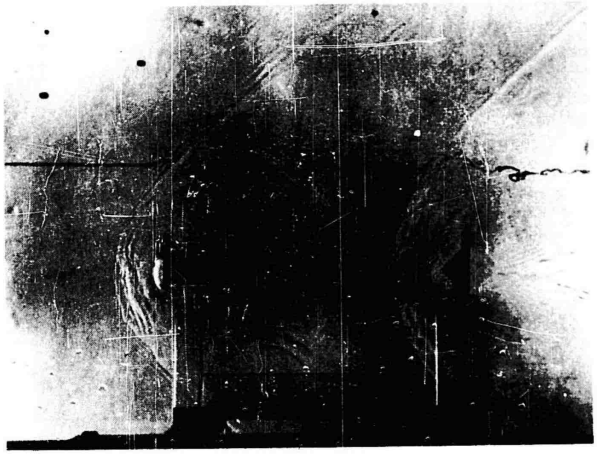

(D) L/D = 8

FIG. 31. REPRESENTATION OF CYLINDER WITH TRAILING CONE (45° HALF ANGLE)

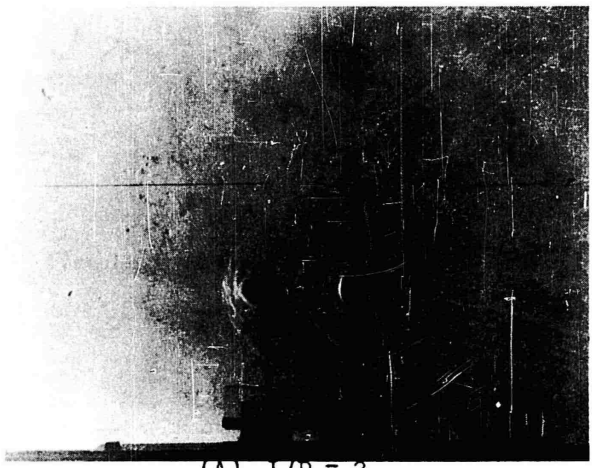

(A) L/D = 2

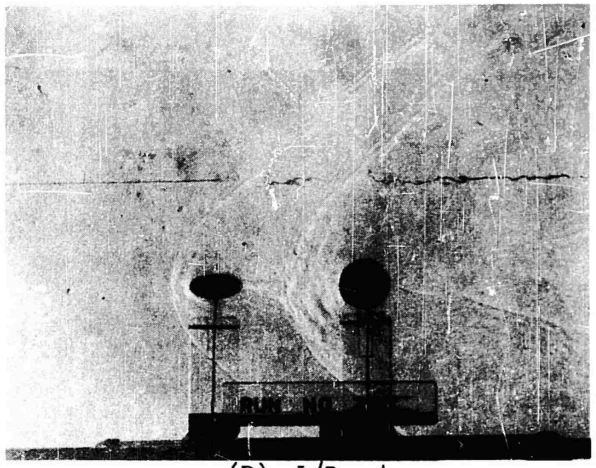

(B) L/D = 4

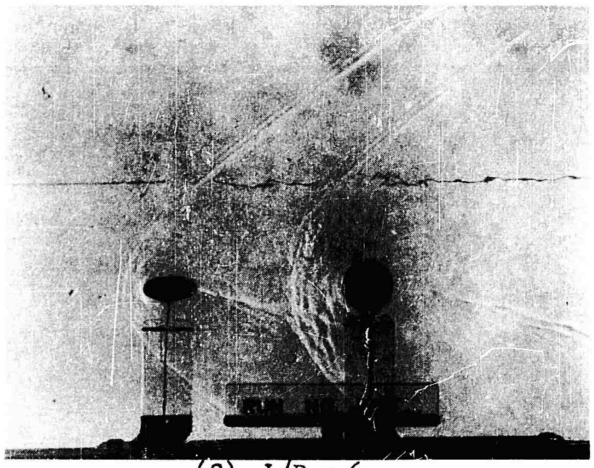

(C) L/D = 6

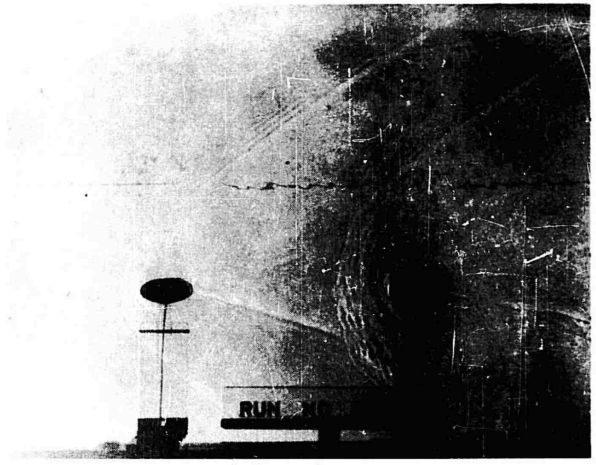

(D) L/D = 8

FIG. 32. REPRESENTATION OF ELLIPSOID WITH TRAILING SPHERE

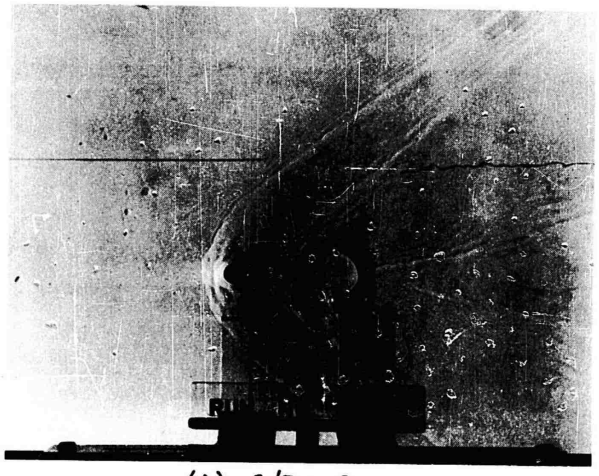

(A) L/D = 2

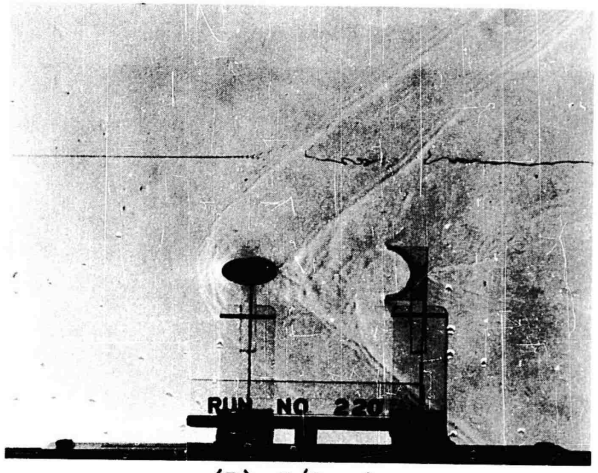


(B) L/D = 4

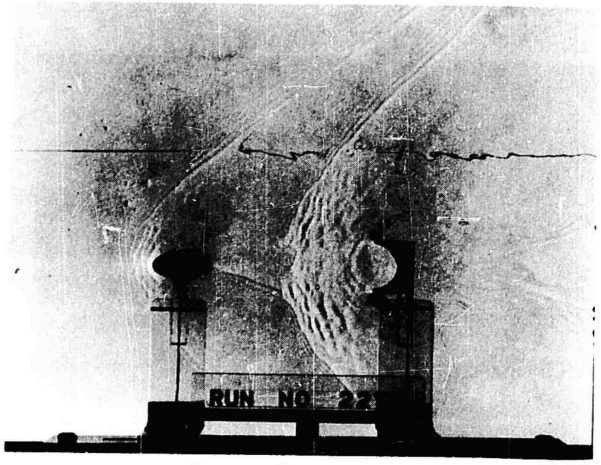


(C) L/D = 6

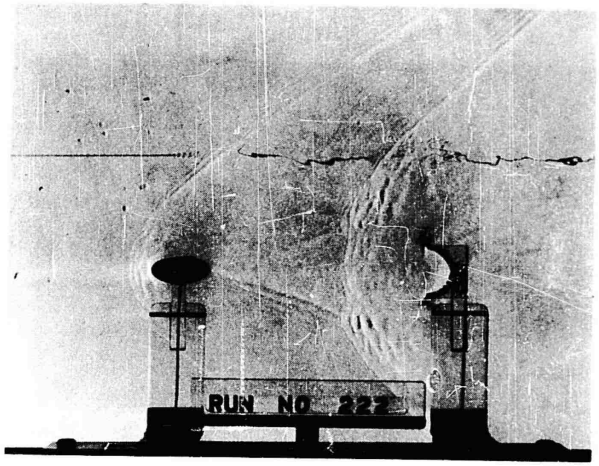


(D) L/D = 8

FIG. 33. REPRESENTATION OF ELLIPSOID WITH TRAILING HOLLOW HEMISPHERE

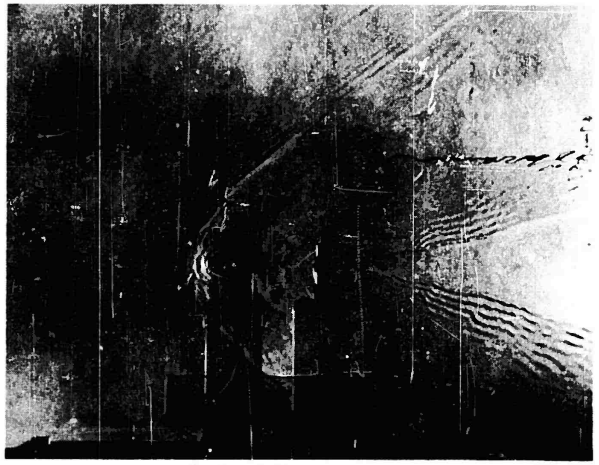

(A) L/D = 2

(B) L/D = 4

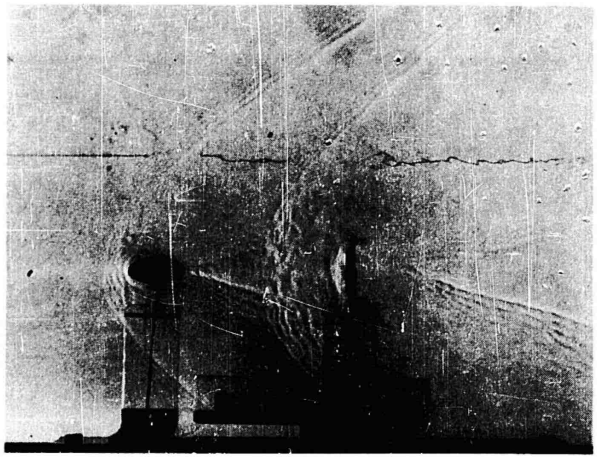

(C) L/D = 6

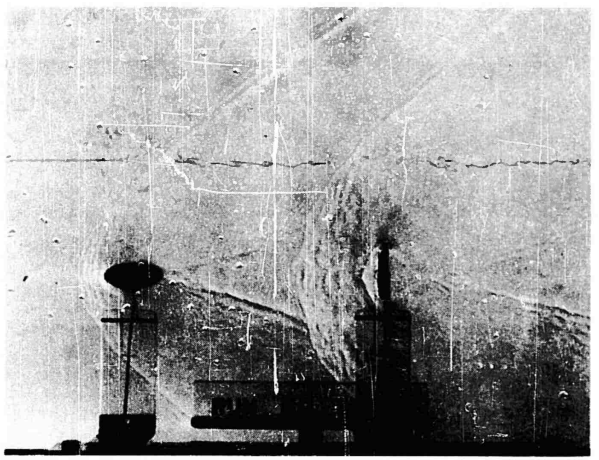

(D) L/D = 8

FIG. 34. REPRESENTATION OF ELLIPSOID WITH TRAILING TRUNCATED CONE

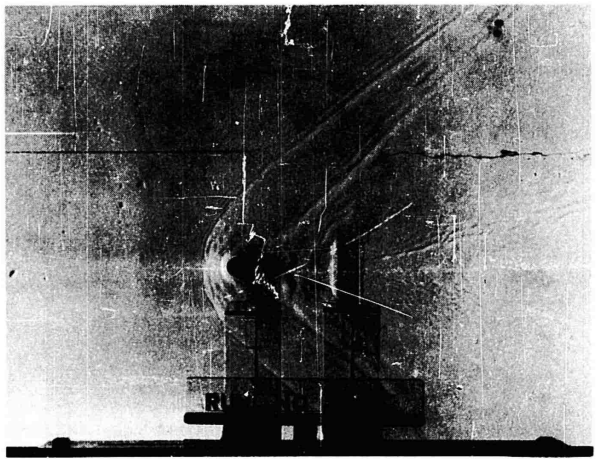

(A) L/D = 2

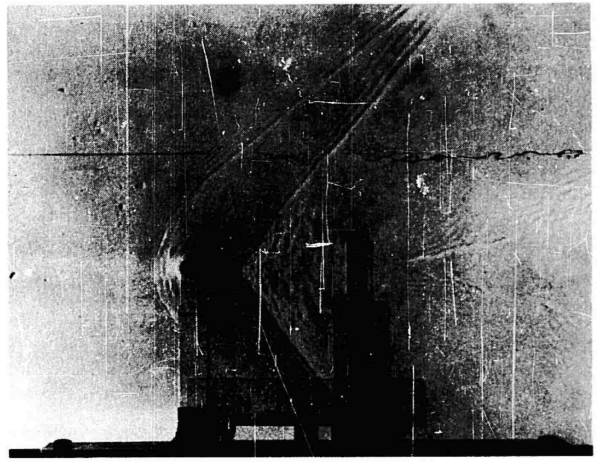

(B) L/D = 4

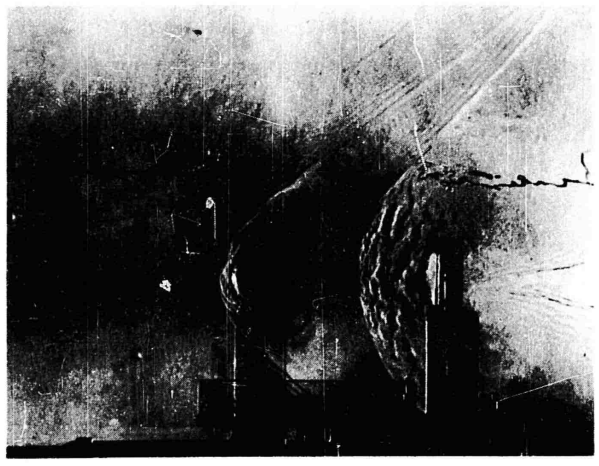

(C) L/D = 6

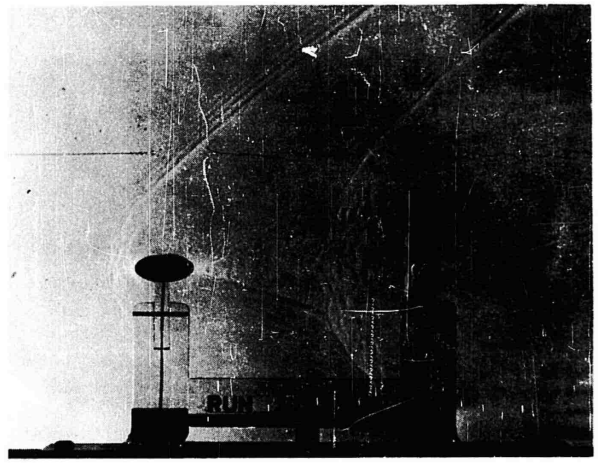

(D) L/D = 8

FIG. 35. REPRESENTATION OF ELLIPSOID WITH TRAILING FLAT PLATE

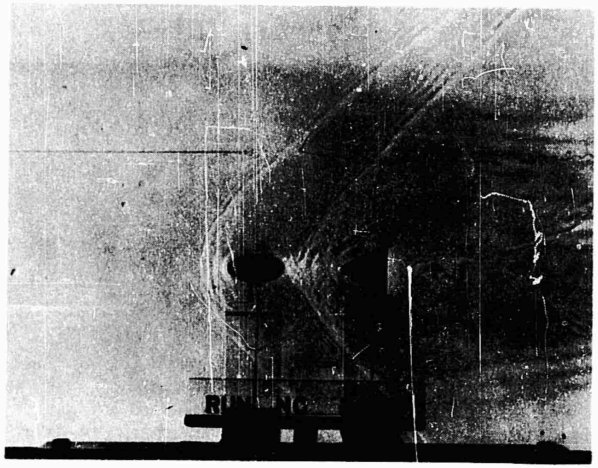

(A) L/D = 2

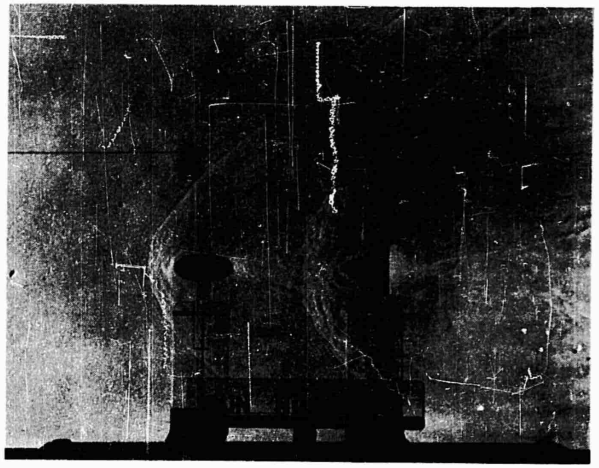

(B) L/D = 4

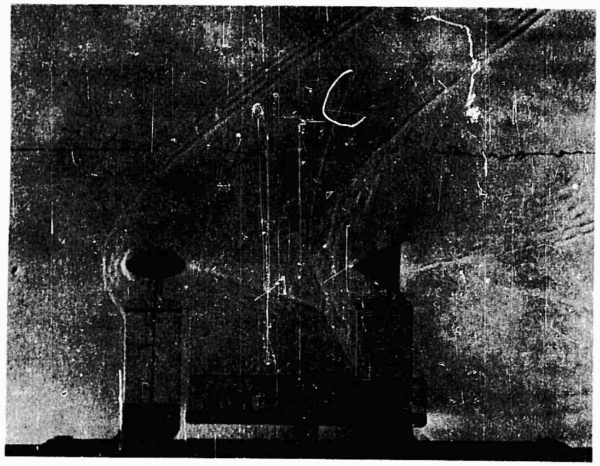

(C) L/D = 6

(D) L/D = 8

FIG. 36. REPRESENTATION OF ELLIPSOID WITH TRAILING CONE (30° HALF ANGLE)

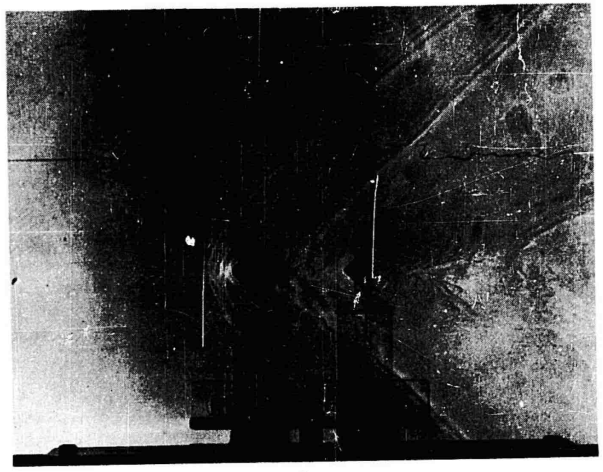

(A) L/D = 2


(B) L/D = 4

(C) L/D = 6

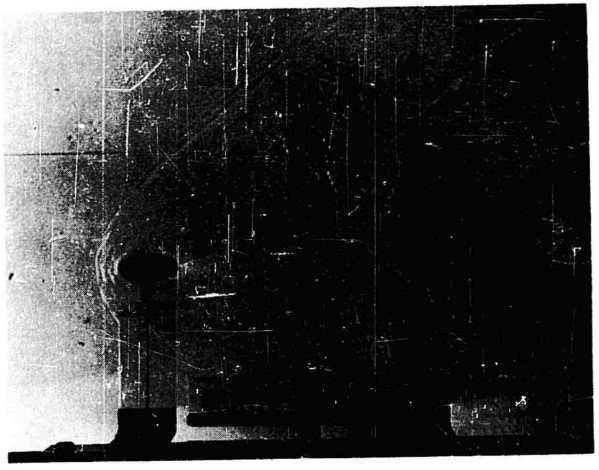

(D) L/D = 8

FIG. 37. REPRESENTATION OF ELLIPSOID WITH TRAILING CONE (45° HALF ANGLE)

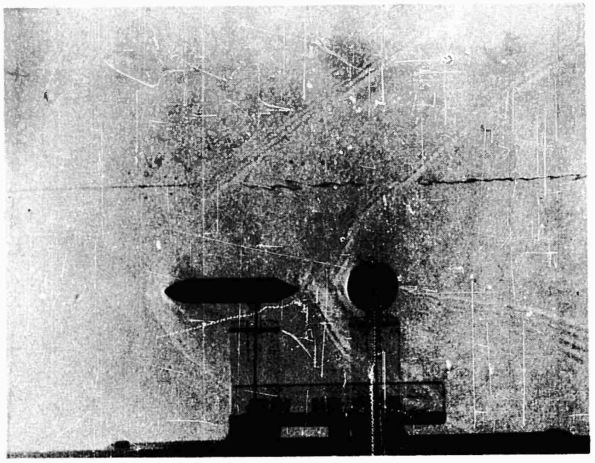

(A) L/D = 2

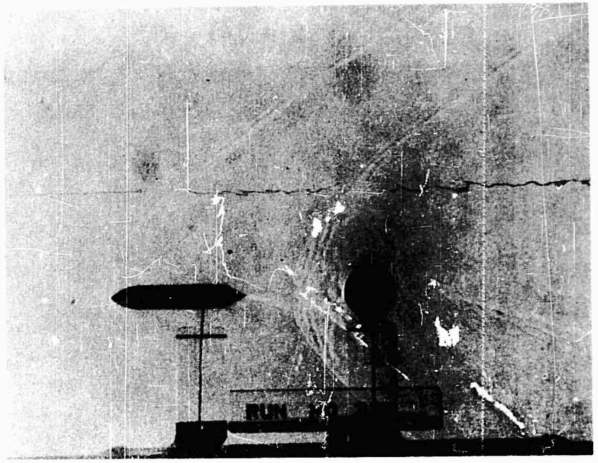

(B) L/D = 4

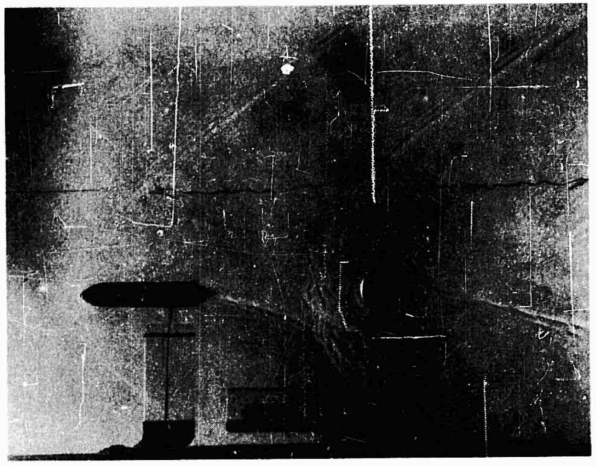

(C) L/D = 6

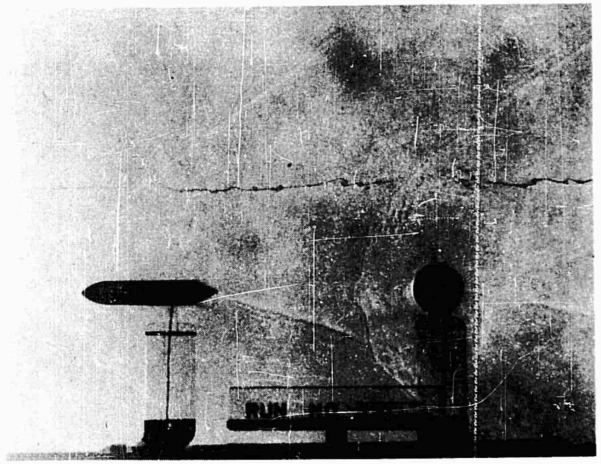

(D) L/D = 8

FIG. 38. REPRESENTATION OF OGIVAL NOSE CYLINDER, CONE TAIL WITH TRAILING SPHERE

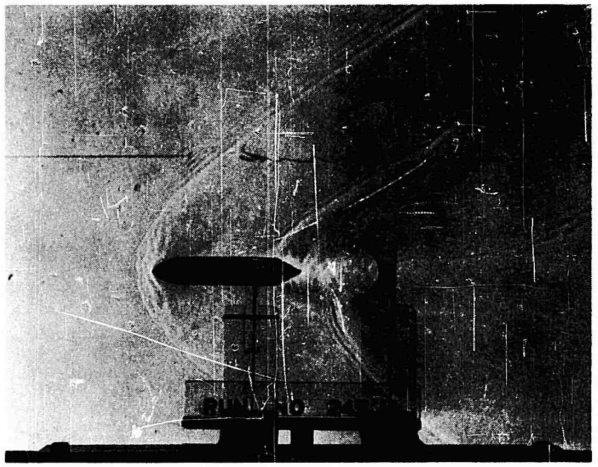

(A) L/D = 2

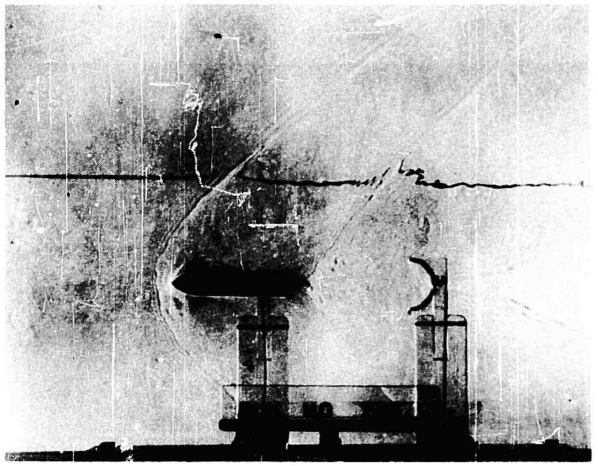

(B) L/D = 4

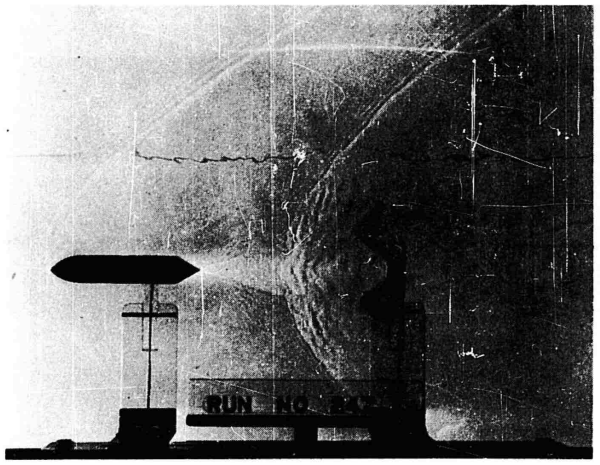

(C) L/D = 6

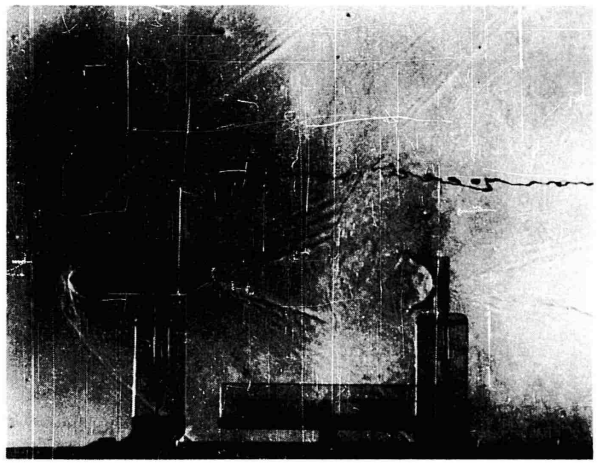

(D) L/D = 8

FIG. 39. REPRESENTATION OF OGIVAL NOSE CYLINDER, CONE TAIL WITH TRAILING HOLLOW HEMISPHERE

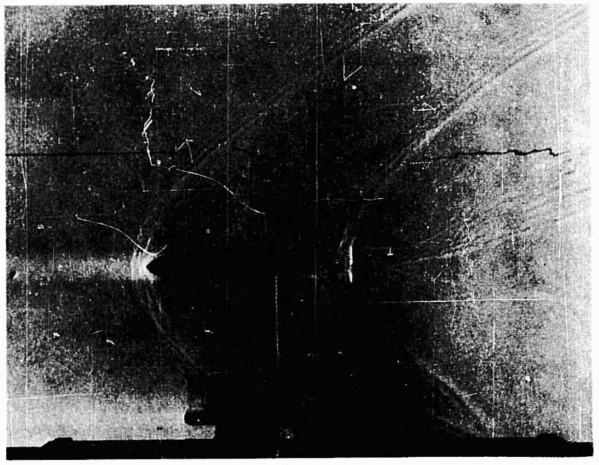

(A) L/D = 2

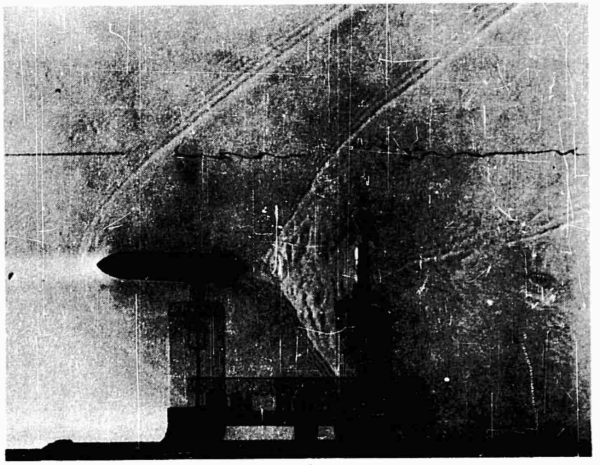

(B) L/D = 4

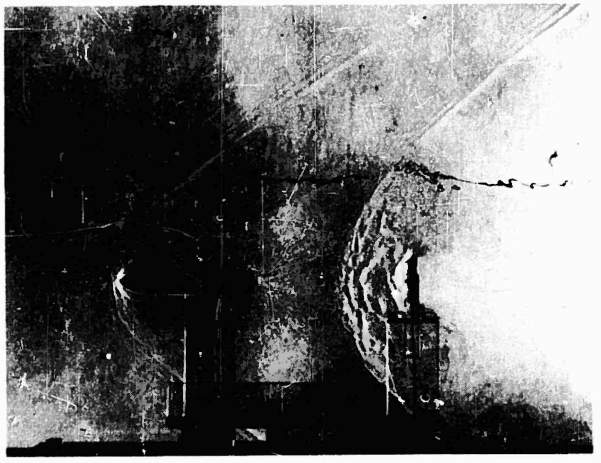

(C) L/D = 6

(D) L/D = 8

FIG. 40. REPRESENTATION OF OGIVAL NOSE CYLINDER, CONE TAIL WITH TRAILING TRUNCATED CONE

(A) L/D = 2

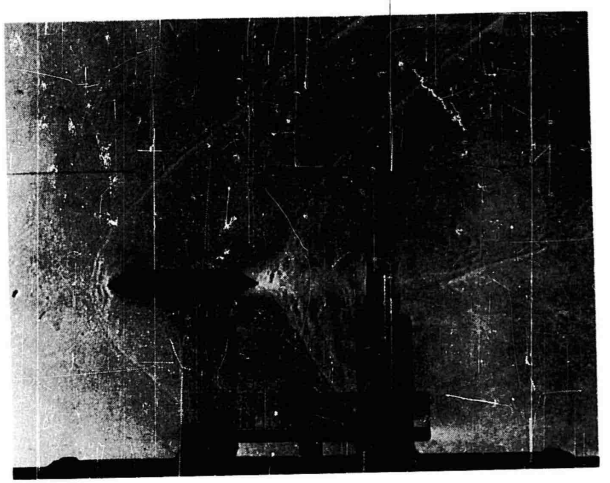

(B) L/D = 4

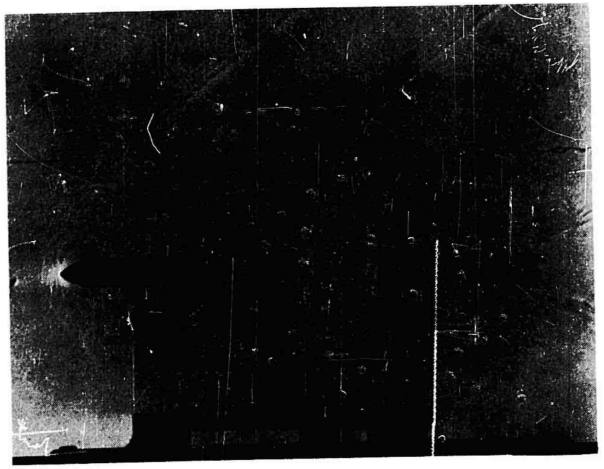

(C) L/D = 6

(D) L/D = 8

FIG. 41. REPRESENTATION OF OGIVAL NOSE CYLINDER, CONE TAIL WITH TRAILING FLAT PLATE

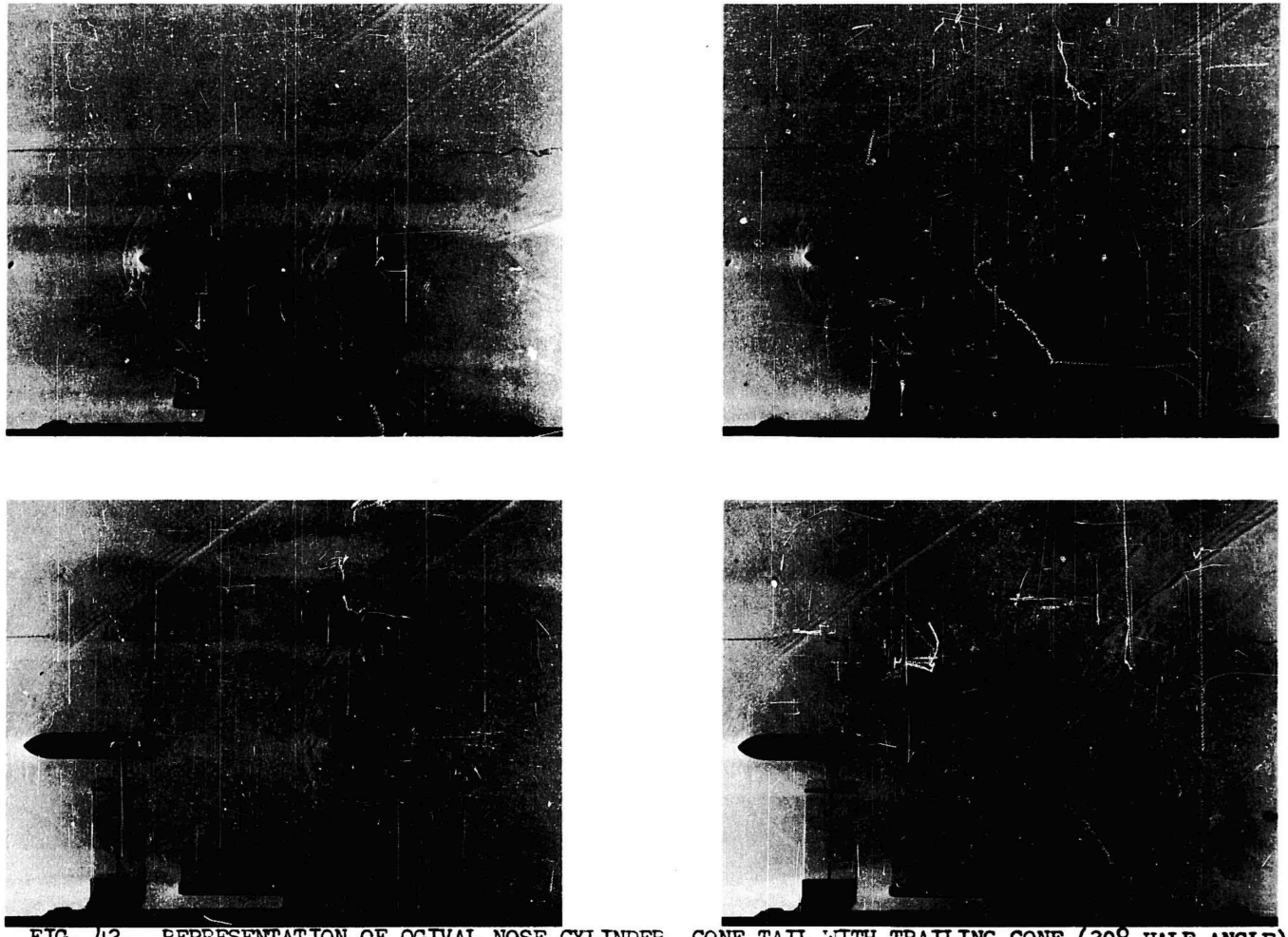

FIG. 42. REPRESENTATION OF OGIVAL NOSE CYLINDER, CONE TAIL WITH TRAILING CONE (30° HALF ANGLE)

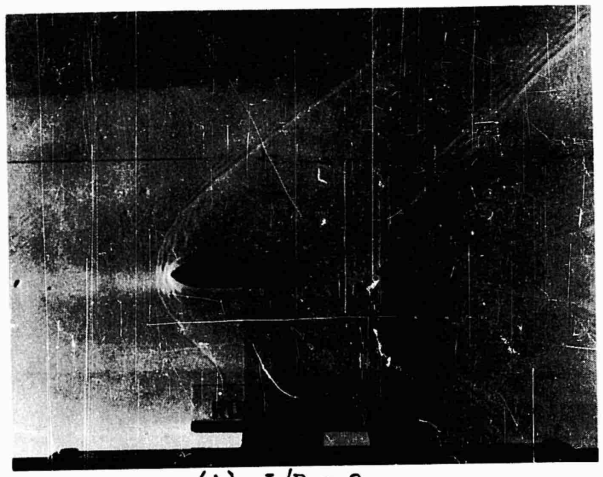

(A) L/D = 2

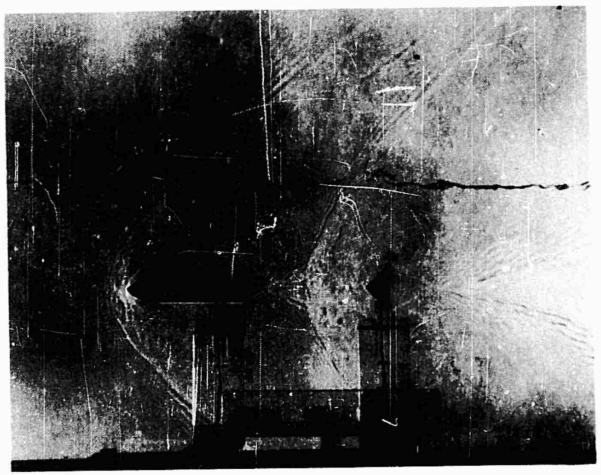

(B) L/D = 4

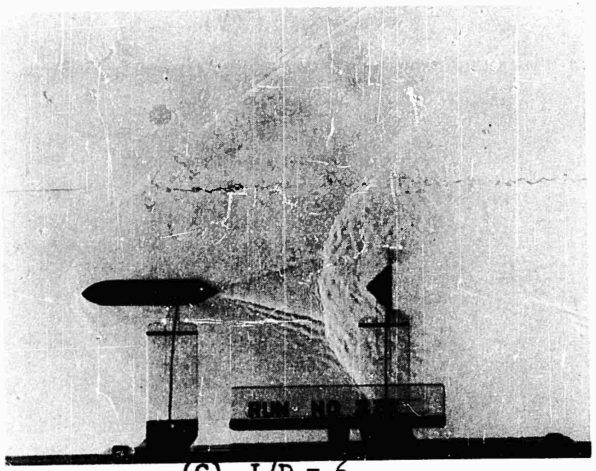

(C) L/D = 6

(D) L/D = 8

FIG. 43. REPRESENTATION OF OGIVAL NOSE CYLINDER, CONE TAIL WITH TRAILING CONE (45° HALF ANGLE)

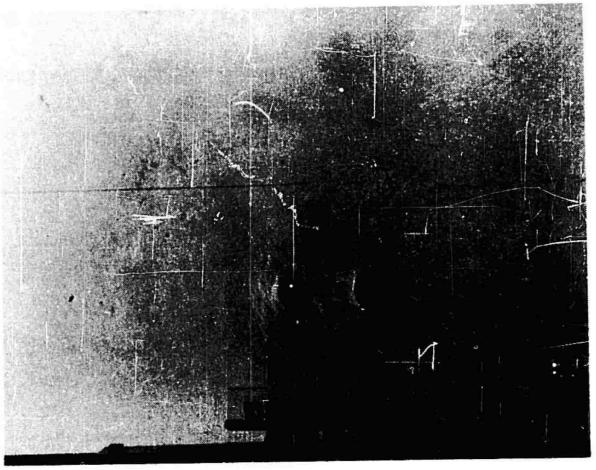

(A) L/D = 2

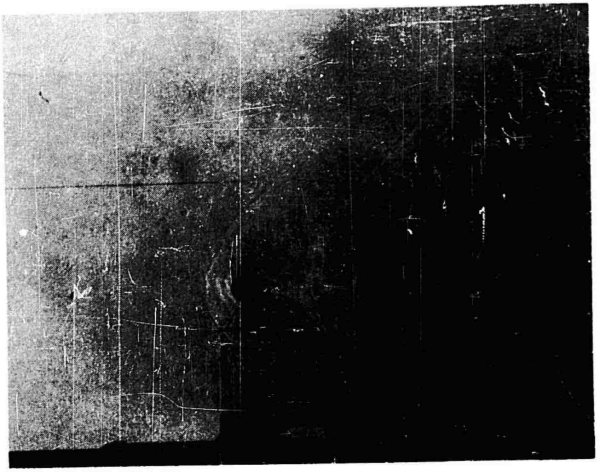

(B) L/D = 4

(C) L/D = 6

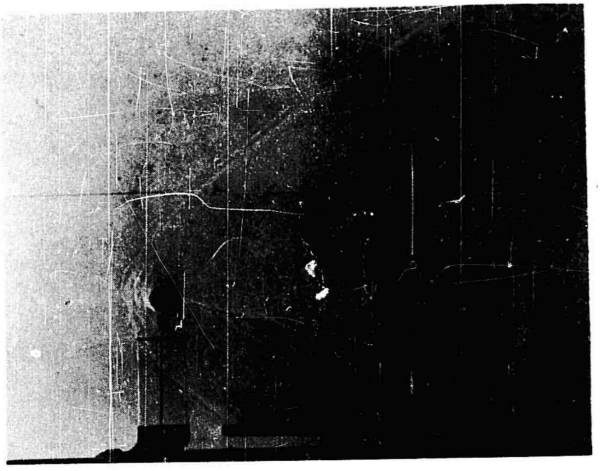

(D) L/D = 8

FIG. 44. REPRESENTATION OF SPHERE WITH TRAILING SPHERE

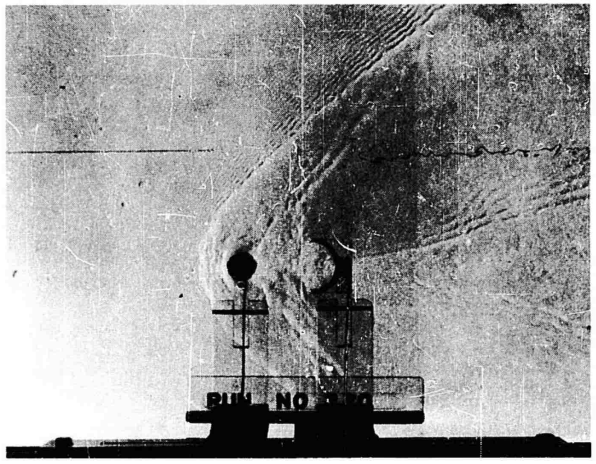

(A) L/D = 2

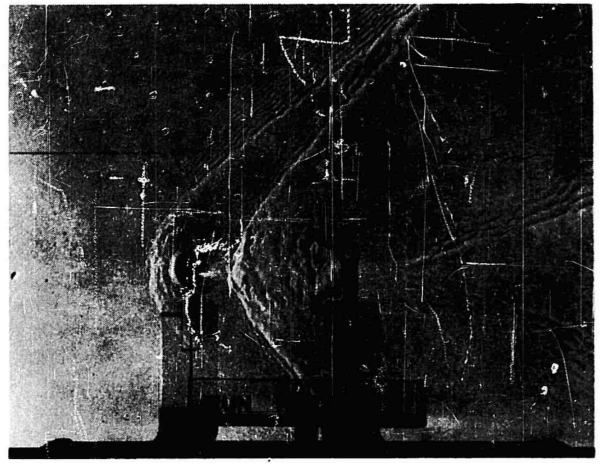

(B) L/D = 4

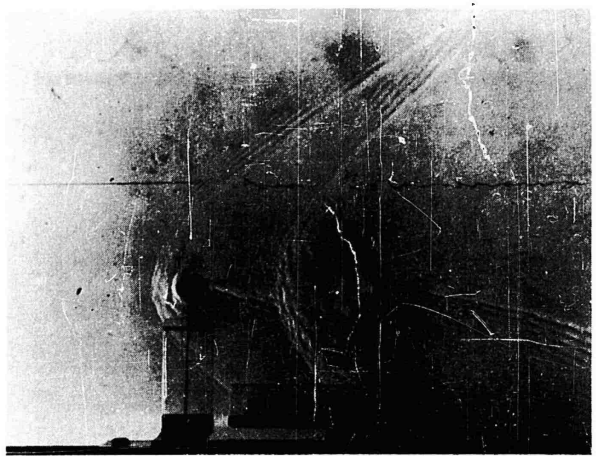

(C) L/D = 6

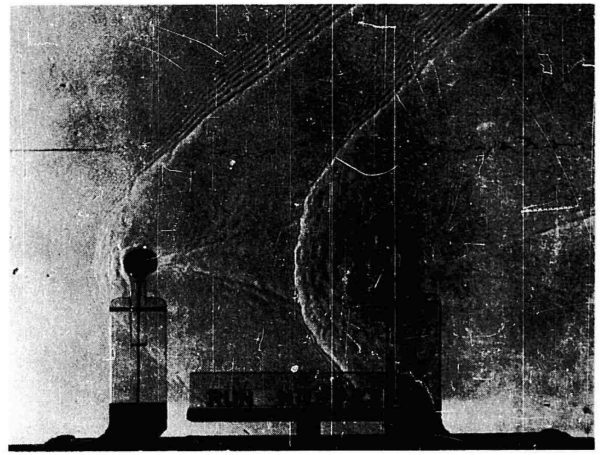

(D) L/D = 8

FIG. 45. REPRESENTATION OF SPHERE WITH TRAILING HOLLOW HEMISPHERE

(A) L/D = 2

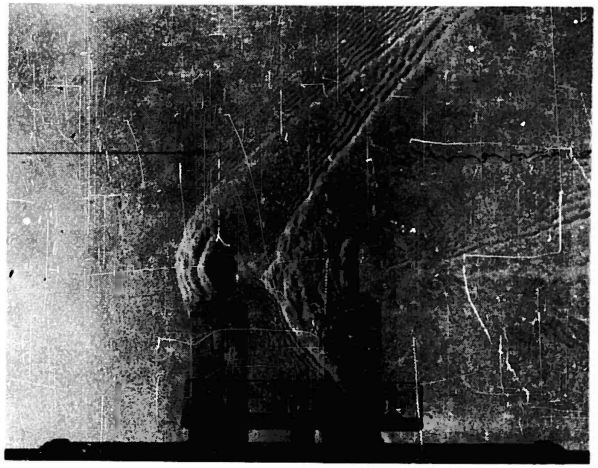

(B) L/D = 4

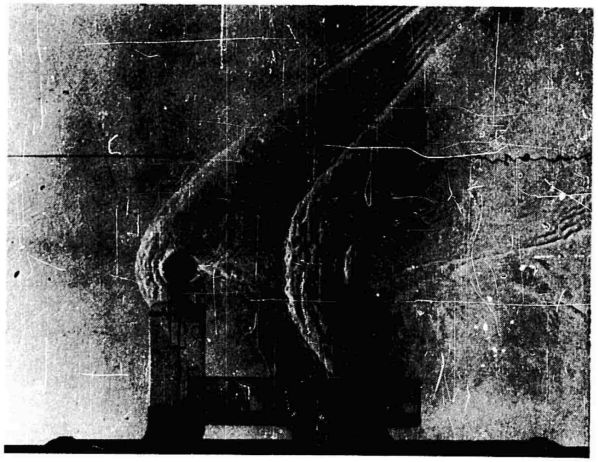

(C) L/D = 6

(D) L/D = 8

FIG. 46. REPRESENTATION OF SPHERE WITH TRAILING TRUNCATED CONE

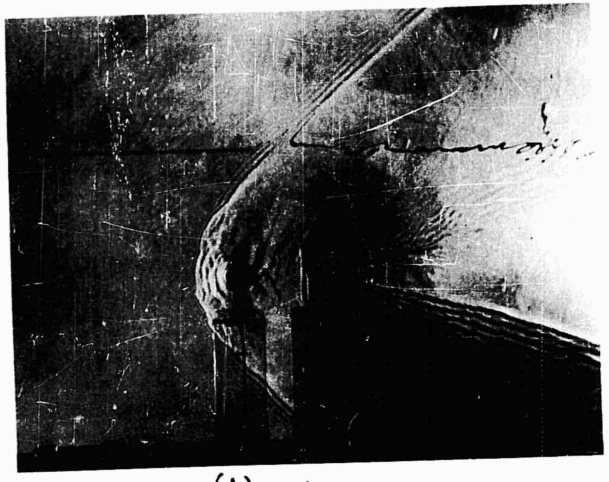

(A) L/D = 2

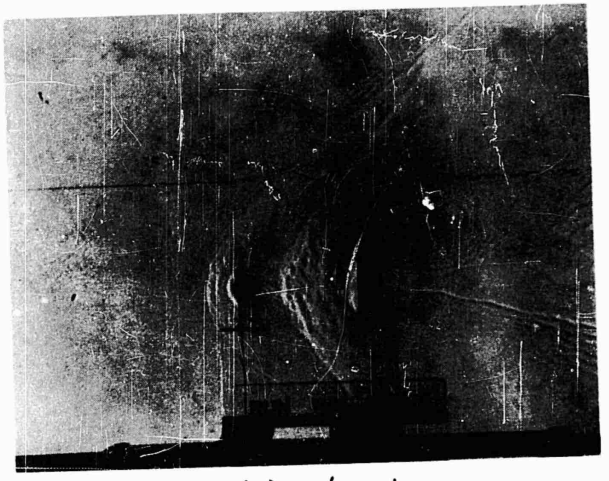

(B) L/D = 4

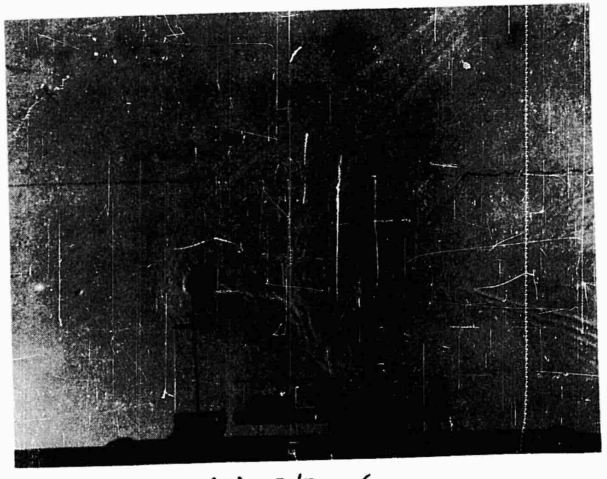

(C) L/D = 6

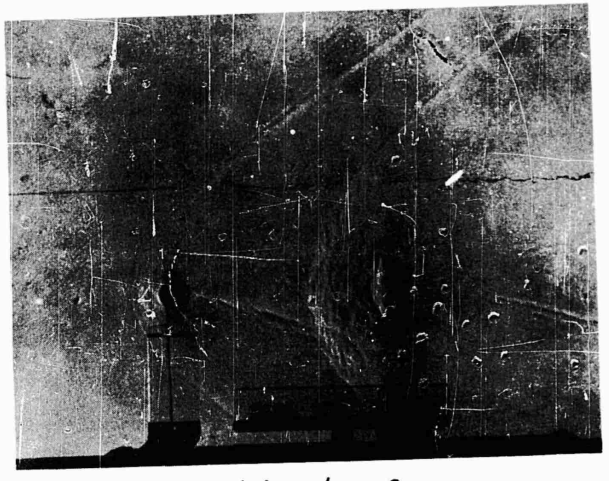

(D) L/D = 8

FIG. 47. REPRESENTATION OF SPHERE WITH TRAILING FLAT PLATE

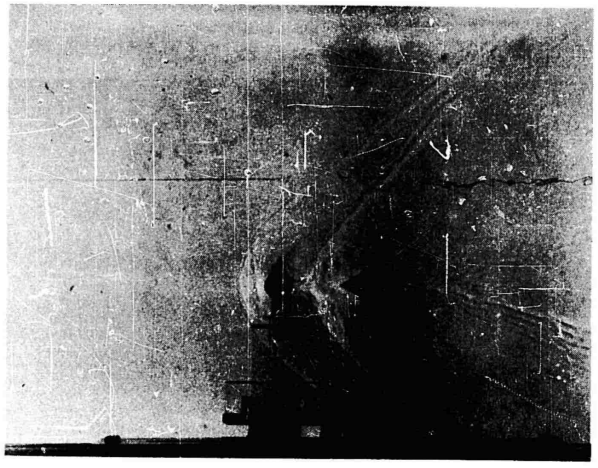

(A) L/D = 2

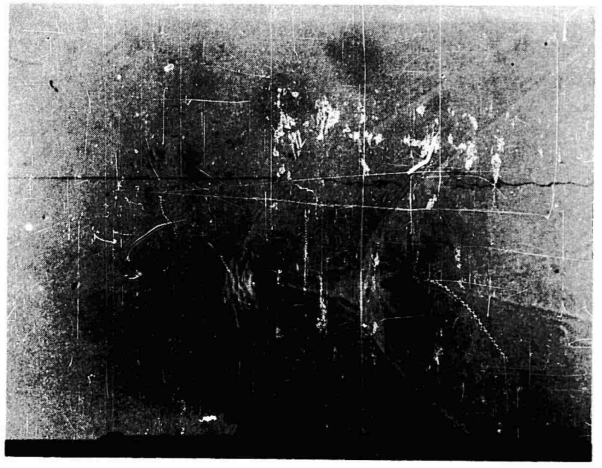

(B) L/D = 4

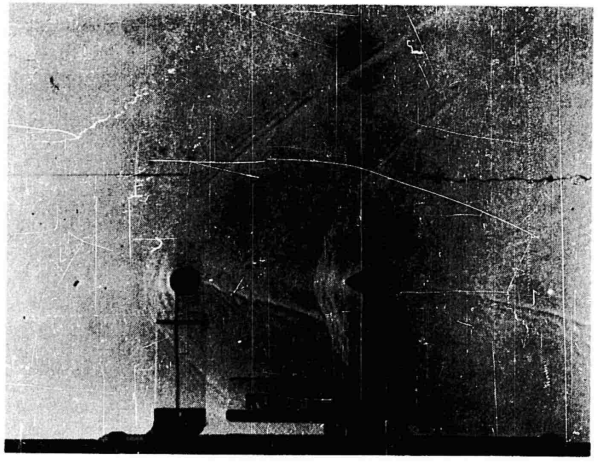

(C) L/D = 6

(D) L/D = 8

FIG. 48. REPRESENTATION OF SPHERE WITH TRAILING CONE (30° HALF ANGLE)

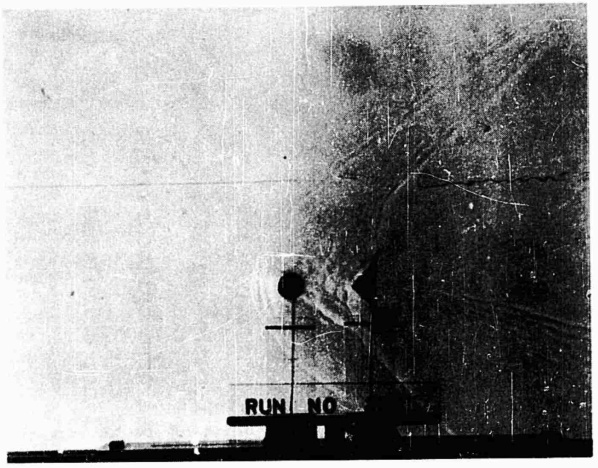


(A) L/D = 2

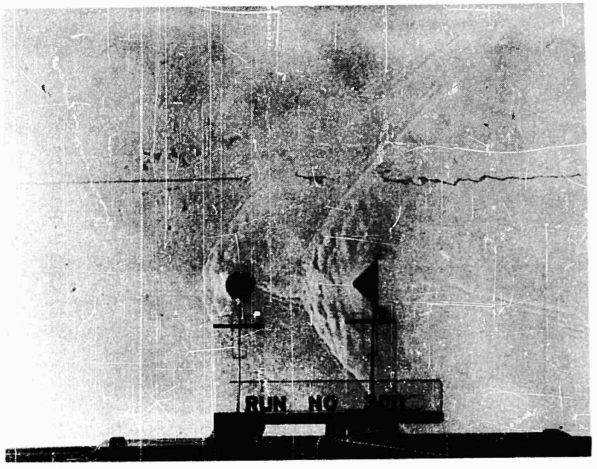


(B) L/D = 4

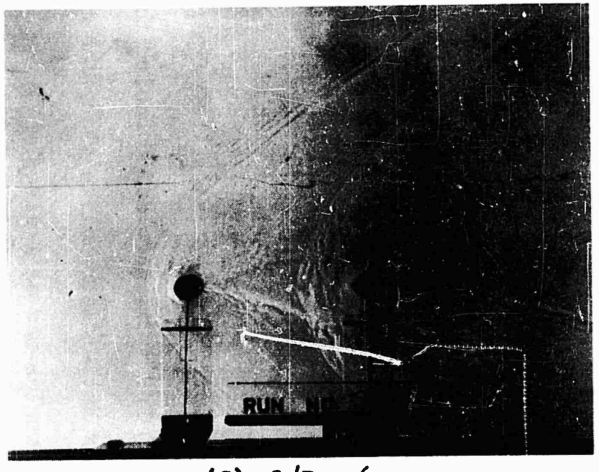

(C) L/D = 6

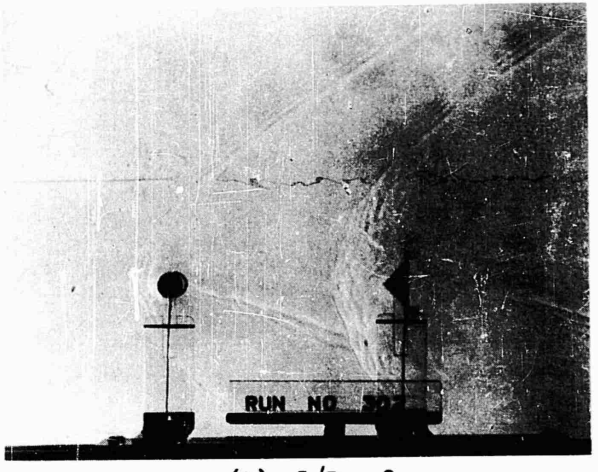


(D) L/D = 8

FIG. 49. REPRESENTATION OF SPHERE WITH TRAILING CONE (45° HALF ANGLE)

similarity of the wave patterns in the two cases. In practically all cases, the detached shock wave appears well established at L/D = 4.

5.3 Experiments to Determine Mach Recovery in the Wake

Having obtained the wave pattern for the different bodies and body combinations, an attempt was made to determine the wake velocity and Mach Number recovery. For this purpose, a 10° double wedge was placed at different L/D ratios axially in the wake of a number of primary bodies. The oblique shock wave angle was measured and the flow Mach Number in the wake was determined from the charts of Reference 6.

The characteristics and limitations of the method of using wedges and cones for Mach Number determination in air flow are well known. When the method was applied to the water flow, some additional restrictions were observed:

When the double wedge was placed close to the primary body, i.e., closer than L/D = 4, the Mach Number determination was very erratic and uncertain. This was due to the fact that, in the wake region close to the body, the flow is quite turbulent and the water surface has numerous crests and troughs. At the instant a photograph is taken, the leading edge of the wedge may be hitting a wave crest, a trough or some intermediate condition and the resultant wave angle will vary accordingly. For this reason, no attempt was made to determine the velocity at distances closer than L/D = 4.

Figure 50 illustrates the wave pattern for the double wedge when set at L/D = 2, 4, 6, and 8 behind the ogival nose cylinder. The Mach Number Ratio distribution along the center line, calculated from the wave angles was as follows:

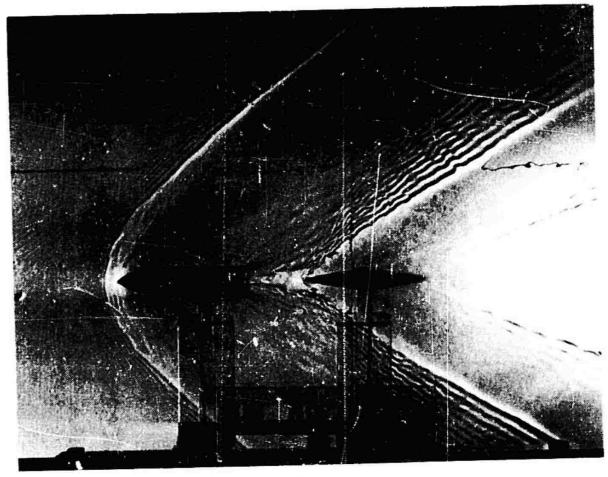

(A) L/D = 2

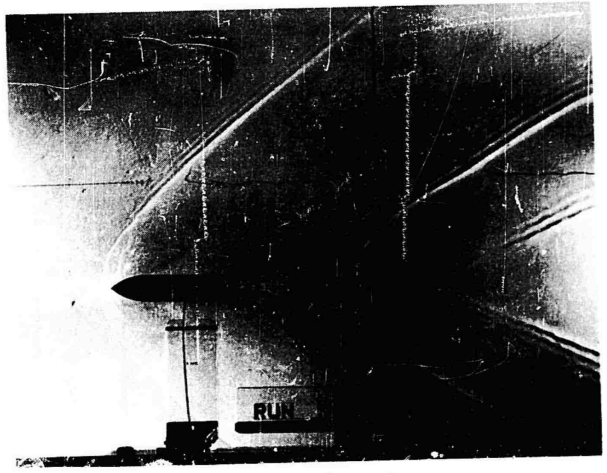


(B) L/D = 4

(C) L/D = 6

(D) L/D = 8

FIG. 50. REPRESENTATION OF OGIVAL NOSE CYLINDER WITH TRAILING DOUBLE WEDGE (16° HALF ANGLE)

| L/D | $\frac{M \text{ wake}}{M \text{ free stream}}$ |
|---|---|
| 4 | 0.895 |
| 6 | 0.950 |
| 8 | 0.975 |

Figures 51 and 52 illustrate the wave patterns for the double wedge behind the models representing the ellipsoid and sphere respectively.

The calculated Mach Number Ratio distribution for these cases was as follows:

| L/D | $\frac{M \text{ wake}}{M \text{ free stream}}$ | |
|---|---|---|
| | Ellipsoid | Sphere |
| 4 | .945 | .925 |
| 6 | .925 | .935 |
| 8 | .925 | .925 |

The experiments to determine quantitatively the Mach Number Recovery in the wake by means of standard wedges were exploratory in character and the results obtained are to be considered of a tentative nature. Validation tests or alternative methods for obtaining quantitative results from the water channel would exceed the scope of the present investigation.

An intrinsic limitation of the method is that it cannot be used for subsonic flow. Separate studies on the wake in this regime have been conducted as a separate phase of the over-all investigation on Aerodynamic Retardation.

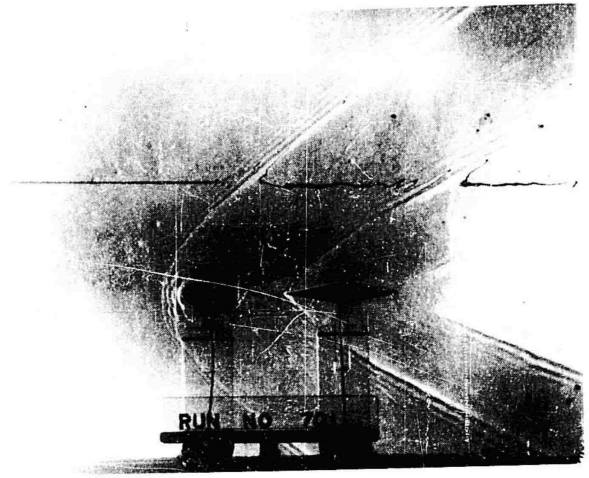


(A) L/D = 2

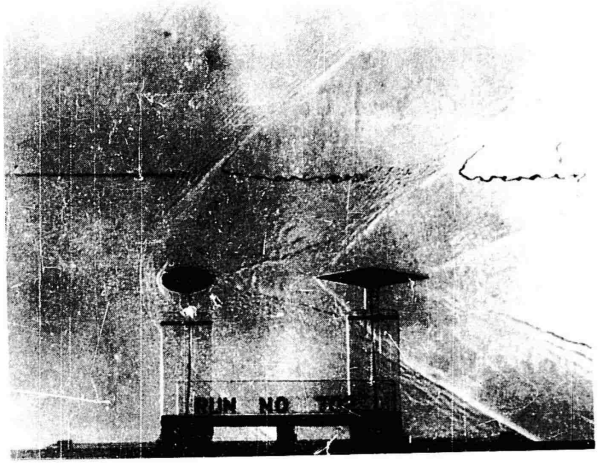

(B) L/D = 4

(C) L/D = 6

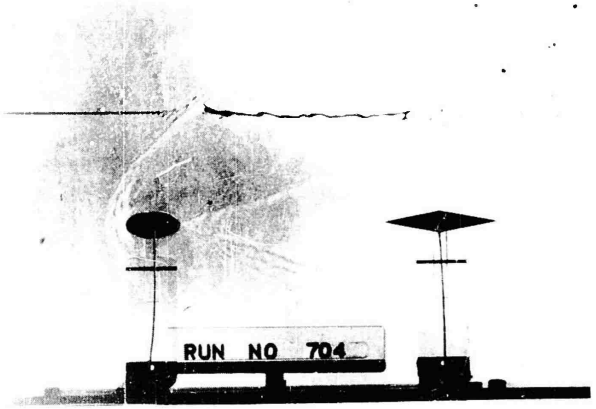


(D) L/D = 8

FIG. 51. REPRESENTATION OF ELLIPSOID WITH TRAILING DOUBLE WEDGE (10° HALF ANGLE)

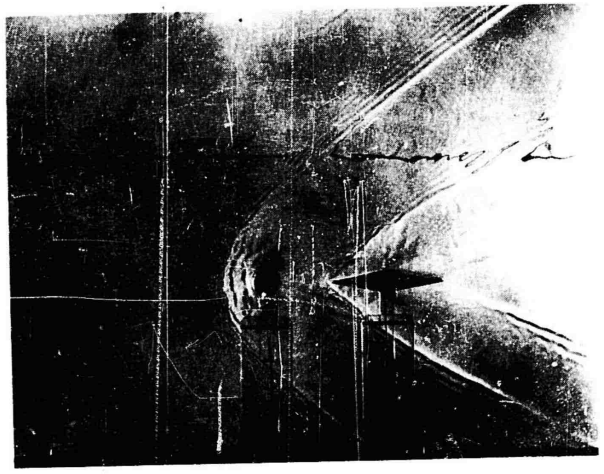

(A) L/D = 2

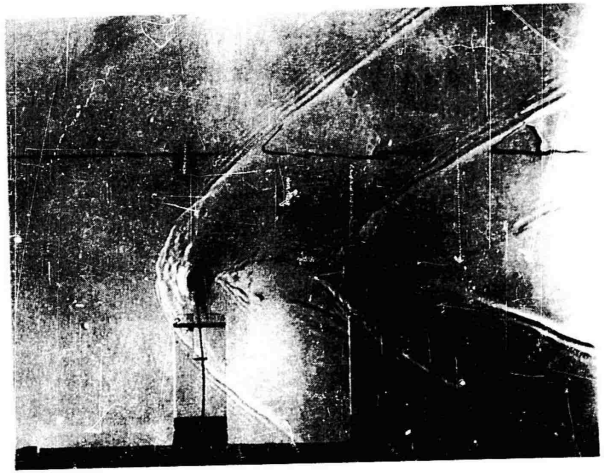

(B) L/D = 4

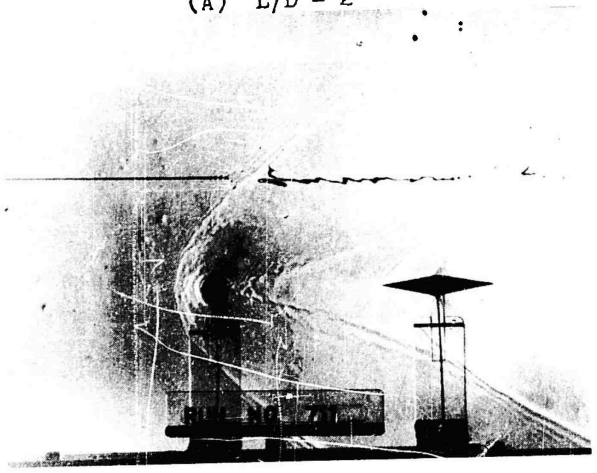

(C) L/D = 6

(D) L/D = 8

FIG. 52. REPRESENTATION OF SPHERE WITH TRAILING DOUBLE WEDGE (10° HALF ANGLE)

## SECTION 6

### Conclusions

1. The water surface wave analogy proved to be a convenient and very inexpensive means for a qualitative investigation of the flow pattern around two dimensional bodies in supersonic flow. It is particularly suitable in the transonic and low supersonic regimes.
2. There appears to be reasonable agreement with regard to the shape of the detached shock wave obtained in the water tank and that calculated from existing theories. However, the stand-off distances obtained experimentally were very much larger (by about 70%) than those calculated from theory.
3. From the experimental wave patterns presented here for a number of primary-secondary body combinations representing existing or potential shapes of flying objects and aerodynamic deceleration devices at a simulated Mach 2, it appears that in most cases, a minimum L/D ratio of 4 is necessary for efficient operation of the retardation device. For primary bodies with a large wake or very blunt secondary bodies, e.g. the hollow hemisphere and flat plate, a ratio of L/D greater than 4 may be necessary.
4. The use of a wedge as an experimental device for Mach Number determination in the wake did not prove very satisfactory. It could not be applied for L.D ratios smaller than 4 and at greater L/D ratios, — the results were not entirely consistent.
5. Theoretical considerations indicate that the water surface analogy might apply to the investigation of non-steady flow problems, such as accelerated or retarded flow. Such applications, if validated, could be very useful in investigations on aerodynamic deceleration devices since similar experiments might be very difficult to produce in transonic or supersonic wind tunnels.

## REFERENCES


1. Preiswerk, E.: Applications of the Methods of Gas Dynamics to Water Flows with Free Surfaces, NACA TM 934 and 935, 1940.
2. Lemeshewsky, A. A.: A Visual Investigation of the Interaction of Shock Waves from a Body in Curvilinear Diving Flight by Simulated Surface Waves on Water. University of Minnesota Thesis, 1955.
3. Moeckel, W.E.: Approximate Method for Predicting Form and Location of Detached Shock Waves Ahead of Plane or Axially Symmetric Bodies. NACA TN 1921, 1949.
4. Laitone, E. V.: A Study of Transonic Gas Dynamics by Hydraulic Analogy. Journal of the Aeronautical Sciences, Vol. 19, No. 4, April, 1952.
5. Crlin , W. J., Lindner, N. J. and Bitterly, J. G.: Application of the Analogy Between Water Flow With a Free Surface and Two-Dimensional Compressible Air Flow. NACA Report 875, 1946.
6. General Electric Co.: Water Analogy to Two-Dimensional Air-Flow. G. E. Report No. 55218, August, 1947.
7. Geer, J. R.: A Study of the Wake at Supersonic Air Flow of an Elliptical Body-Flat Disk Combination Using Hydraulic Analogy to Compressible Air Flow. University of Minnesota Thesis, 1957.
8. Heberle, J. W., Wood, G. P. and Goodrum, P. B.: Data on Shape and Location of Detached Shock Waves on Cones and Spheres. NACA TN 2000, 1950.
9. Shapiro, A. H.: The Dynamics and Thermodynamics of Compressible Fluid Flow, Ronald Press, New York.